

SPIE PRESS

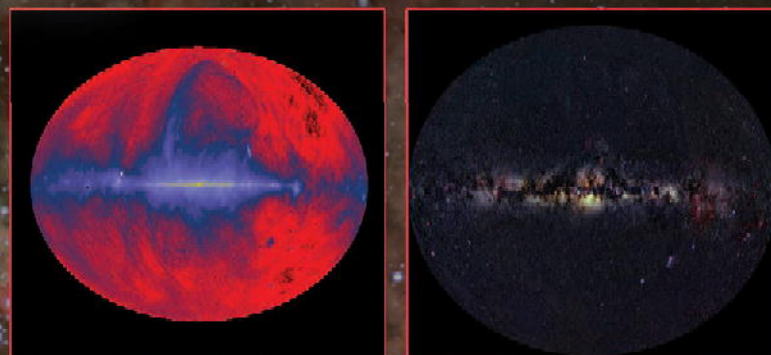


SPIE

Alien Vision

Exploring the Electromagnetic Spectrum with Imaging Technology

SECOND EDITION



Austin Richards

Alien Vision

Exploring the Electromagnetic
Spectrum with Imaging Technology

SECOND EDITION

Alien Vision

Exploring the Electromagnetic
Spectrum with Imaging Technology

SECOND EDITION

Austin Richards

SPIE
PRESS

Bellingham, Washington USA

Library of Congress Cataloging-in-Publication Data

Richards, Austin.

Alien vision : exploring the electromagnetic spectrum with imaging technology /
Austin Richards. – 2nd ed.

p. cm. – (Press monograph ; 205)

Includes bibliographical references and index.

ISBN 978-0-8194-8535-9

1. Imaging systems. 2. Electromagnetic waves. 3. Spectrum analysis. I. Title.

TK8315.R53 2011

621.36'7–dc22

2010046664

Published by

SPIE
P.O. Box 10
Bellingham, Washington 98227-0010 USA
Phone: +1 360.676.3290
Fax: +1 360.647.1445
Email: Books@spie.org
Web: <http://spie.org>

Copyright © 2011 Society of Photo-Optical Instrumentation Engineers (SPIE)

All rights reserved. No part of this publication may be reproduced or distributed in any form or by any means without written permission of the publisher.

The content of this book reflects the work and thought of the author(s).

Every effort has been made to publish reliable and accurate information herein, but the publisher is not responsible for the validity of the information or for any outcomes resulting from reliance thereon.

Printed in the United States of America.

Cover background: “Runaway Star in the Tarantula Nebula,” courtesy of NASA, ESA, C. Evans (Royal Observatory Edinburgh), N. Walborn (STScI), and ESO.



Contents

List of Figures	vii
Preface.....	xv
Acknowledgments	xviii
Introduction	xix
Chapter 1 Infrared and Ultraviolet: The Edges of the Rainbow	1
Near-Infrared Imaging.....	6
Night Vision and Surveillance with Near-IR Imaging.....	7
Exploiting the Deep Penetration of NIR and SWIR Light.....	12
Art Conservation	16
Military Uses of SWIR Imaging	20
Ultraviolet Imaging	21
Animal Ultraviolet Vision	28
Optical Properties of Materials in the Near-IR and Near-UV	30
Atmospheric Effects in the IR and UV Wavebands	34
Infrared and Ultraviolet Light Sources	35
Infrared Photography and Heat Detection	38
Chapter 2 Thermal Imaging: We All Glow in the Dark	41
Reflectivity of Materials	48
Midwave and Longwave IR Imaging Systems.....	48
Surveillance and Law Enforcement	51
Industrial Thermography	53
Imaging Invisible Gases.....	56
Test Range Radiometry	56
High-Speed Thermography	57
Thermal Imaging and Biology.....	59
Thermal Imaging in Astronomy.....	63

Chapter 3 Microwave and Millimeter-Wave Imaging: Piercing the Veil	67
Sub-Millimeter-Wave Imaging: T-Rays	69
Millimeter-Wave Imaging: Seeing Through Clothing and Fog.....	71
Radio Astronomy: The Foundations of Radio-Wave Imaging	74
Radar Imaging: A Microwave Searchlight	79
Small-Scale Imaging Radar.....	85
Chapter 4 X Rays and Gamma Rays: Crookes Tubes and Nuclear Light	89
Gamma Rays.....	91
High-Energy Astronomy	104
Gamma-ray Imaging	107
PET Scans: Observing Living Tissue with Gamma Rays	108
Chapter 5 Acoustic Imaging: Seeing with Sound.....	115
Underwater Acoustic Imaging.....	116
Ultrasound Medical Imaging.....	120
Acoustic Daylight Imaging.....	122
Acoustic Imaging of Sound Sources	124
Chapter 6 Sweeping through the Spectrum: Comparative Imagery	127
Milky Way Images from Radio to Gamma Ray	132
Milky Way Image Descriptions.....	133
Epilogue	139
Glossary	143
Bibliography	153
Index.....	155

List of Figures

1	Electromagnetic spectrum.	xxii
1.1	The near-UV, visible, near-IR, and SWIR wavebands.	2
1.2	Sunlight split into some of its components by a prism.	2
1.3	Plate from W. Herschel's infrared paper (1800).	4
1.4	Block diagram of near-IR and near-UV photographic apparatus.	6
1.5	Robert Wood in the UV band.	7
1.6	M3 sniperscope, Korean War era.	8
1.7	The author with a working WWII-era C-3 near-IR imager.	8
1.8	Night-vision goggles with head mount.	9
1.9	Near-IR image showing dark-adapted eyes. (<i>Courtesy of Dannen Harris</i>)	10
1.10	Three views of a factory: visible, no camouflage (top); visible, camouflage (middle); near-IR, camouflage (bottom). (<i>Courtesy of Eastman Kodak, Inc.</i>)	11
1.11	False color key to LANDSAT image of San Francisco Peninsula (red: high reflectance at blue wavelengths; green: high reflectance at near-infrared wavelengths; blue: high reflectance in visible wavelengths). Built-up areas appear purple or gray, white areas are high albedo objects, vegetation appears green because of its high near-IR reflectance, and clear water appears black.	12
1.12	Visible (left) and SWIR (right) images of water in a plastic cup. (<i>Courtesy of FLIR</i>)	13
1.13	(a) Visible: 400–750 nm; (b) NIR: 830–1100 nm; (c) SWIR: 1400–1700nm; (d) SWIR: 2000–2500um. (<i>Courtesy of FLIR</i>)	14
1.14	Near UV: 365 nm (left) and shortwave UV: 254 nm (right) images of an altered document.	14
1.15	Four views of a paper label on a cardboard box: (a) visible: 400–750 nm; (b) NIR: 830–1100 nm; (c) SWIR: 1400–1700 nm; (d) SWIR: 2000–2500 um. (<i>Courtesy of FLIR</i>)	15
1.16	Two views of a torn paper label with printing underneath: left—365 nm; right—254 nm.	15
1.17	VIS and NIR images of a cotton shirt showing a GSR pattern. (<i>Courtesy of Heidi Nichols, Miami-Dade County Medical Examiner's Office</i>)	16
1.18	Early 19th century headstone with staining and lichen growth: left—VIS; right—780–1100 nm.	17

1.19 The author in a loud and admittedly tacky shirt made of rayon: left—VIS; right—NIR (780–1100 nm)	17
1.20 Visible image of <i>Natura</i> and two details in visible and near-IR light. (<i>Courtesy of Editech</i>)	18
1.21 Visible (400–750 nm), NIR (830–1100 nm), and SWIR (1400–1700 nm) images of a test panel with oil paint swatches and underdrawing media. Paint swatches from left to right: burnt umber, burnt sienna, raw sienna, and ochre. Underdrawing media from top to bottom: silver, ivory black, lamp black, vine black, charcoal in gum arabic. (<i>Courtesy of FLIR and LACMA</i>).	19
1.22 Ruysdael painting imaged in visible (400–750 nm) [top and bottom-left] and SWIR (1400–1700 nm) [bottom-right]. (<i>Images courtesy of Yosi Poseilov, Los Angeles County Museum of Art</i>) . . .	20
1.23 Mahogany veneer with well-done repair: left—VIS; right—780–1100 nm.	21
1.24 (a) Airborne Laser Test Bed in flight; (b) SWIR aiming and focusing optics on the nose of the ALTB; (c) SWIR image of ALTB firing at a Scud missile—the missile is on the left side of the image; (d) Scud missile mounted on a mobile launcher. Figures 1.24(a)–(c) courtesy of the Missile Defense Agency.	21
1.25 CD jewel case with scratches: left—visible; right—near-UV.	23
1.26 Magazine cover (top) and details imaged with visible light (bottom left) and shortwave-UV light (bottom right). (<i>Courtesy of Sirchie Fingerprint Laboratory</i>)	24
1.27 Visible (left) and near-UV (right) images of a five-month-old bite mark on a living person. (<i>Photos courtesy of Stephen Warlen and the Kansas City Police Department Crime Lab</i>)	25
1.28 Epoxy floor sealant shoe mark on a tile floor: left—VIS; right—near-UV (396 nm).	25
1.29 Shoemark on vinyl tile with floor wax: left—VIS; right—near-UV (365 nm).	25
1.30 Fresh and old paint on a stucco wall: left—VIS; right—near-UV (330–400 nm).	26
1.31 Near-UV image of polar bears. (<i>Courtesy of Dr. David Lavigne</i>)	27
1.32 Visible (left) and near-UV (right) images of Canadian Arctic military camouflage. (<i>Courtesy of Dr. David Lavigne</i>)	27
1.33 Visible (left) and near-UV (right) images of skin cancer. (<i>Courtesy of Dr. Norman Goldstein</i>)	28
1.34 Visible (left) and near-UV (right) images of Black-Eyed Susans. (<i>Courtesy of Prof. Tom Eisner</i>)	29
1.35 Visible (left) and near-UV (right) images of <i>Goneopteryx cleopatra</i> . (<i>Courtesy of Edward Aicken</i>)	30
1.36 Visible (left) and near-UV (right) images of coral reefs and fish. (<i>Courtesy of Prof. Thomas Cronin and the Journal of Fish Biology</i>)	30

1.37	Images of BK7 glass and fused silica discs in three narrow UV bands. (<i>Courtesy of David Hayes</i>)	31
1.38	From upper left to bottom right: SWIR (2000–2500 nm), SWIR (950–1700 nm), visible (400–750 nm), and near-UV (350–380 nm) images of a human eye. (<i>Courtesy of FLIR and Rand Molnar</i>)	32
1.39	SWIR, visible, and near-UV images of the author. (<i>Courtesy of FLIR and Rand Molnar</i>)	33
1.40	Top–VIS image of oil rig at 47 km range. Bottom–SWIR (950–1700 nm) image. (Courtesy of FLIR)	34
1.41	The setting moon over Nellis Air Force Base in near-UV, VIS, near-IR, and midwave IR wavebands. (<i>Midwave IR image courtesy of FLIR</i>)	35
1.42	Visible (left) and SWIR (right) images of a methanol fire. (<i>Courtesy of FLIR</i>)	36
1.43	Composite visible and UV (240–280 nm) image of methanol fires. (<i>Courtesy of Ofil Ltd., Nes-Ziona, Israel</i>)	37
1.44	Composite visible and UV (240–280 nm) image of power line corona. (<i>Courtesy of Ofil Ltd., Nes-Ziona, Israel</i>)	38
1.45	Visible (left) and near-UV (right) images of fuel rod assembly in a storage pond. The missing rods make the marked holes glow brighter because nothing is blocking the light paths. (<i>Photo courtesy of Channel Systems</i>)	38
1.46	Shortwave IR image of a lit cigarette illuminating a bathroom. (<i>Courtesy of FLIR</i>)	39
1.47	Visible (left) and SWIR (right) images of hot and cold stove burners. (<i>Courtesy of FLIR</i>)	40
2.1	The infrared spectrum in relation to visible light.	42
2.2	A child watching television: left–VIS; right–3–5 micrometers. (<i>Courtesy of FLIR</i>).	42
2.3	MWIR (3–5 mm) image of pyramid and Sphinx. (<i>Courtesy of Stan Laband</i>)	44
2.4	Plastic plant pot on wood chips in sunlight: left—VIS; right—MWIR (3–5 mm).	45
2.5	Thermal scar left by plant pot: left—VIS; right—MWIR (3–5 mm). (<i>Courtesy of FLIR [IR] and Patrick Stanbro [visible]</i>)	45
2.6	Visible and MWIR (3–5 mm) images of a floor with heat footprints. (<i>Courtesy of FLIR</i>)	46
2.7	MWIR (3–5 mm) image of the author. (<i>Courtesy of FLIR</i>)	46
2.8	Visible (left) and MWIR (3–5 mm) (right) images of the author's eye. (<i>Courtesy of FLIR</i>)	46
2.9	A boy with his arm inside a black polyethylene garbage bag: left—VIS; right—MWIR (3–5 mm). (<i>Courtesy of FLIR</i>)	47
2.10	Visible (left) and MWIR (3–5 mm) (right) images of a man sitting in a car. (<i>Courtesy of FLIR and Patrick Stanbro</i>)	49

2.11	Visible (left) and MWIR (3–5 mm) (right) images of a man reflected in a brushed stainless steel refrigerator door. (<i>Courtesy of FLIR and Patrick Stanbro</i>)	49
2.12	Cooled MWIR (3–5 mm) camera. (<i>Courtesy of FLIR</i>)	50
2.13	Block diagram of a cooled MWIR (3–5 mm) camera.	50
2.14	Visible and LWIR images of person in smoke-filled building. (<i>Courtesy of FLIR</i>)	52
2.15	Jesusita fire at 10-km range in Santa Barbara, California: left—VIS; right—MWIR (3–5 mm). (<i>Courtesy of FLIR</i>)	52
2.16	Handgun in bushes at night: left—VIS; right—LWIR (8–13 μm). (<i>Courtesy of FLIR</i>)	52
2.17	Burglar sneaking in the dark: left—VIS; right—MWIR (3–5 mm). (<i>Courtesy of FLIR</i>)	52
2.18	Visible (left) and MWIR (3–5 mm) (right) images of a living room. (<i>Courtesy of FLIR and Patrick Stanbro</i>)	54
2.19	Thermal image of unmarked graves. (<i>Courtesy of Gary J. Weil, Entech Engineering, Inc.</i>)	54
2.20	Heated seats in a car: left—VIS; right—MWIR (3–5 mm). (<i>Courtesy of FLIR and Patrick Stanbro</i>)	55
2.21	Visible (top) and MWIR (3–5 mm) (bottom) images of energized transformers. (<i>Courtesy of FLIR</i>)	55
2.22	Visible (left) and MWIR (3–5 mm) (right) images of a high-speed circuit board. (<i>Courtesy of FLIR</i>)	56
2.23	Propane gas leak imaged with a special 3.3 micrometer midwave-IR camera. (<i>Courtesy of FLIR</i>)	57
2.24	Harrier jet hovering in place during an airshow: top—VIS; middle—MWIR (3–5 mm); bottom—NIR (0.78–1.1 μm). (<i>Courtesy of FLIR</i>)	58
2.25	Chinook helicopter taking off at night: left—VIS; right—MWIR (3–5 mm). (<i>Courtesy of FLIR</i>)	59
2.26	A 168 grain .30 caliber bullet in flight: top—MWIR (3–5 mm); bottom—VIS. (<i>Courtesy of FLIR and Vision Research</i>)	59
2.27	VIS and MWIR (3–5 mm) images of a cat. (<i>Courtesy of FLIR</i>)	61
2.28	Visible (left) and MWIR (3–5 mm) (right) images of blood flow in a forearm. (<i>Courtesy of FLIR</i>)	61
2.29	MWIR (3–5 mm) image of hand with a missing finger. (<i>Courtesy of FLIR</i>)	61
2.30	Visible (left) and MWIR (3–5 mm) (right) images of a fingertip. (<i>Courtesy of FLIR</i>)	62
2.31	Hummingbird in flight—MWIR (3–5 mm). (<i>Courtesy of FLIR</i>)	63
2.32	LWIR image of a bee ball (left) and visible image of a dead hornet dragged by bees (right). (<i>Courtesy of Dr. Masato Ono, Tamagawa University, Tokyo</i>)	63
2.33	Eclipsed Moon imaged in 4.29- μm waveband. (<i>Courtesy of DCATT Team, MSX Project, and BMDO</i>)	65

3.1	The long-wavelength region of the electromagnetic spectrum.	69
3.2	T-Ray image of an integrated circuit. (<i>Courtesy of Prof. Daniel Mittleman and Prof. Martin Nuss</i>).	70
3.3	T-ray image of a leaf at 48-hour interval. (<i>Courtesy of Prof. Daniel Mittleman and Prof. Martin Nuss</i>).	70
3.4	Visible (top) and T-ray (bottom) images of a milk chocolate bar with almonds. (<i>Courtesy of Picometrix, Inc.</i>)	71
3.5	Side view of concealed contraband under clothing.	73
3.6	Visible (left) and mmW (right) images of a man with concealed guns. (<i>Courtesy of Millivision Corporation</i>)	73
3.7	Visible (top) and mmW (bottom) images of a runway in zero-visibility fog. (<i>Courtesy of Northrup Grumman Corporation</i>) . .	74
3.8	Passive millimeter-wave camera on aircraft nose. (<i>Courtesy of Northrup Grumman Corporation</i>)	75
3.9	Karl Jansky and his steerable 14.6-m wavelength radio antenna. (<i>Courtesy of NRAO/AUI</i>)	76
3.10	Microwave sky in the 73-cm waveband. (<i>Courtesy of NASA</i>) . . .	76
3.11	Aitoff projection of the visible sky. (<i>Courtesy of Axel Mellinger</i>) .	78
3.12	Block diagram of radio telescope and celestial source. The telescope has a narrow field of view (the “beam”) that scans the source.	78
3.13	Parkes Observatory. (<i>Courtesy of David McClenaghan, CSIRO</i>) .	79
3.14	Airborne radar system schematic.	80
3.15	Model of SIR-C/X-SAR imaging radar antenna array.	81
3.16	Radar image of Angkor in Cambodia. (<i>Courtesy of NASA</i>)	82
3.17	Radar image of Wadi Kufra, Libya. (<i>Courtesy of NASA</i>)	83
3.18	Lake Vostok imaged by Radarsat with 6-cm microwaves. (<i>Courtesy of Canadian Space Agency</i>)	84
3.19	Visible and microwave images of Venus. (<i>Left image courtesy of Calvin J. Hamilton, right image courtesy of NASA</i>)	85
3.20	Radar image of Maat Mons. (<i>Courtesy of NASA</i>)	86
3.21	Visible (left) and MIR (right) images of an antitank mine. (<i>Courtesy of Lawrence Livermore National Laboratory</i>)	86
3.22	Visible (left) and MIR (right) images of metal structures in concrete slab. (<i>Courtesy of Lawrence Livermore National Laboratory</i>)	87
4.1	The short-wavelength region of the electromagnetic spectrum. . . .	90
4.2	Schematic of an x-ray shadowgram.	93
4.3	Crookes tube schematic.	93
4.4	The first radiograph. (<i>Courtesy of the American College of Radiology</i>)	94
4.5	Hand of Mihran Kassabian, x-ray martyr. (<i>Courtesy of American College of Radiology</i>)	94

4.6	Kassabian's x-ray laboratory. (<i>Courtesy of American College of Radiology</i>)	95
4.7	X-ray studio advertisement. (<i>Courtesy of American College of Radiology</i>)	95
4.8	Nelson x-ray power supply. (<i>Courtesy of American College of Radiology</i>)	96
4.9	Shoe-fitting fluoroscope. (<i>Courtesy of Dr. Paul Frame</i>)	97
4.10	Radiograph of a foot in a shoe. (<i>Courtesy of American College of Radiology</i>)	97
4.11	X-ray shadowgram of a lily. (<i>Courtesy of Steve Meyers</i>)	98
4.12	Movie poster from <i>X: The Man with the X-ray Eyes</i> . (<i>Courtesy of MGM</i>)	99
4.13	Thomson Twins imaged by a fluoroscope. (<i>Courtesy of Hergé/Moulinsart</i>) © Hergé/Moulinsart 2010.	99
4.14	Visible and x-ray images of a painting. (<i>Courtesy of the J. Paul Getty Museum, Los Angeles</i>)	100
4.15	Mummy being loaded into CAT scanner. (<i>Courtesy of Prof. Clive Baldock</i>)	101
4.16	CAT-scan front view of a mummy. (<i>Courtesy of Prof. Clive Baldock</i>)	101
4.17	CAT-scan cross section of a mummy. (<i>Courtesy of Prof. Clive Baldock</i>)	102
4.18	X-ray CAT scan of the mummy Nesperennub, an Egyptian priest who was mummified in approximately 800 BCE. (<i>Photo courtesy of SGI</i>)	103
4.19	A color image of Nesperrenub's cartonnage casket, which has remained sealed for almost 3000 years. (<i>Photo courtesy of the British Museum</i>)	103
4.20	A close-up x-ray CAT scan of Nesperrenub's hands showing various ornamental rings. (<i>Image courtesy of SGI</i>)	104
4.21	Marijuana concealed behind a false wall in a truck. (<i>Courtesy of American Science and Engineering</i>)	104
4.22	Backscatter x-ray image of a man. (<i>Courtesy of American Science and Engineering</i>)	105
4.23	The Sun imaged with soft x rays. (<i>Courtesy of Yohkoh/SXT</i>)	106
4.24	Gamma-ray imaging with radioactive source and film.	108
4.25	Visible (left) and gamma-ray (right) images of a marble statue. (<i>Courtesy of CEA</i>)	109
4.26	Schematic diagram of a PET scan.	110
4.27	Heart muscle viability indicated by PET scans: left image shows loss of blood flow in regions, right image shows metabolic activity. (<i>Courtesy of Dr. David Lilien, Biomedical Research Foundation of Northwest Louisiana</i>)	111
4.28	Normal brain (left) and brain with Alzheimer's disease (right) PET scans. (<i>Courtesy of Dr. Michael E. Phelps, UCLA School of Medicine</i>)	112

4.29	Epileptic brain PET scan. (<i>Courtesy of Dr. Michael E. Phelps, UCLA School of Medicine</i>)	112
4.30	GRIS images of depleted uranium (left) and plutonium fuel rods (right). (<i>Courtesy of Lawrence Livermore National Laboratory</i>) . .	113
4.31	Rendering of GRIS inspection of a Peacekeeper missile in its silo. (<i>Courtesy of Lawrence Livermore National Laboratory</i>)	114
4.32	GRIS image of a Peacekeeper missile warhead package. (<i>Courtesy of Lawrence Livermore National Laboratory</i>)	114
5.1	Schematic of ship's depth finder.	117
5.2	Sonar towfish with undersea cable. (<i>Courtesy of Garry Kozak, L-3 Klein</i>)	118
5.3	(a) Front view and (b) top view of sonar towfish with sonar beams. (<i>Courtesy of John Perry Fish</i>).	119
5.4	The <i>Empire Knight</i> imaged with sonar. (<i>Courtesy of Garry Kozak, L-3 Klein</i>)	119
5.5	Another sonar image of the <i>Empire Knight</i> . (<i>Courtesy of Garry Kozak, L-3 Klein</i>)	120
5.6	(a) Sonar scan of a lake with a drowning victim at the bottom; (b) detail of drowning victim. (<i>Courtesy of Gary Klein</i>).	121
5.7	Fetal ultrasound image. (<i>Courtesy of Siemens Healthcare, Ultrasound</i>)	122
5.8	Ultrasound image of a fetus with Doppler false color. (<i>Courtesy of Siemens Healthcare, Ultrasound</i>)	122
5.9	ROMANIS acoustic imaging sensor. (<i>Courtesy of Mandar Chitre and Venugopalan Pallayil, Acoustic Research Lab, Tropical Marine Science Institute, National University of Singapore</i>)	124
5.10	(a) ANI target and (b) an acoustic noise image of the target. (<i>Courtesy of Mandar Chitre and Venugopalan Pallayil, Acoustic Research Lab, Tropical Marine Science Institute, National University of Singapore</i>).	125
5.11	Acoustic image series of a TGV trainset. (<i>Courtesy of TNO-TPD, Delft, the Netherlands</i>)	126
5.12	TGV Thalys trainset and SYNTACAN acoustic imaging array. (<i>Courtesy of TNO-TPD, Delft, the Netherlands</i>).	126
6.1	Millimeter-wave ($\lambda = 3300 \mu\text{m}$) photo. (<i>Courtesy of Trex Enterprises</i>)	128
6.2	Longwave infrared ($\lambda = 8\text{--}9 \mu\text{m}$) photo. (<i>Courtesy of FLIR</i>)	128
6.3	Midwave infrared ($\lambda = 3\text{--}5 \mu\text{m}$) photo. (<i>Courtesy of FLIR</i>)	129
6.4	Shortwave infrared ($\lambda = 2\text{--}2.5 \mu\text{m}$) photo. (<i>Courtesy of FLIR</i>)	130
6.5	Near-infrared ($\lambda = 0.9\text{--}1.68 \mu\text{m}$) photo. (<i>Courtesy of FLIR</i>)	130
6.6	Very near-infrared ($\lambda = 0.83\text{--}1.1 \mu\text{m}$) photo.	130
6.7	Visible ($\lambda = 0.4\text{--}0.7 \mu\text{m}$) photo.	131
6.8	Near-ultraviolet ($\lambda = 0.35\text{--}0.38 \mu\text{m}$) photo. (<i>Courtesy of Rand Molnar</i>)	131

6.9 Shortwave ultraviolet ($\lambda = 0.254 \mu\text{m}$) photo. (<i>Courtesy of Patrick Stanbro</i>)	132
6.10 X ray ($\lambda \sim 2.5 \times 10^{-5} \text{ mm}$) of a human head. (<i>Courtesy of LACMA</i>).	132
6.11 Multiwavelength Milky Way images	134
6.12 Five images of Vela. (<i>Courtesy of the Astrophysics Data Facility, NASA Goddard Space Flight Center</i>).	136

Preface

The inspiration for *Alien Vision* came from two other illustrated science books that I have long admired. Both are visual explorations of nature that use imaging technology to transcend the limitations of human visual perception. The first is *The Powers of Ten*, by Phillip and Phylis Morrison,* which takes the reader on a pictorial journey through 40 powers of ten in size scale, starting with a one-meter square image of a couple sleeping on a park lawn. Each successive section of the book changes the scale of the image by a factor of ten, zooming out to view the park, then Chicago, then Lake Michigan, then North America, then Earth, and so on, until finally the square image is so large that it encompasses a multitude of galaxies. Then the “camera” zooms in on the man’s hand, on a mosquito feeding there, then on bacteria on the mosquito, and so on, stopping at the subatomic particles whirling around in the nucleus of a single atom. There is also a movie version of this book available that includes a sequence where the observer rushes in from viewing distant clusters of galaxies to the hand of the sleeping man! *The Powers of Ten* explores nature in the *scale* domain, exploring size scales that are much larger and much smaller than the size scale of human visual perception.

The second book is *Stopping Time—The Photographs of Harold Edgerton*.† The photographs in this book show commonplace events captured with high-speed cameras using electronic flash units and special shutters invented by Prof. Edgerton and his colleagues at the Massachusetts Institute of Technology. Events that happen in thousandths or millionths of a second are captured on film: a bullet passing through an apple, the first atomic bomb test an instant after detonation, a football player kicking a football. Edgerton’s work is an exploration of images of the world in the *time* domain. The Eames Office, makers of the film version of *The Powers of Ten*, have also produced a film called *The Powers of Time*‡ which explores the universe in 37 orders of magnitude of time, from the tiny attosecond to 31 billion years. These time scales are much shorter and much longer than the time scale of human visual perception.

My idea was to apply this same idea of a visual exploration of the universe to the electromagnetic spectrum itself, which could be considered the domain of *wavelength*. Instead of exploring the universe in many size or time scales, my book would take the reader on a tour of all the possible “colors” of light, from long-wavelength radio waves to extremely short gamma rays. These are wavelengths of light that are much longer and much shorter than the narrow wavelength range of human visual perception. It would be as though the readers each had a knob on

**The Powers of Ten*, Phillip and Phylis Morrison and the Office of Charles and Ray Eames, Scientific American Library, New York (1982).

†*Stopping Time-The Photographs of Harold Edgerton*, Harold Edgerton, Abrams, New York (1987).

‡*The Powers of Time* (1996), by Eames Demetrios for the Eames Office.

their heads that they could tune like a radio dial and change the “color response” of their eyes out of the visible spectrum and into the infrared, ultraviolet, and beyond. I worked for a time as an astrophysicist and was always fascinated by the way we observe the sky with instrumentation that extends the human visual sense into new realms of the electromagnetic spectrum beyond the visible portion. An astronomy teacher of mine once remarked that if our eyes could only detect radio waves instead of what we call visible light, then we would not see the stars at all. Instead, we would see a sky full of big clouds and swirls of cold interstellar gas, with compact radio sources sprinkled throughout. The familiar night sky we see is only one of many possible skies overlaid on top of one another. I wondered if hypothetical aliens on some distant planet might see a radio sky with their peculiar visual apparatus. Extraterrestrial aliens aside, with imaging technology we have the ability to synthesize our own version of “alien vision.”

This book is not intended as a comprehensive survey of imaging technology. Rather, it is a compilation of images and descriptions of imaging technology that convey a sense of what nature looks like when imaged with “invisible light.” Descriptions of the imaging technology (electronic sensors and photographic film) are non-technical in nature, and I include pictures of actual imaging devices only in cases where the layperson can appreciate the design of the device. I have attempted to include a visible-light picture of the same scene or object next to every “invisible light” image, but these visible-light counterparts were not always available.

The majority of the research for this book was carried out through Internet searches, which uncovered many images and articles on imaging. I located the authors of this web content, and these helpful colleagues transmitted additional articles and digital images to me via e-mail from all over the world. I obtained many of the infrared images in Chapters 1 and 2 using cameras provided by my present employer, FLIR in Santa Barbara, California. I have attempted to obtain the highest-resolution images available, but many of the electronic sensors used to image in invisible wavebands of light have limited resolution, and the resulting images can sometimes appear quite grainy in comparison with their visible-light counterparts. Since the first edition of the book, the number of pixels of many thermal IR sensors has increased from 80,000 to over 1 million. I attempted to “upgrade” IR images whenever possible, though in some cases it was not practical or possible to do so. In some cases, the ultimate resolution of an image is limited by the wavelike properties of light, properties that make it impossible to resolve features that are smaller than a wavelength. I have used metric units throughout, and terms or jargon in boldface are included in a glossary at the end of the book. Metric units are very appropriate in a book like this, because I don’t think I have ever heard of anyone using Imperial units as a measure of wavelength!

I refer to electromagnetic waves as light throughout this book. Some would question that usage, preferring to reserve the term “light” for visible light only. Everything else would then be called electromagnetic radiation. I dislike this usage of the word radiation to describe lightwaves in a book like *Alien Vision*. To the layperson, the word radiation calls to mind ionizing particles or gamma rays. Some workers in the infrared industry use the term energy rather than light. They will say

“shortwave infrared energy” rather than “shortwave infrared light.” I don’t like this term much either—it is too vague. Energy has many different forms, but light is a very specific manifestation of energy.

Acknowledgments

Many thanks are in order for the generosity and helpfulness of the people and organizations that gave me permission to use images or offered suggestions: Victoria Charters; Peter Richards; Elma O'Donaghue and Yosi Pozeilov of LA County Museum of Art; John Lovberg and Chris Martin of Trex Enterprises; Prof. Axel Mellinger of Central Michigan University; Lawrence Wolff of Equinox Corporation; Prof. Gary Settles of Penn State University; Stephen Warlen of the Kansas City Police Crime Laboratory; Cliff Anger of Itres Corporation; Gerry Holst; Dr. Larry Yujiri of TRW, Inc.; Graham Rockley of Ashwin Systems Corp.; Richard Huguenin of Millimetrix Corp.; Jay Robinson, Stan Laband, David Risdall, Ron Carrelejo, and Vu Nguyen of FLIR; Chris Johnston, Kurt Heidner, and Elliot Rittenberg of IRCameras.com; Dr. Greg Bearman of Jet Propulsion Laboratory; Dr. Thomas Cronin of the University of Maryland, Baltimore County; Prof. Thomas Eisner of Cornell; Dr. Masato Ono of Tamagawa University, Tokyo; Dr. Justin Marshall and Kylie Jennings of the University of Queensland; Nancy Adams of Kodak Corp.; Dr. Martin Nuss of Bell Labs – Lucent Technologies; John Perry Fish; Dr. Michael E. Phelps of the UCLA School of Medicine; Clive Baldock of the Queensland University of Technology; Calvin Hamilton; Dr. Scott Klioze of the University of Florida; The American College of Radiology; Dr. David Lilien of the Biomedical Research Foundation of Northwest Louisiana; Yvonne Szafran of the Getty Conservation Institute; Dr. Klaus Ziock and Dr. Steven Azevedo of the Lawrence Livermore National Laboratory; Zahi Lindner of Ofils Ltd., Israel; Kathryn Charles-Wilson of British Museum Images; Sophie Lonsky of SGI; Maurizio Seracini of Editech; Peter Horemans of Moulinart, Belgium; Prof. John David Jackson of UC Berkeley; Dr. Paul Frame of Oak Ridge Associated Universities; Shaula Coyl of the LA County Museum of Art; Dr. David Alexander of the Lockheed Martin Solar and Astrophysics Lab; Seth Digel of NASA; John Potter of the National University of Singapore; Peter Taylor; Brian Nagourney; Stan Voynick; Prof. Robert Romer and Prof. Kannan Jagannathan of Amherst College; Rand Molnar of Brooks Institute of Photography; Rick Twardy of ATNF CSIRO; Tony Bacarella; and Dannen Harris. A special thanks to the late Prof. William Youngren (my stepfather) for his edit of the original manuscript and encouragement to write this book, which was conceived during a road trip the two of us took in January 1998.

Austin Richards, Ph.D. (www.austinrichards.com)
Santa Barbara, California, December 2010

Introduction

At each end of the solar spectrum the chemist can detect the presence of what are known as “actinic” rays. They represent colors – integral colors in the composition of light – which we are unable to discern. The human eye is an imperfect instrument; its range is but a few octaves of the real “chromatic scale.” I am not mad; there are colors that we cannot see. And, God help me! The Damned thing is of such a color!

- From “The Damned Thing” by Ambrose Bierce (1893)

Dr. Waldman, I learned a great deal from you at the university about the violet ray, the ultraviolet ray, which you said was the highest color of the spectrum. You were wrong. Here in this machinery I have gone beyond that. I have discovered the great ray that first brought life into the world!

- Dr. Henry Frankenstein, from the motion picture *Frankenstein, the Man Who Made a Monster* (1931)

Vision ranks highest in the hierarchy of human senses. Our eyesight informs our perception of the world to a tremendous extent. We grow so accustomed to seeing the world a certain way that it is easy to forget that our vision is, in certain respects, quite limited. For example, the optical properties of the eye are such that we cannot resolve objects below a certain size scale without a microscope or magnifying lens. Nor is the eye infinitely fast in its response time. The chemical and electrical properties of the eye and brain impose speed limits on human visual perception: events such as the motion of a bullet through an apple occur in time scales too small to perceive. Stopping the flight of the bullet requires cameras with very fast shutter speeds or strobe lights. In both of these cases, imaging technology enhances human visual perception, enabling us to explore the world of very small things and very fast things.

Imaging technology can also explore another fundamental limitation of human visual perception, one that concerns the nature of light itself. When we look at a candle flame, light emitted by the hot gases travels into our eye and produces chemical and electrical signals that the brain interprets as an image. But the human

eye is sensitive to light only within a narrow range of color, and when one looks at a candle flame, one sees only a fraction of all the light emitted by the flame! We distinguish these two classes of light in the following way. The light that our eyes use for vision is called **visible light**. Visible light comes in all the colors of the rainbow, from red to violet. Light that falls outside of this color range does not produce a visual sensation. Hereafter this will be referred to as **invisible light**. It should be noted that invisible light does not have “color” as we know it, since color is a construct of human perception rather than an absolute property of light. A bit later, I will define more appropriate means of describing the quality called color of both visible and invisible light.

Invisible light surrounds us at all times, even when our eyes tell us we are in the dark, and objects that appear non-luminous to the eye are always emitting invisible light. Many sources of visible light, such as the Sun, are also emitters of copious invisible light. A beam of sunlight passed through a prism splits into a rainbow pattern of colors from red through violet. At each end of the pattern the colors appear to fade into darkness, but this effect is a limitation of the eye. That apparent darkness contains invisible light, for the pattern from the prism extends out beyond what the eye sees, and it can be detected with imaging technology. In fact, there is an almost infinite range of light beyond the visible. Imagine that you could only hear one note out of the 88 notes on a piano, or that the only color you could see was one particular shade of green, and you will have some idea of the limitations of our visual apparatus. We do not normally think about this ubiquitous invisible light, just as we do not normally think about the fact that we exist at the bottom of an ocean of air that is many miles deep. But invisible light is there nonetheless, and very interesting things are revealed when we use it to image the world. In most cases, an image of an object or scene made with invisible light is totally different from an image of the same object or scene made with visible light. The reason for this is that some materials heavily absorb visible light yet freely pass invisible light, while others pass visible light but strongly absorb invisible light. An object or material that we think of as opaque such as a block of wood may appear transparent to an invisible-light imaging system; conversely, objects or materials that are transparent to visible light such as window glass may appear opaque when imaged with invisible light. This book contains images (made with visible and invisible light) and descriptions of both types of materials.

Imaging with invisible light is a relatively recent advance, requiring technology invented since the end of the 19th century. In recent decades, the technology of imaging with invisible light has grown at an amazing rate, especially in the area of electronic detectors. Whenever possible for purposes of comparison, images made with invisible light are presented alongside images of the same scene or object made with visible light. In the cases when only the image made with light from outside our color perception range is shown, the visible-light image was either not available, would be completely black, or is obvious as to its appearance.

Describing invisible light

Since we cannot see invisible light with our eyes, we cannot describe it by its color. A different convention is needed, one based on the physical properties of light itself. What is light, and what property of it is perceived as color by the eye? Classical physics describes light as an **electromagnetic wave** that propagates at a fixed speed through empty space, a disturbance in the **electromagnetic field**. Scientists describe the “color” of an electromagnetic wave or **light wave** in terms of its **wavelength**, its **frequency**, or its **energy**. The wavelength of light is defined as the distance between crests of waves that propagate in the electromagnetic field. If one places a free electric charge in the path of the wave, the charge will move in response to the oscillations of the electromagnetic field of the wave, just as a buoy moves up and down on the surface of the ocean when water waves pass underneath it. The frequency of a light wave is defined as the number of oscillations of the electromagnetic field per second. The wavelength and frequency of an electromagnetic wave are related by the following expression:

$$c = \lambda v$$

where c is the **speed of light** in empty space, λ is the wavelength, and v is the frequency. Note that frequency and wavelength are inversely proportional to each other: the higher the frequency of the light wave, the shorter the wavelength. The energy of light is defined in the following way. **Quantum theory** predicts that light waves transfer energy to matter and vice-versa in discrete bundles called **photons**. The energy of a photon in a lightwave is related to its frequency of the lightwave by the expression $E = hv$, where v is the frequency in cycles per second and h is **Planck's constant**. Wavelength, frequency, and energy are all used to describe lightwaves, and the full range of wavelengths, frequencies, or energies of light is called the **electromagnetic spectrum**.

The various colors of visible light are described generally in terms of wavelength, since it is the easiest parameter to measure directly. For example, red laser pointers emit light with a wavelength of 635 **nanometers**, abbreviated as nm. Wavelength is a very useful way to describe light in the middle regions of the electromagnetic spectrum, but it is not so useful at the edges. At very high energies the wavelength of light is so short and its frequency so high that it is impractical to measure either its wavelength or frequency, and therefore it is conventional to quantify a lightwave by the amount of energy it transfers in a collision with matter, i.e. the energy of its photons. At very low energies, the wavelengths of lightwaves become very long and difficult to measure, while frequencies can be measured directly. Thus, these very low energy light waves are described in terms of frequency. All three descriptors are used throughout this book, with a bias toward wavelength.

Figure 1 is a diagram of the electromagnetic spectrum with wavelength indicated in metric length units. The energy of light decreases with wavelength; thus, energy decreases from top to bottom in the figure. The range of wavelengths shown spans

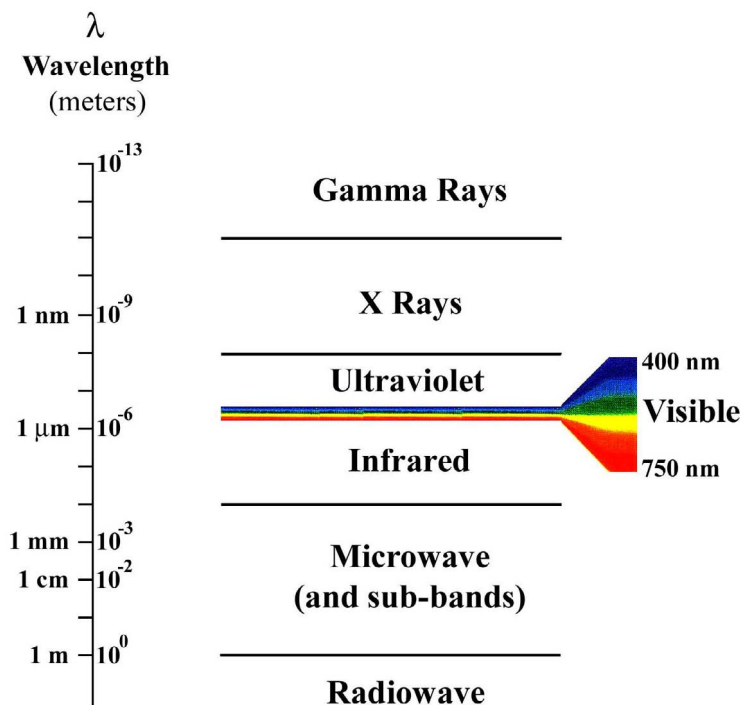


Figure 1 Electromagnetic spectrum.

18 powers of ten, and is divided into regions called **wavebands**. The diagram does not represent the entire electromagnetic spectrum, but it encompasses the wavelengths of light used to make the images in this book and the vast majority of wavelengths of light studied by scientists. The most familiar classifications of wavebands are indicated by regions that span a portion of the spectrum, the **radiowave**, **microwave**, **infrared**, **visible**, **ultraviolet**, **x-ray** and **gamma-ray** wavebands. These areas are not strict definitions—there is some overlap between wavebands, and there are also subclassifications within wavebands. These sub-bands are described in more detail in subsequent chapters. Visible light, the light that our eyes use to collect visual information, is merely a narrow strip within the scale of the electromagnetic spectrum. Our eyes see light in the wavelength range from 400–750 nm, and that is all!

The visible waveband is flanked by the infrared (“below red”) and ultraviolet (“beyond violet”) wavebands. These names are based on the wavebands’ position in the spectrum relative to visible light, but the other wavebands have names that are quite independent of any reference to visible light or even light at all. This naming convention is a consequence of the history of their discovery —x rays and gamma rays, for example, were initially thought to be particles (or “rays”) rather than lightwaves. It is often more convenient to describe x rays and gamma rays in terms of energy rather than wavelength or frequency, since the wavelengths are so extremely short and the frequencies so high that they can be difficult or impossible

to measure directly. Microwaves and radio waves are also lightwaves; though, like x rays and gamma rays, they interact with matter in a manner that is very different from visible light. Most people do not think of radiowaves as low-energy cousins of visible lightwaves. But they are indeed lightwaves, and are often described in terms of their frequency, since we can directly measure the oscillation frequency of electric charges induced by passing radio waves.

Each chapter of this book describes a different waveband of the electromagnetic spectrum, with selected images to illustrate the unique properties of that waveband. The book begins with the infrared and ultraviolet wavebands, since the imaging technology—such as cameras, film, and filters—is familiar at these wavelengths near to our own visual range. Moving further out into the spectrum, subsequent chapters present images produced by the more exotic technologies needed to image **thermal infrared**, microwave, and radio wavebands; yet we will still be in the range of light that is emitted by objects (such as people, animals and machines) at terrestrial temperatures. Then comes the highest-energy, shortest-wavelength region of the spectrum, where light is either man made—such as that produced by an x-ray tube or radar transmitter—or produced in the extreme conditions found in celestial objects e.g., the Sun or in nuclear explosions. Some of the imaging devices used at the extreme ends of the electromagnetic spectrum look nothing like a visible-light camera, but they produce images that can be visually interpreted. The book also includes images produced by sound waves for those cases where imaging with light waves is impossible, such as with a ship sunk at the bottom of the ocean. The final chapter studies a scene or object as seen through various wavelengths of light, tuning that imaginary knob on our head to adjust the wavelength of the light we see. But first, on to the edges of the rainbow: the infrared and the ultraviolet wavebands of the electromagnetic spectrum.

Chapter 1

Infrared and Ultraviolet: The Edges of the Rainbow

The **near-infrared (near-IR)** and **near-ultraviolet (near-UV) wavebands** flank the visible spectrum of light. Their relationship to the visible waveband is shown in Fig. 1.1, along with the **short wave infrared (SWIR)** waveband, described shortly. The chemistry of our eyes bounds our color vision; near-IR photons do not have enough energy to stimulate our eyes, and the lenses of our eyes block near-UV light. Though we cannot see these “colors” of light, they are close cousins to the ones we can see. The optical properties of glass and photographic film in the near-IR and near-UV wavebands are similar enough to their properties in the visible waveband that scientists have been able to image in the near-IR and near-UV wavebands using special filters and films for over a century. These modified camera systems reveal a surprising view of familiar objects and materials. The changed appearance of the familiar or the revelation of things unseen is the essence of “alien vision” (i.e., the imaging of the world in wavebands of light that human eyes cannot see). Alien vision suggests extraterrestrial beings that see with invisible light, yet there are familiar creatures around that see light that we cannot; for instance, butterflies, birds, and honeybees are sensitive to near-UV light. Ultraviolet vision is quite common in the animal kingdom, particularly among invertebrates. In fact, there are many examples of markings and patterns on animals and plants that appear to act as signals or cues to animals with near-UV vision. These markings were unknown until the advent of ultraviolet imaging technology in the early part of the 20th century.

Light in both the near-IR and the near-UV wavebands is easy to generate with a prism: let a narrow shaft of sunlight enter a darkened room, place a glass prism on a table so as to intersect the shaft of light, and place a white screen behind the prism. The prism bends the light rays according to their color, with red bent the least and violet bent the most. This wavelength-dependent **refraction** is a property of the glass known as **dispersion**. The white beam of light becomes a rainbow projected onto the screen, with the familiar colors arranged in order of increasing frequency and decreasing wavelength: red, orange, yellow, green, blue and violet, as shown in Fig. 1.2. As we move along the pattern, we pass through orange, then red, and then the red becomes a deeper shade of red, like the color of dying embers in a fire. Finally, the red light appears to fade out completely; we have reached the near-IR

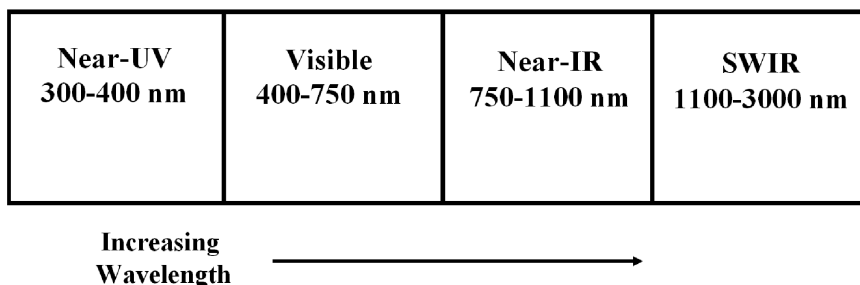


Figure 1.1 The near-UV, visible, near-IR, and SWIR wavebands.

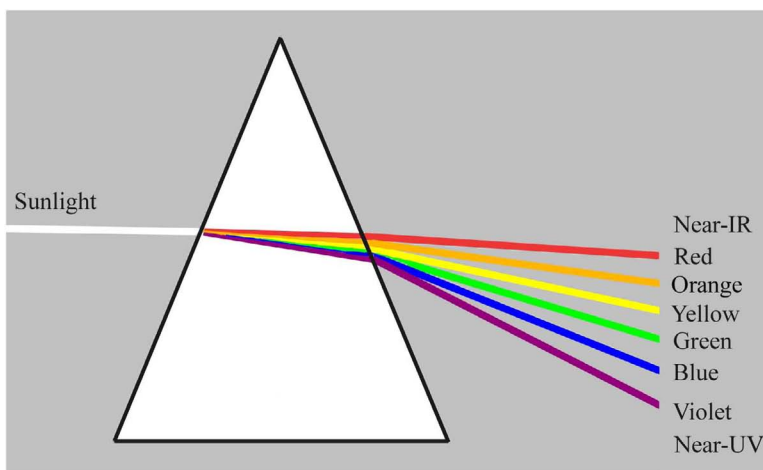


Figure 1.2 Sunlight split into some of its components by a prism.

region of the spectrum. Our eyes are unable to perceive this light, although we can feel its heat if the source is bright enough.

We cannot see near-IR light because near-IR photons do not have enough energy to trigger the chemical reactions in the eye that lead to the visual perception of light. This characteristic of near-IR light underscores an important fact about light: the longer the wavelength, the lower the energy of its photons. In fact, we cannot see any light with wavelengths longer than red—that is, a wavelength of about 750 nm—nor can any animal discovered so far. This is because all known animal visual systems are based on the same light-sensitive chemical, known as **rhodopsin**. The chemical reactions necessary to produce a signal in the retina have a threshold energy that is higher than the energy imparted by light with wavelengths longer than 750 nm. We can otherwise detect near-IR light as the molecules in our skin readily absorb it, producing the warm sensation we feel when we bask in sunlight.

The near-IR waveband was the first portion of the electromagnetic spectrum outside the visible waveband to be discovered, by astronomer Sir William Herschel (1738–1822) in 1800. He devised an apparatus with a prism and three blackened thermometers, and measured the transfer of heat from various color components of

sunlight refracted through the prism to the thermometers, which had been placed in the path of the refracted rays of sunlight (the blackening of the thermometers increases the absorption of energy from the incident light). The thermometers registered a temperature change even when placed in the dark region just beyond the red part of the rainbow pattern. Herschel concluded that there were invisible light rays heating the thermometers, and he wrote about this discovery in a paper for the *Philosophical Transactions of the Royal Society*:

“It being now evident that there was a refraction of rays coming from the sun, which, though not fit for vision, were yet highly invested with a power of occasioning heat...”¹

Figure 1.3 shows the best illustration of the apparatus from this seminal paper.

Sir Isaac Newton had discovered in the 17th century that a ray of sunlight could be dissociated into the familiar colors of the rainbow with a prism. Herschel expanded on Newton’s research by postulating the existence of an additional prismatic component of light that was invisible, which he named the “thermometrical spectrum” (the term “infrared” was coined later). He postulated that the “construction of the organs of sight” allowed for the entry of visible light, and that light in the thermometrical spectrum was stopped in the “coats and humours of the eye,” which accounted for our inability to see it. The idea of invisible light was met with a great deal of resistance in the scientific community, but Herschel was eventually proved right—invisible light did exist.

Sir William’s son, Sir John Herschel, continued his father’s experiments with infrared light and published a paper in 1840 that described an apparatus he used for recording infrared images of the solar spectrum—the first invisible-light imaging technology. The apparatus consisted of a prism that imaged sunlight onto very thin black paper soaked in an alcohol/colored dye solution he called “rectified spirit of wine.”² The lightwaves absorbed onto the paper produced different rates of evaporation of the dye solution, which resulted in varying film thickness with attendant colors (like the colors of a thin film of oil in a puddle). This technique was refined in the 1930s by Marianus Czerny (1896–1985), who invented the “Evaporograph”—an infrared imaging system that used a thin film of volatile oil applied to a thin absorbing membrane. Practical infrared imaging did not really start until the invention of infrared-sensitive photographic film based on the light-sensitive dye kryptocyanine in the 1930s.

Returning to the sunbeam and prism experiment, consider the other edge of the rainbow pattern projected onto the white screen. When human eyes look at the screen just beyond the deepest violet light, they no longer perceive any light at all. Therein lies the near-ultraviolet (near-UV) region of the spectrum, which begins

¹W. Herschel, “Experiments on the refrangibility of the invisible rays of the Sun,” *Phil. Tran. Roy. Soc.* **90**, 284–347 (1800).

²J.F.W. Herschel, “On the chemical action of the rays of the solar spectrum on preparations of silver and other substances, both metallic and non-metallic, and on some photographic processes,” *Phil. Trans. Roy. Soc.* **130**, 1–59 (1840).

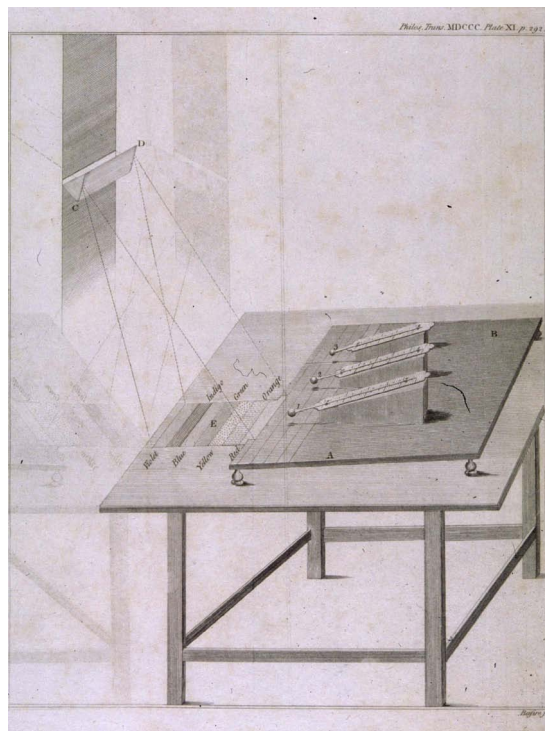


Figure 1.3 Plate from W. Herschel's infrared paper (1800).

where our eyes' sensitivity leaves off, at a wavelength of about 400 nm. Sir William Herschel also examined this part of the spectrum with his prism-and-thermometer apparatus but found no perceptible temperature increase when his thermometer was placed in the dark space next to the violet band of light. This led him to conclude that there were no rays beyond violet:

“By these last experiments I am sufficiently convinced that no rays, which exist outside the violet, can have any provable force, neither in the forms of light, nor of heat, and that these two forces prolong along the prismatic spectrum, and ends there where the farthest violets disappear.”³

Johann Wilhelm Ritter (1776–1810), a contemporary of Herschel, discovered near-UV light in 1801. Ritter used a similar prism and screen apparatus to create a rainbow pattern. But instead of a thermometer, he used silver chloride crystals as a detector. The crystals darkened more rapidly when exposed to the near-UV light from the prism than they did when exposed to visible colors of light. Herschel's thermometer was not sufficiently sensitive to detect near-UV light, which led to his

³W. Herschel, “Experiments on the refrangibility of the invisible rays of the Sun,” *Phil. Tran. Roy. Soc.* **90**, 284–347 (1800).

incorrect conclusion that light beyond violet did not exist. Not only does near-UV light exist, but many animals can see it. The human retina is somewhat sensitive to near-UV light, but we cannot see it because the crystalline lens of our eye absorbs light below 400 nm. This is believed to be an evolutionary solution to the problem of chromatic aberration, a wavelength-dependent focusing of light by a lens that becomes more apparent at shorter wavelengths.⁴ Some people are missing the lens of their eye, either through accident, disease, or a birth defect. This condition is known as aphakia, and these people can see into the near-UV, although the thick eyeglasses needed to focus light on their retinas absorb ultraviolet fairly well. Some experiments have been carried out on subjects with aphakia using quartz lenses that have a higher transmission in the UV than conventional glass lenses. These subjects could read an optometrist's wall chart with 365-nm light alone, something most people cannot do.⁵ People can indirectly detect intense sources of ultraviolet light as a bluish haze caused by fluorescence within the eye, but this is not the same as ultraviolet vision, since the blue light that is perceived is visible light, not ultraviolet.

We can make images using light in the near-IR and near-UV wavebands using standard cameras, film and filters. The near-IR waveband encompasses the region of the electromagnetic spectrum between 750 nm and 1100 nm. The cutoff at 1100 nm is the wavelength at which silicon detectors become insensitive. At these wavelengths, glass is still transparent, which enables us to take photographs with ordinary camera optics and special film designed to respond to near-IR light (like the human eye, regular photographic film is insensitive to infrared light and has little sensitivity to red light, which is why many darkroom safelights are a deep red). If a filter that allows infrared light to pass but blocks out visible light is placed over the lens, the resulting picture is a true near-IR image.

Figure 1.4 shows a block diagram of this camera system, which can be used for near-UV imaging as well. These images can often reveal interesting features that the eye cannot detect; for example, many different materials that appear to have the same hue and intensity as each other when imaged in visible light appear very different from each other in the near-IR.

As is the case with infrared light, ultraviolet light interacts differently with materials than does visible light, and looking at the world with ultraviolet vision can allow us to sometimes see things that are invisible to the unaided human eye. How can we see the world in near-ultraviolet light without removing our eye lenses, which is an unpleasant prospect? As with near-IR light, ordinary film and camera optics will function with near-UV light. A regular camera still functions in the region of the spectrum from a wavelength of 400 nm (where human visual sensitivity cuts off) down to about 300 nm, where ordinary glass lenses become opaque.⁶ Unlike infrared pictures, which require special film, near-UV pictures

⁴T. Goldsmith, "Hummingbirds see near ultraviolet light," *Science* **207**, 786–788 (1980).

⁵The 365-nm light comes from a mercury vapor lamp known as a Wood's Lamp. This experiment was carried out in 1956. Kennedy, D. & Milkman, *R.D. Biol. Bull.* **111**, 375 (1956).

⁶The antireflection coatings on quality lenses are optimized for visible light, and thus are not ideal for UV photography.

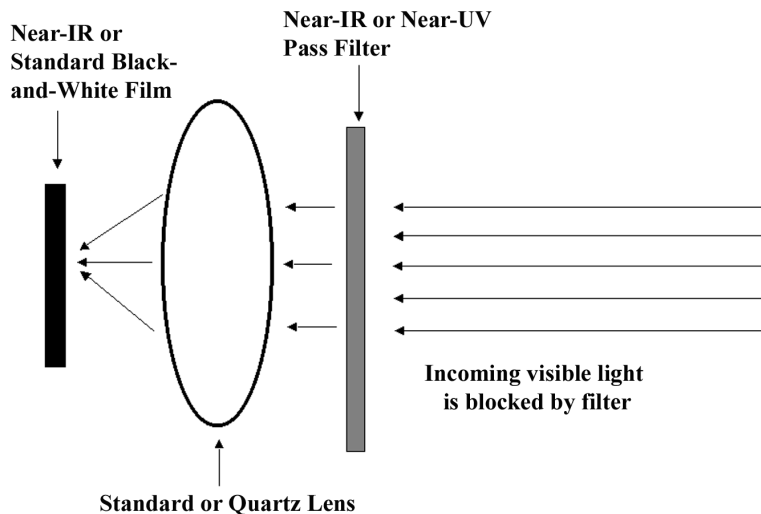


Figure 1.4 Block diagram of near-IR and near-UV photographic apparatus.

can be taken with conventional film. Regular Kodak Panchromatic Tri-X film (as well as many other black-and-white films) are sensitive down to approximately 300 nm in wavelength, and when combined with a filter that passes near-UV light only, they enable us to take near-UV photographs that are sometimes quite different from visible-light images. The photographic apparatus is the same as that used for near-IR imaging, as shown in Fig. 1.4. Professor Robert Wood described the first near-UV transmitting filter. The filter blocked out visible light and enabled him to capture the first near-UV images in the 1910s using standard black-and-white film.⁷ One of the earliest known UV images is shown in Fig. 1.5.

If we wish to extend the sensitivity of our photographic apparatus to wavelengths shorter than 300 nm, we must use special quartz lenses or else a pinhole camera, which quite literally uses a tiny pinhole instead of a lens. Some types of regular black-and-white film will still work down to around 250 nm, but special films become necessary at wavelengths below 200 nm, as regular gelatin photographic emulsions become very absorbent below that point. The near-UV images presented in this chapter were all taken with various filters made of special filter glasses. These filter glasses transmit UV light in various bands but then cut off sharply in the visible spectrum. There are also a variety of electronic imaging cameras that are sensitive to near-UV light, such as **silicon-intensified target (SIT)** and **back-thinned CCD** cameras. In 1969, Professor Thomas Eisner and his colleagues used a near-UV-sensitive video camera to mimic insect vision.⁸ Visible-light electronic sensors can be coated with fluorescent materials that shift the wavelength of the ultraviolet light into the longer visible-light wavelengths that the array can detect.

⁷A.R. Williams, G. Williams, *Jour. Biol. Phot.* **61**, 115–132 (1993).

⁸T. Eisner et al., *Science* **166**, 1172–1174 (1969).



Figure 1.5 Robert Wood in the UV band.

Near-Infrared Imaging

The near-infrared band is usually defined as 750 nm to 1100 nm, 750 nm being the edge of normal human vision and 1100 nm being the cutoff wavelength for silicon detectors. This is the first infrared band where photographs were taken, and the first band of invisible light to be used in electronic imaging.

Night Vision and Surveillance with Near-IR Imaging

The ability to see in the dark without being detected must be one of mankind's oldest wishes. Early human beings equipped with modern night-vision devices would have been able to see if a predator was lurking outside in the darkness without the predator knowing it was being watched. Night vision is crucial to modern warfare, and military forces of the world have committed extensive resources to the problem of target identification in various lighting and weather conditions. The need for covert night vision led to the development of infrared viewing systems such as the **sniperscope**, which enabled Allied soldiers in WWII to see in the darkness with covert light sources invisible to unaided eyes. The imaging system was mounted on the M1 carbine rifle, and gave the shooter about a 70-yard range to accurately hit enemy soldiers in total darkness.

Figure 1.6 illustrates a typical sniperscope design used during the Korean War. These devices employed an **imaging tube** similar to a television-camera tube but sensitive to near-IR light. The soldiers would illuminate the target with searchlights equipped with special filters that blocked all visible light but passed near-IR light. This system has the distinct disadvantage that an enemy equipped with a similar

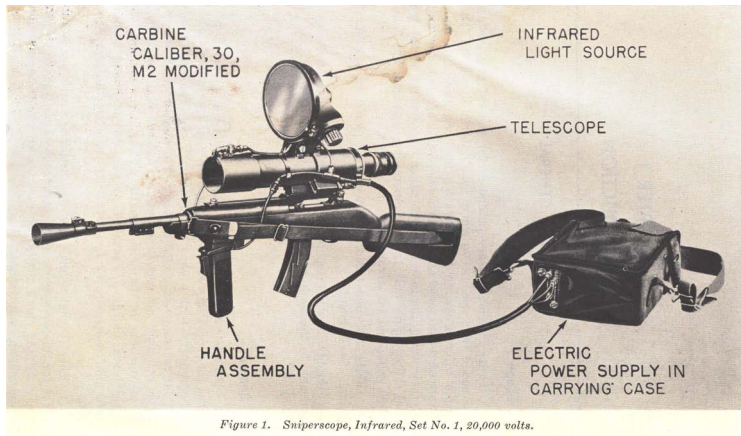


Figure 1. Sniperscope, Infrared, Set No. 1, 20,000 volts.

Figure 1.6 M3 sniperscope, Korean War era.

IR viewer can see the searchlight and shoot at it. These systems were first fielded on Okinawa during WWII and were very effective.

Near-infrared lights were also used for signaling between Navy ships. The X-12 train light is an example of this technology. It consists of an incandescent lamp with multiple redundant filaments, surrounded by a cylindrical black glass filter that passes near-infrared light only. These lights were hung on various parts of the ship and kept on continuously at night. Friendly ships equipped with near-IR viewers could see the train lights. These viewers used image converter tubes that respond to near-IR light. Figure 1.7 shows a C-3 viewer which is equipped with a long focal length reflective optic. The author is holding one that still works!

Subsequent developments in night-vision technology that have occurred over the last 50 years have resulted in systems that are much smaller, lighter, and more sensitive than the early image tubes. These devices can be worn on the head in a goggle configuration (as shown in Fig. 1.8) or mounted on small arms to enable a person to see fairly well in extremely low light levels (almost as low as overcast



Figure 1.7 The author with a working WWII-era C-3 near-IR imager.



Figure 1.8 Night-vision goggles with head mount.

starlight) by amplifying existing light, thus eliminating the need for an infrared searchlight. These devices are known as image intensifiers, and they image with visible as well as near-IR light out to a wavelength of about 900 nm. This extended spectral sensitivity adds to the overall brightness of the scene due to the presence of near-IR **night glow**, and allows for the use of covert signaling devices used primarily in law enforcement applications. For example, there are commercially available miniature infrared beacons that can be attached to the roof of a vehicle and then tracked from the air by law enforcement with night-vision devices.

It is interesting to look at a person in total darkness with a near-IR viewer and a purely near-infrared light source. Human skin reflects equally well no matter what the skin color, so that dark-skinned people appear the same color as light-skinned people. Eye pupils dilate completely, giving them a glowing-eye appearance, due to the human retina's high reflectivity in the near-IR and red regions of the spectrum. This reflectivity is the reason why flash photographs often show the subject's eyes glowing with a dull red color. The subject's pupils opened to admit more light into the eye, enabling better vision in the low-light situation that required the use of the flash in the first place. Some cameras with built-in flash units attempt to prevent this "red-eye" effect by emitting a series of flashes right before the picture is taken, which causes the subject's pupils to close, eliminating or reducing the retinal reflection. Figure 1.9 shows a near-IR image of the author with dark-adapted eyes taken with a silicon CCD camera. Illumination was provided by a light-emitting diode source that emits IR light at wavelengths around 850 nm. This light is totally invisible to the human eye, so my pupils were fully dilated.

Near-IR imaging in aerial surveillance has had a long and interesting history. For example, during World War II, a great deal of effort was made to conceal strategic targets from enemy bombers and observation planes. Often, factories and other stationary objects were concealed with painted cloth, netting, and artificial trees to make them difficult for enemy aircraft to detect. It was realized that this camouflage looks different when imaged with near-IR light, and research at



Figure 1.9 Near-IR image showing dark-adapted eyes. (*Courtesy of Dannen Harris*)

Eastman Kodak, Inc. led to the invention of high-speed infrared film. The first commercial infrared film based on kryptocyanine had low sensitivity and was therefore unsuitable for military applications. Kodak's high-speed film made it possible to detect camouflage with aerial reconnaissance. Figure 1.10 shows three views of a factory, reproduced from a Kodak advertisement from 1943. The top image shows a standard aerial picture of a factory, a high-value target that can be very easily spotted from the air.

The middle image shows a conventional visible-light photograph of the factory covered with camouflage (netting, green cloth, artificial trees). The factory is quite well concealed, at least from reconnaissance aircraft forced to fly at high altitudes to avoid anti-aircraft artillery. The bottom image is a picture of the camouflaged factory made with Kodak Aero Infrared film, a film that is sensitive in both the visible and the near-IR wavebands out to about 900 nm.

Unlike real vegetation, which is highly reflective in the infrared, the artificial vegetation appears black in the infrared image, since the green cloth and netting material does not reflect infrared well. Notice that the real grass and vegetation in the near-IR image appears snow-white; this is healthy vegetation, which has a very high reflectivity to near-IR light due to the presence of the molecules chlorophyll and xanthophyll. Diseased, dehydrated, or otherwise stressed vegetation shows a marked decrease in near-IR reflectivity, and agriculturists exploit this property of vegetation in remote sensing applications, as shown in the next example of near-IR imaging.

Leaves and grass are highly reflective in the near-IR band, and infrared photography is often used to evaluate the extent of urban development, since it enhances the visual contrast between “green space” and built-up areas. Figure 1.11 is a LANDSAT image of the San Francisco peninsula in California, which has a different color representation than that of our eyes due to the varying levels of IR reflectance. This is known as **pseudocolor** or **false color**, and we will encounter it repeatedly in this book as a means of visually representing invisible wavebands

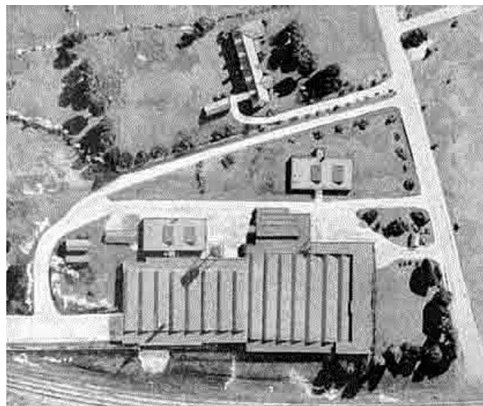


Figure 1.10 Three views of a factory: visible, no camouflage (top); visible, camouflage (middle); near-IR, camouflage (bottom). (*Courtesy of Eastman Kodak, Inc.*)

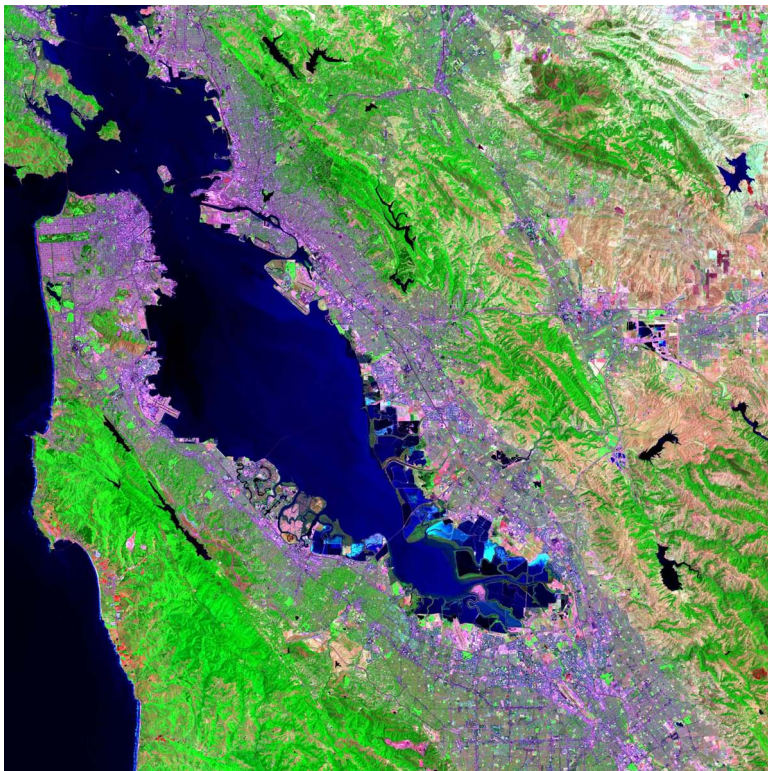


Figure 1.11 False color key to LANDSAT image of San Francisco Peninsula (red: high reflectance at blue wavelengths; green: high reflectance at near-infrared wavelengths; blue: high reflectance in visible wavelengths). Built-up areas appear purple or gray, white areas are high albedo objects, vegetation appears green because of its high near-IR reflectance, and clear water appears black.

of light using different colors. The Marin Headlands in the upper left corner are heavily vegetated, as are the East Bay hills to the right and the mountains in the lower right corner. Urban areas show up as light gray, indicating that they have a lower near-infrared reflectance. Buildings, streets, and parking lots absorb much more near-infrared light, raising the summer temperature in some cities by as much as 5 to 10 degrees centigrade over that of nearby heavily vegetated areas (the so-called “heat island” effect).

Exploiting the Deep Penetration of NIR and SWIR Light

Infrared light often is reflected off surfaces differently from visible light, which is the principle behind the detection of the camouflaged factory in Fig. 1.10. Infrared light is also absorbed and transmitted differently than visible light, and this property can be used to see through layers of material that absorb visible light but transmit infrared.

The absorption or transmission of infrared light in a particular molecular material (e.g. wood, paper, ink, leaves, glass) is determined by the presence or

absence of infrared **excitation modes** in the electromagnetic structure of the material.⁹ These excitation modes manifest themselves as a strong response of the electrons in the material to light of a particular frequency (or equivalently, wavelength). As I discussed in the introduction, electrons move in response to the electric field of the lightwave. If the electrons are constrained (bound to a molecule, for example), then they respond strongly to lightwaves with a particular frequency. For example, water molecules have a strong **absorption band** at a 1450-nm wavelength—light at this wavelength tends to be highly absorbed. This light causes an excitation of the bond between hydrogen and oxygen atoms in a water molecule. The excitation is akin to a rapid stretching and contracting of this bond, which is called a stretch mode. Water is only weakly absorbent in the visible waveband, especially to blue light. We can visualize the infrared absorption of water with SWIR imaging technology. Figure 1.12 show a glass of water viewed in both visible light and SWIR light in the 900–1680-nm waveband.

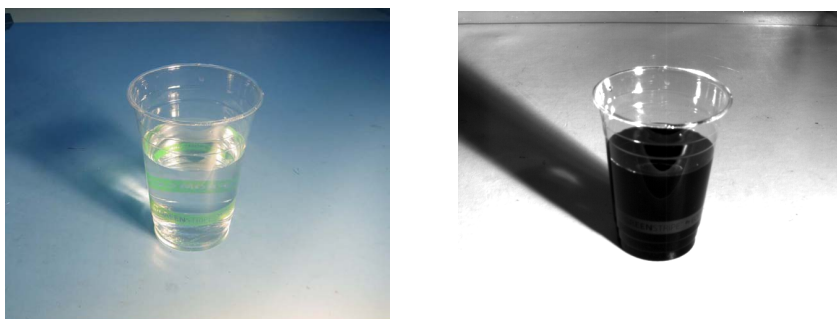


Figure 1.12 Visible (left) and SWIR (right) images of water in a plastic cup. (Courtesy of FLIR)

The water looks like strong coffee because near-IR and SWIR light is strongly absorbed by liquid water, owing to the presence of molecular absorption bands in water at various wavelengths, including 760, 970, 1190, and 1450 nm. The infrared image of the glass of water shows that the light within the camera's spectral sensitivity (900–1680 nm) is highly absorbed and thus would not be useful for imaging underwater. The absorption of near-IR light in liquid water continues into the visible waveband on the red end (as well as into longer-wavelength IR wavebands). Going deeper underwater, red light is absorbed first, which makes water look blue at depths beyond several meters.

Criminologists often use near-infrared imaging techniques to examine documents for possible alterations. Figure 1.13 shows a series of images of a

⁹Metals are highly reflective to light over an enormous range of wavelengths. The electrons in metal are only weakly bound to individual atoms, and thus do not exhibit the same response to light as electrons bound to individual atoms or molecules. The theory of reflectivity of metallic and nonmetallic materials is beyond the scope of this book. It is explained very well in the book *Optics* by E. Hecht (Addison-Wesley, 1998).

document that has had typescript defaced by ballpoint pen ink and correcting fluid (“whiteout”). The first IR image was taken with a silicon CCD sensor with a black glass near-IR pass filter—the waveband is 830 to 1100 nm. The second IR image was taken with an electronic camera with an **indium gallium arsenide** sensor (InGaAs for short) that is filtered to image in the 1500–1700-nm waveband. This is part of the SWIR waveband, because the spectral region from 1100 nm to 3000 nm is designated as the SWIR (short-wave infrared) band.

It is very interesting to look at this same piece of paper in the UV bands as well. There the ink and whiteout are highly opaque, especially in the shortwave UV band, as shown in Fig. 1.14. The near-UV image is 365 nm, and the shortwave UV image is 254 nm. The whiteout is anything but white in the UV band. UV imaging is a very effective way to examine a questioned document.

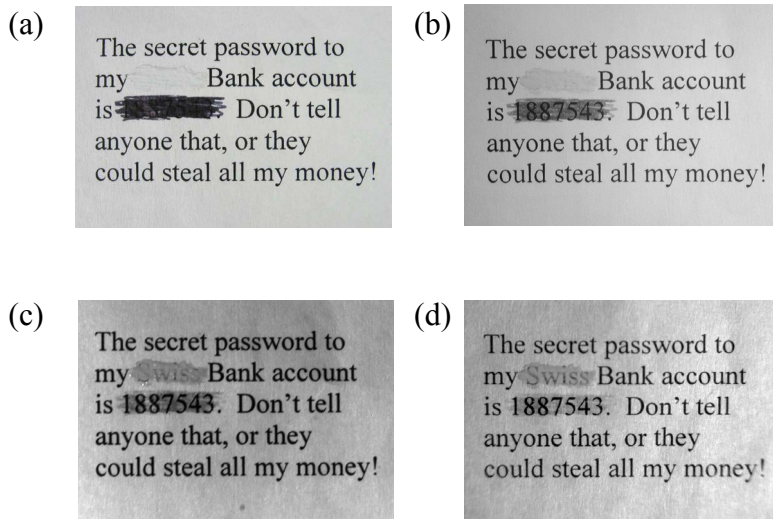


Figure 1.13 (a) Visible: 400–750 nm; (b) NIR: 830–1100 nm; (c) SWIR: 1400–1700nm; (d) SWIR: 2000–2500um. (Courtesy of FLIR)

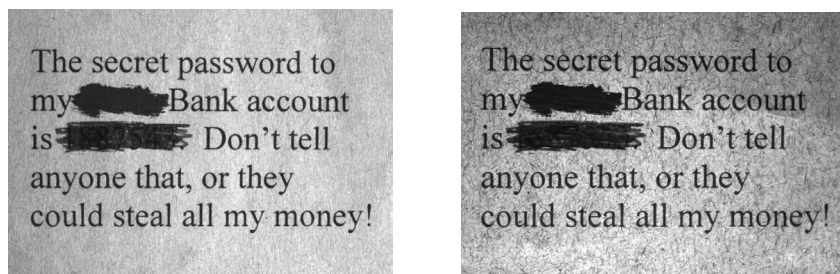


Figure 1.14 Near UV: 365 nm (left) and shortwave UV: 254 nm (right) images of an altered document.

Near-IR light can penetrate through thin paper as well. Figure 1.15 shows four images of a paper label on cardboard in four different wavebands. Note that the penetration improves as the wavelength of light gets longer. There is less scattering of the light rays off the fibers in the paper label.

As with the whiteout and ink in the preceding altered document example, the paper label becomes increasingly opaque in the UV band, as shown in Fig. 1.16. The near-UV image is 365 nm and the shortwave UV image is 254 nm. The shortwave UV image shows some staining on the paper under the numeral 3.

Forensics photographers use various invisible-light wavebands to uncover evidence at crime scenes or on crime victims. Sometimes the evidence is difficult or impossible to see with the naked eye, and sometimes the invisible-light band reveals information that is not otherwise apparent. Figure 1.17 shows a visible-light image of a polo-style shirt with a bullet hole in it.

What is not apparent in this VIS image is the ring of gunshot residue around the hole, indicating the bullet's entry point. In many cases where a person has been shot



Figure 1.15 Four views of a paper label on a cardboard box: (a) visible: 400–750 nm; (b) NIR: 830–1100 nm; (c) SWIR: 1400–1700 nm; (d) SWIR: 2000–2500 nm. (*Courtesy of FLIR*)



Figure 1.16 Two views of a torn paper label with printing underneath: left—365 nm; right—254 nm.

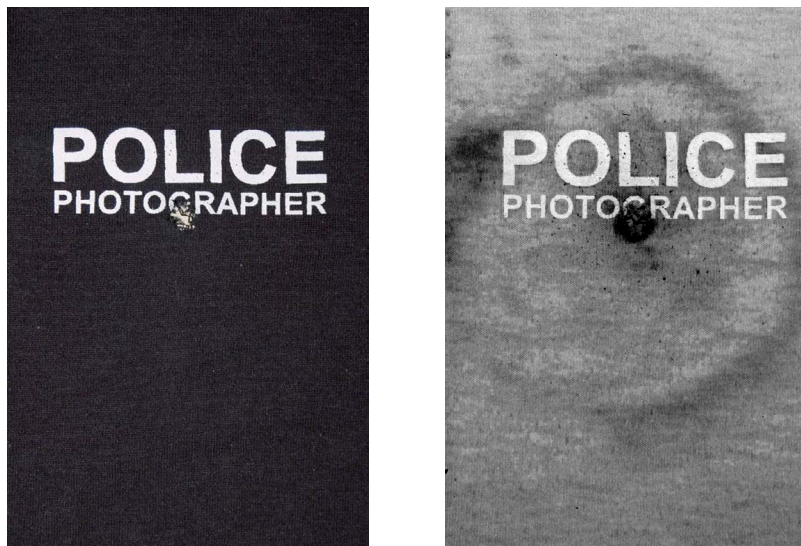


Figure 1.17 VIS and NIR images of a cotton shirt showing a GSR pattern. (*Courtesy of Heidi Nichols, Miami-Dade County Medical Examiner's Office*)

at close range, there is a distinctive pattern of gunshot residue (GSR). This material can be a mixture of burned and unburned smokeless powder, and burnt primer. GSR patterns can be used to match a particular firearm to a victim's article of clothing. The NIR image (780–1100 nm) shows the ring of GSR because the dark-colored cotton shirt is much more reflective in the NIR band—the dye pigment is essentially transparent, and we see a reflection off the cotton itself. Measurements of the GSR ring's diameter on the shirt compared to lab measurements made with a gun found at the crime scene can suggest a value for the distance between the shooter and the victim, with a smaller diameter indicating a closer range.

This phenomenon is very useful in forensics investigation: distracting patterns or colors disappear or are greatly reduced in contrast when imaged in the near-IR band. Figure 1.18 shows a tombstone in a Quaker cemetery on Nantucket Island, Massachusetts, in the VIS and NIR bands. The lichens and discoloration make it very hard to read the inscription by eye. The near-IR image makes it possible to more easily read the name of the deceased: Sarah Hamblin. Of course, a much better way to read all the text is a gravestone rubbing made with a charcoal pencil and a sheet of paper held against the surface. Rubbing is not always allowed though, especially on softer marble headstones.

The elimination or reduction of color in an image can be also used for industrial inspection purposes. Figure 1.19 shows two views of a very loud shirt worn by the author. The buttons are hard to see in the VIS image, but they stand out very clearly in the NIR image.



Figure 1.18 Early 19th century headstone with staining and lichen growth: left—VIS; right—780–1100 nm.



Figure 1.19 The author in a loud and admittedly tacky shirt made of rayon: left —VIS; right—NIR (780–1100 nm).

Art Conservation

Art conservationists, like criminologists, are concerned about authentication and identification. They use near-IR imaging to image through visibly opaque but infrared-transparent materials, like the age-darkened varnish on some old paintings. Figure 1.20 shows three views of a painting by Otto Marseus entitled *Natura*, which is displayed in the Galleria Palatina in Florence. The full painting is shown in the top image, with the red box in the lower left corner corresponding

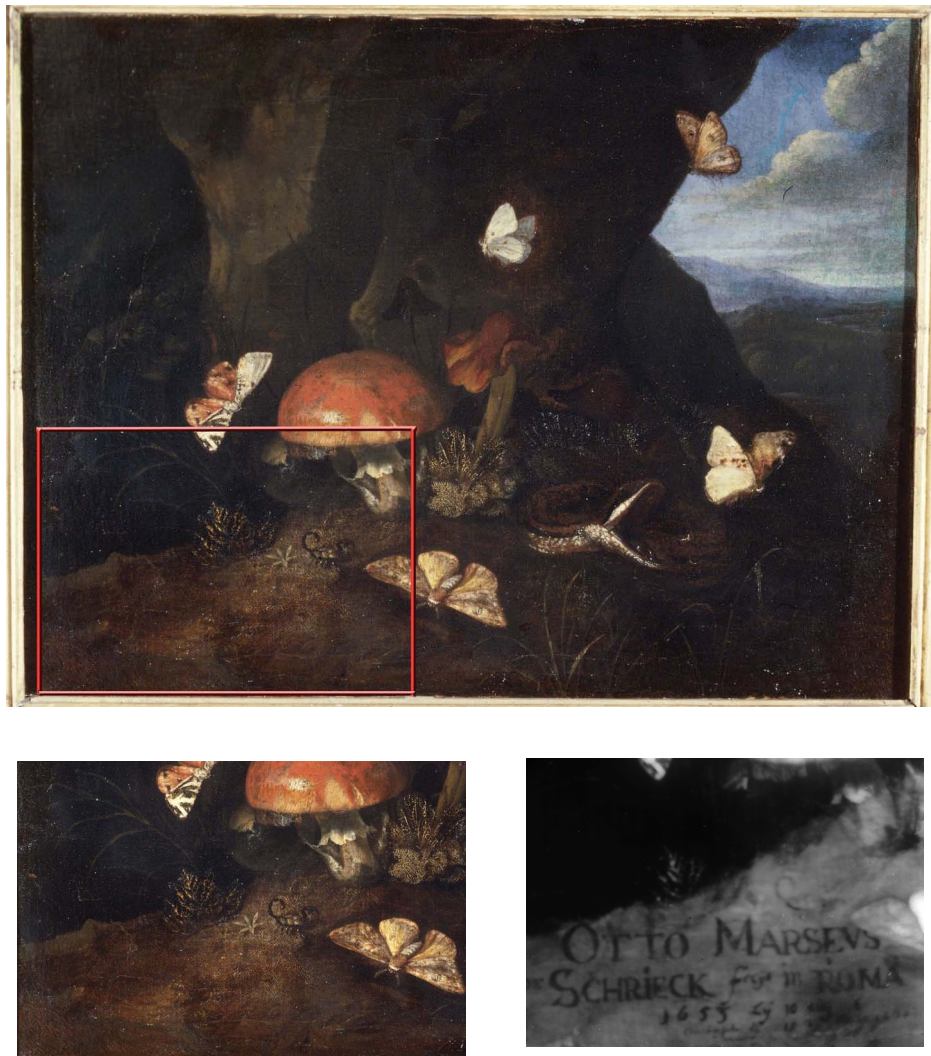


Figure 1.20 Visible image of *Natura* and two details in visible and near-IR light. (Courtesy of Editech)

to the details shown in the two bottom images. The dark varnish obscures the signature of the artist as seen in visible light, but the near-IR image reveals the artist's name and the date of the painting.

Certain paints, like aged varnish, are transparent to infrared light and opaque to visible light. Figure 1.21 shows three views (visible, NIR and SWIR) of a special test panel painted with a variety of colors of oil-based pigment. All of the pigments shown are quite opaque to visible light. The test panel has various drawing media such as charcoal and pencil drawn across it underneath the pigment stripes. Note that as the wavelength increases, the paint stripes become more and more transparent. This property of infrared light helps art conservators authenticate paintings by revealing the underdrawing without disturbing the paint layers.

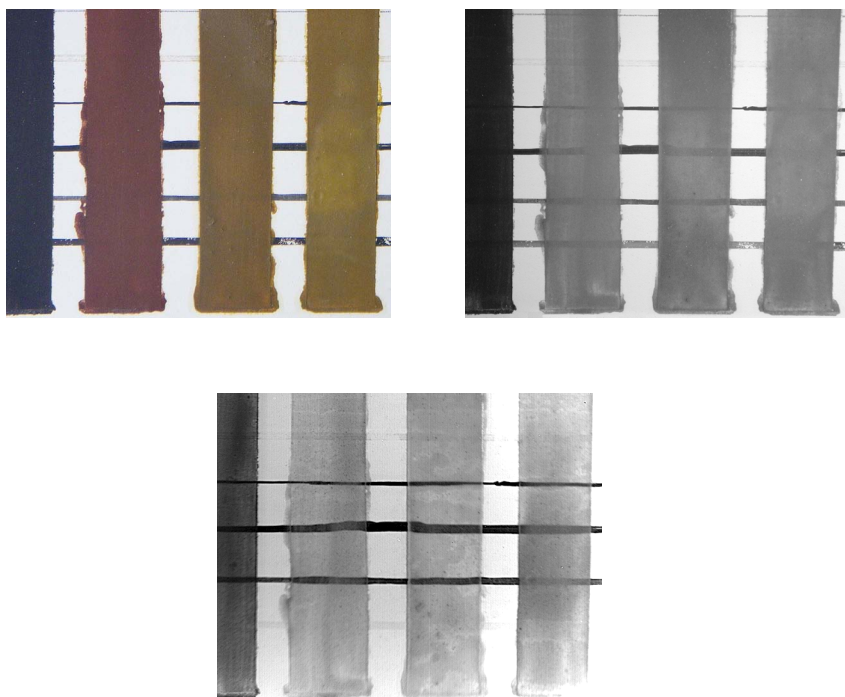


Figure 1.21 Visible (400–750 nm), NIR (830–1100 nm), and SWIR (1400–1700 nm) images of a test panel with oil paint swatches and underdrawing media. Paint swatches from left to right: burnt umber, burnt sienna, raw sienna, and ochre. Underdrawing media from top to bottom: silver, ivory black, lamp black, vine black, charcoal in gum arabic. (*Courtesy of FLIR and LACMA*).

The Dutch artist Salomon van Ruysdael drew an interesting underdrawing on one of his paintings that is almost a scribble and very different in nature to the end product. Figure 1.22 shows a painting of his called *Landscape with Deer Hunters* imaged in both color visible and SWIR light, with the details from the lower left of the painting. Ruysdael drew loops (probably with a lead pencil) to suggest foliage around the tree, and zigzag lines to delineate the landscape. We know that Ruysdael used underdrawing in his early works—other landscape paintings from this period (1630s) show similar underdrawing beneath the paint, but he stopped using the technique later in his career. The figures are all drawn without the use of underdrawing.

Subsurface analysis is especially valuable in the antiques market, which contends with many forms of deception. Many pieces of antique furniture are sold as being unrestored, when in fact they have sometimes been quite extensively modified. A very common example of this involves repairs to wood veneers. Veneers were attached to a substrate of heavier, stronger wood using animal glues. Over time this glue can weaken, creating loose pieces of veneer that can get torn off over the years. Figure 1.23 shows a piece of mahogany that has been veneered. A repair made to the veneer panel was done with wax filler and then cunningly

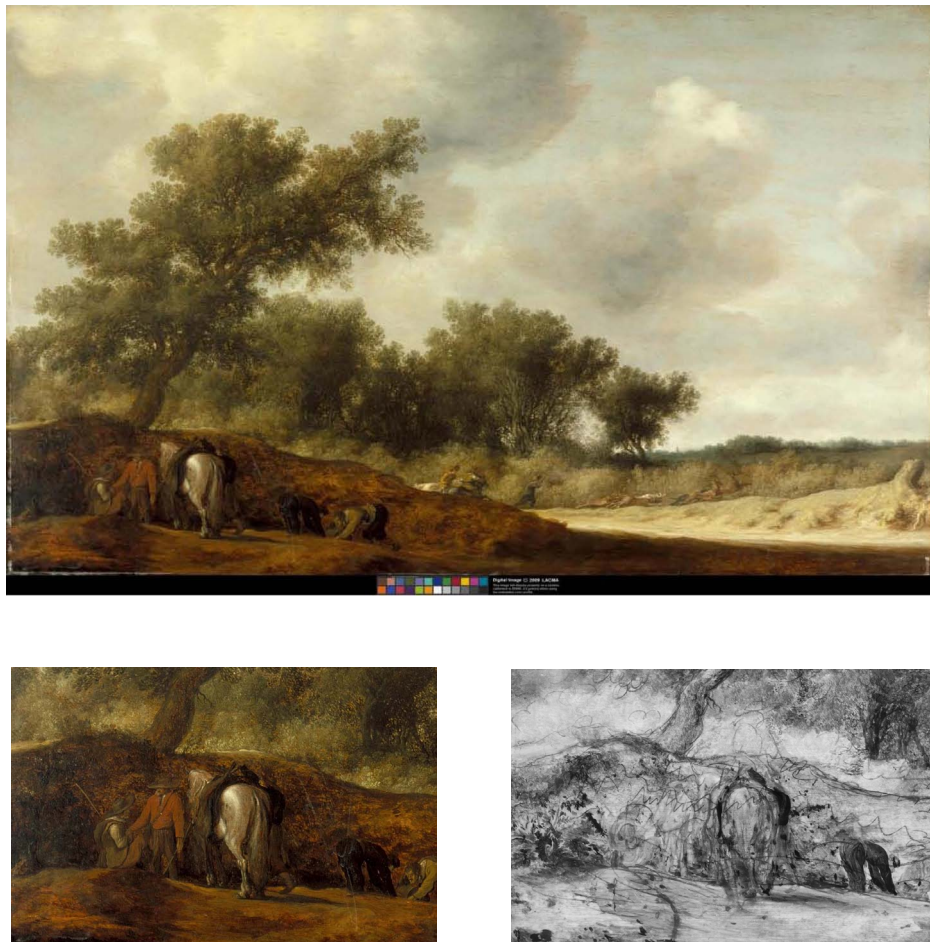


Figure 1.22 Ruysdael painting imaged in visible (400–750 nm) [top and bottom-left] and SWIR (1400–1700 nm) [bottom-right]. (*Images courtesy of Yosi Poseilov, Los Angeles County Museum of Art*)

painted to match the veneer. The paint is transparent to near-IR, showing the dark filler wax between the pieces of veneer.

Military Uses of SWIR Imaging

There are many uses for SWIR imaging in military applications, including visualization of laser designators, detecting camouflage, and range-gated imaging, which is a special technique for seeing through snow, rain and dust. One very interesting example of SWIR imaging is shown in Fig. 1.24: a test in February 2010 of the missile-destroying capability of the Airborne Laser (ABL) system, a specially modified Boeing 747 with a huge SWIR chemical laser weapon integrated into the entire rear of the plane. The beam, which has a wavelength of 1310 nm, emerges from an optical system on the “chin” of the plane.

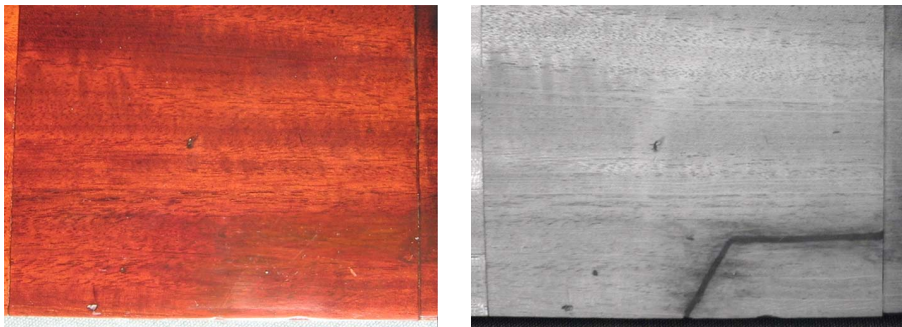


Figure 1.23 Mahogany veneer with well-done repair: left—VIS; right—780–1100 nm.

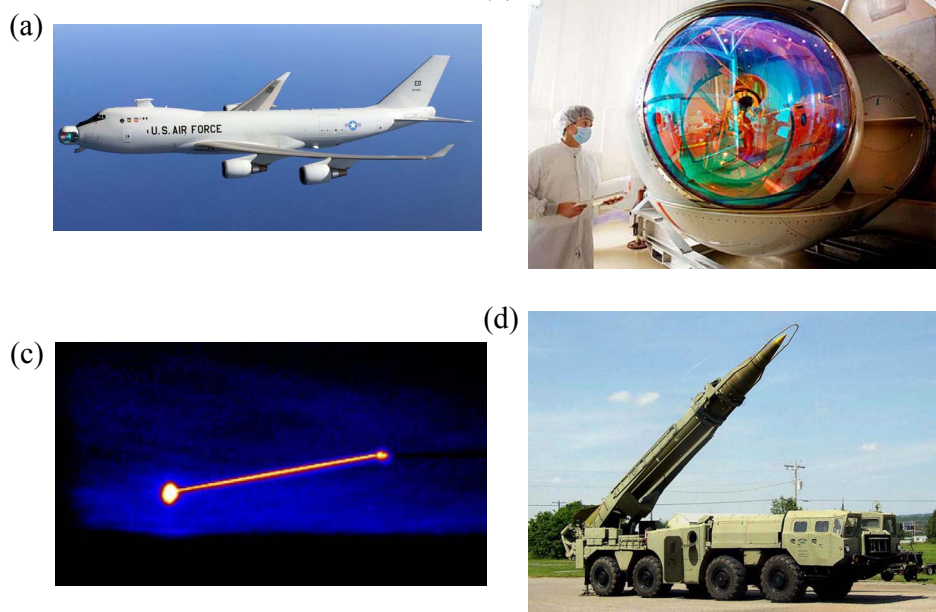


Figure 1.24 (a) Airborne Laser Test Bed in flight; (b) SWIR aiming and focusing optics on the nose of the ALTB; (c) SWIR image of ALTB firing at a Scud missile—the missile is on the left side of the image; (d) Scud missile mounted on a mobile launcher. Figures 1.24(a)–(c) courtesy of the Missile Defense Agency.

Figures 1.24a and 1.24b show the ABL plane and a close-up of the laser focusing optics. Figure 1.24c shows a frame from a SWIR video of the engagement. The target on the left of the image is a Scud missile (see Fig. 1.24d) that was destroyed several minutes after takeoff; the plane is on the right side with the laser beam making contact with both objects. Further details such as the engagement range and laser power have not been released publically.

The idea behind this system posits that the laser heats the surface of a missile in flight until structural failure occurs. The heat distorts the metal aerodynamic surfaces of the missile, making it unstable in flight and leading to its violent breakup.

Ultraviolet Imaging

The phenomena seen with ultraviolet imaging tend to be complimentary to phenomena seen with near-IR imaging. UV light has both higher-energy photons and shorter wavelengths relative to VIS and near-IR light. These two differences account for the very different appearance of many materials when imaged with UV, VIS and near-IR imaging systems.

The applications for UV imaging can be divided into three classes: imaging visibly transparent materials due to their UV opacity; imaging tiny structures or texture on surfaces that are not apparent to visible light; and imaging ultraviolet light sources that have little or no emission in other bands such as the visible or near-infrared. This section includes examples of each of these classes.

Consider photon energy and how it makes UV behave differently from IR. Relative to visible light, UV light tends to be either absorbed or reflected from the very top surface rather than penetrating into a given material, especially if the material is composed of organic molecules. This is in contrast to near-IR and SWIR light, which tends to penetrate into these same types of materials deeper than visible light and much deeper than UV light. The difference is the energy of the photons in these wavebands and the way they interact with materials. UV photons are more energetic than visible-light photons. They are therefore more likely to be absorbed by many materials, as the higher photon energies stimulate quantum-state transitions in both atoms and molecules that result in the UV photons being absorbed. Shortwave infrared light does not have the right photon energies to be absorbed in the same way—it takes more material to absorb it. Many materials composed of organic molecules are prone to absorb UV and transmit near-IR. Some inorganic materials like window glass will absorb UV and transmit VIS and near-IR. Still other inorganic materials like quartz have such tightly bound electrons in their structure that they transmit UV, VIS and near-IR light. Metals are in a class by themselves. They have very loosely bound electrons, so there is little penetration into their surface by UV, VIS or near-IR light, or indeed any wavelength of light shorter than x rays.

The shorter wavelength of UV light is apparent when one reflects it off of surfaces with imperfections on them. This phenomenon is important to optics manufacturers who are very concerned with the surface polish on glass lenses and other optical materials. Surface scratches and stains may not be readily apparent to visible-light inspection methods. The scratches show up because of the shorter wavelength, while the stains can show up because they are organic molecules that absorb UV photons. A nice example of scratches showing up appears in Fig. 1.25, which shows a CD jewel case in both the visible band and in the near-UV band. There are two reasons the images are different: the plastic is slightly more reflective in the near-UV band than in the visible band, so the surface is already a little easier to see, and the tiny scratches on the surface scatter the near-UV light waves. The scratches are too small to readily scatter visible light waves—the waves tend to “average out” the surface scratch, as though they are sampling a larger area of the surface on both sides of the scratch. One sees this when working with infrared



Figure 1.25 CD jewel case with scratches: left—visible; right—near-UV.

optics—the surface finish tolerances are much looser than with visible light lenses because they can be. For example, a sanded piece of metal that is a very diffuse reflector of visible light can look like an almost perfect mirror to a thermal infrared camera!

Ultraviolet imaging is useful for some types of forensic analysis, which is often concerned with seeing invisible traces of a crime that may have been overlooked by naked-eye inspection. For example, shortwave ultraviolet imaging has proven to be quite useful in locating and recording latent fingerprints (fingerprints that have not been processed with powder or fuming and that are not readily apparent to the naked eye). Fingerprint analysis has long been a vital tool to law enforcement, since fingerprints are often left behind at crime scenes and are unique to an individual. There are two types of prints, oily and sweaty. Both are often very difficult to see with the unaided eye, even with a magnifying glass, because the skin oils and dried sweat tend to be transparent to visible light. These skin oils do not transmit shortwave UV light readily, and the salt crystals in sweaty prints tend to scatter shortwave UV light more than visible light. These two UV optical properties can be exploited to detect both types of fingerprints on nonporous surfaces without physical contact. This is sometimes crucial to preserve evidence, as dusting for fingerprints can destroy or blur them out.

Figure 1.26 shows a magazine cover imaged in visible light as well as a magnified view of an area of the magazine imaged in both the visible band and with shortwave UV light. The red box superimposed on the magazine cover shows the area with the sweaty fingerprints, which appear brighter than the paper background. The salt crystals in the prints diffusely reflect the UV light into the camera, while the paper absorbs the UV, giving the resulting image a great deal of contrast.

These images were taken with an electronic viewing scope and a UV light source that illuminated the magazine with 254-nm light. The viewing scope is an image intensifier consisting of a light-sensitive photocathode (a glass window coated with a special electrically charged conductive coating) that converts incident light into electrons, which then are amplified and converted back into visible light by a phosphor screen. Note that the fingerprint in the near-ultraviolet image is not fluorescing (emitting light at a visible wavelength in response to an ultraviolet excitation); rather, the salt crystals are reflecting UV light back into the ultraviolet



Figure 1.26 Magazine cover (top) and details imaged with visible light (bottom left) and shortwave-UV light (bottom right). (*Courtesy of Sirchie Fingerprint Laboratory*)

detector. There are many other forensic materials (urine, semen, hair, fibers) that do fluoresce in the presence of ultraviolet light. In that case, the investigator's eyes can detect the visible fluorescence, and he or she need only employ an ultraviolet light source such as a **black light**.

Reflected ultraviolet light photography can sometimes be used to detect bruises and wounds such as bite marks many weeks after the wounds were inflicted, when the wounds are virtually undetectable to the naked eye. The wounds exhibit a change in pigmentation that may be caused by disturbance to the pigment production of the injured basal cells.¹⁰ Figure 1.27 shows examples of an old bite mark that is still visible to reflected-UV imaging.

Many organic materials such as waxes, oils, adhesives and paints absorb or scatter UV light strongly. Figure 1.28 shows a terra cotta tile floor with a shoe impression that is only apparent to near-UV imaging.

The impression was formed by an epoxy floor sealant that was tracked onto the tile floor by a workman. The epoxy tends to scatter UV light, making it look white in the image.

Figure 1.29 shows a vinyl floor tile which has been covered with floor wax. A shoe impression shows up quite dramatically in the near-UV image relative to the

¹⁰R. Barsley, M. West, and J. Fair, "Forensic Photography — Ultraviolet Imaging of Wounds on Skin," *The American Journal of Forensic Medicine and Pathology* 11(4), 300–308 (1990).



Figure 1.27 Visible (left) and near-UV (right) images of a five-month-old bite mark on a living person. (*Photos courtesy of Stephen Warlen and the Kansas City Police Department Crime Lab*)

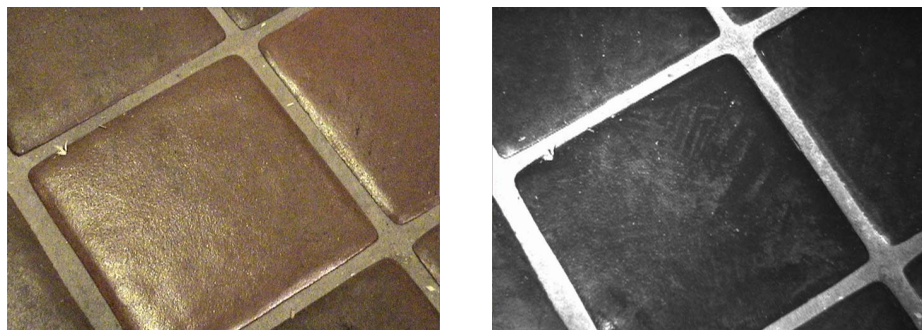


Figure 1.28 Epoxy floor sealant shoe mark on a tile floor: left—VIS; right—near-UV (396 nm).



Figure 1.29 Shoemark on vinyl tile with floor wax: left—VIS; right—near-UV (365 nm).

color image. The wax tends to either absorb or scatter UV light (depending on the illumination angle). The shoe impression changes the texture of the wax surface and affects how light is scattered from it.

Paint is generally composed of a transparent organic resin or polymer with pigment particles suspended in it. As we have seen earlier in this chapter, the pigment particles may not scatter NIR or SWIR light sufficiently to make the paint opaque. In the UV band, conventional paint is always opaque. The reflectivity of the paint surface can vary greatly over time, especially for exterior paint exposed to sunlight, and this property can be exploited to tell old paint from new. Figure 1.30 shows a stucco wall that has been recently repainted near ground level. The fresh paint is relatively unoxidized, such that UV light is absorbed by the polymer binder. The older paint that has been exposed to California sunshine is oxidized and denatured. This inorganic surface layer tends to reflect UV light.

Near-ultraviolet imaging can be used to defeat camouflage because a number of organic materials reflect visible light, but absorb near-UV light. This can make visibly white objects appear dark against a white background that reflects near-UV light. For instance, a polar bear appears white to the mammalian eye because its fur is highly reflective to visible light. The bears are therefore camouflaged when viewed against snow and ice. Many other Arctic animals have evolved this “cryptic coloration”: the Arctic hare, the snowy owl, and the baby harp seal. Two scientists studying herds of harp seals lying on sea ice found that they could not easily count the entire herd using aerial photographs, since the white seal pups were invisible in conventional photographs. These scientists found that photographs taken with light in the near-UV band revealed the baby seal pups; the pups’ fur, being composed of organic molecules, absorbs light in the near-UV and makes them appear dark against snow (snow is highly reflective in both the ultraviolet and visible wavebands). This technique works on polar bears as well, as shown in Fig. 1.31, a near-UV (350–380 nm) photograph of a female polar bear with three cubs. The bears appear almost as dark as grizzly bears in the near-UV.

The scientists also found that the standard military-issue Arctic camouflage issued to Canadian troops was rendered ineffective by their photographic technique. Soldiers on Arctic duty wear snow-colored parkas and pants and



Figure 1.30 Fresh and old paint on a stucco wall: left—VIS; right—near-UV (330–400 nm).



Figure 1.31 Near-UV image of polar bears. (*Courtesy of Dr. David Lavigne*)

transport gear on white sleds, all of which appear very dark when imaged in the near-UV (350–380 nm), as shown in Fig. 1.32.

Ultraviolet light can penetrate some materials that are opaque to visible light and can sometimes reveal information about underlying substances. This property allows for noninvasive analysis of materials. For example, ultraviolet imaging has an interesting application in dermatology. Human skin is normally opaque to ultraviolet light, as the chemical pigment melanin absorbs it. Thus, people with normally pigmented skin appear much darker in the ultraviolet than they do in the visible. If the melanin is destroyed over time by exposure to ultraviolet light, it can penetrate to sensitive inner layers and cause damage to the basal cells, which are approximately 2 mm below the surface. The damaged skin will look white in color—this is called actinic keratosis. Sometimes skin damage looks darker in the UV band than in the visible band. This is because of hyperpigmentation—the tendency of the skin to react to UV light damage by increasing the amount of melanin in the skin. Light freckling will look much darker. Prior ultraviolet damage

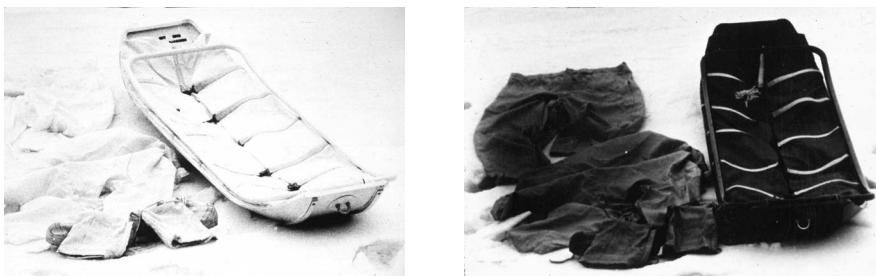


Figure 1.32 Visible (left) and near-UV (right) images of Canadian Arctic military camouflage. (*Courtesy of Dr. David Lavigne*)

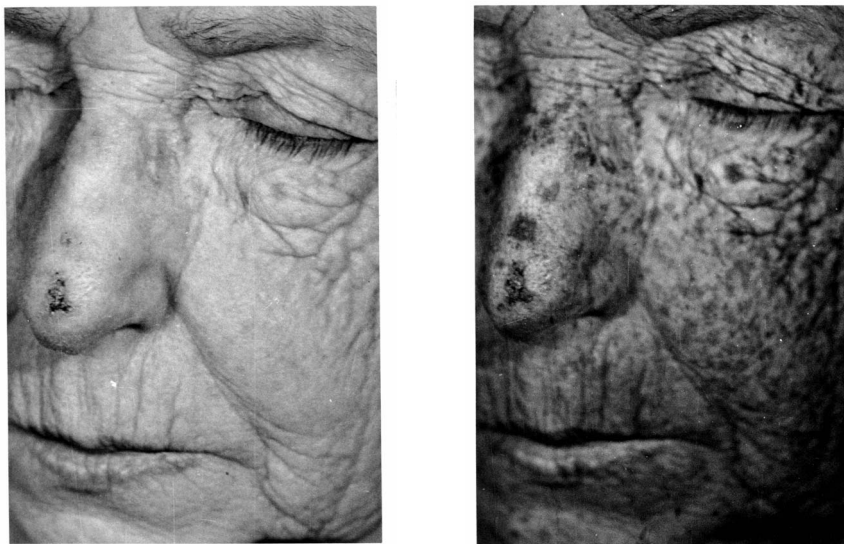


Figure 1.33 Visible (left) and near-UV (right) images of skin cancer. (Courtesy of Dr. Norman Goldstein)

to skin is revealed with near-UV photography, as shown in Fig. 1.33. The near-UV image was taken with conventional black-and-white film and a UV-transmitting filter in the 350–380-nm waveband.

The visible image of skin on the patient's face appears fairly uniform, except for an ulcerating basal-cell cancer on the bridge of her nose. The ultraviolet photograph reveals many dark patches in the deep skin layers, some of which are just hyperpigmentation, while others are precancerous lesions. There are also two other basal-cell cancers on this patient: one on the nose just above the ulcerating cancer and one under the left eye. This ultraviolet photography technique can aid in earlier diagnosis of skin cancer, as precancerous lesions tend to look darker in the ultraviolet than when viewed in the visible.

Animal Ultraviolet Vision

There are many animals and plants that have ultraviolet markings and patterns that were visible only to animals with ultraviolet vision until UV imaging technology revealed them to us. Some insects—notably bees—have visual sensitivity to ultraviolet light in the 300–400-nm region of the spectrum. This ultraviolet vision can see markings and patterns on flowers that we humans cannot. Figure 1.34 shows three Black-Eyed Susan flowers (*Rudbeckia hirta*) imaged in both the visible and near-UV (350–380 nm) regions of the spectrum.

The visible image shows a uniform yellow color throughout, except for the dark center, but the near-UV image reveals a complex pattern of light and dark zones, which serve to guide the pollinating honeybee to its destination. These patterns are known as nectar guides and are believed to play a role in insect pollination.



Figure 1.34 Visible (left) and near-UV (right) images of Black-Eyed Susans. (Courtesy of Prof. Tom Eisner)

Many flowers will appear uniformly white in visible light, but they are seen to have dark regions near the center of the blossom when imaged in ultraviolet light. This dark color is due to the presence of UV-absorbing compounds called flavanols.¹¹ Ultraviolet imaging is useful for the scientific identification of flowers that have nectar guides, as many flower species are difficult to differentiate on the basis of visible color. Ultraviolet “colors” strongly affect the behavior of moths and other light-seeking insects, which will fly to light sources covered with ultraviolet-passing filters, although the filtered sources appear dark to human eyes.

The butterfly is another insect that can see into the ultraviolet. In fact, butterflies have the widest color sense of any known organism. One Japanese species has five different **photoreceptors**—two more than we have—and can see colors from red to near-UV.¹² Figure 1.35 shows two views of a Cleopatra butterfly (*Goneopteryx cleopatra*). The butterfly looks uniformly yellow to our eyes, but interesting patterns are revealed in the near-UV waveband (350–380 nm). The Cleopatra belongs to a large family of butterfly species (*Pieridae*) that to our eyes appear very similar to one another, generally having a nondescript white or yellow color.

However, the near-UV wing markings shown in this image are an example of how nature distinguishes this species from other yellow-colored members of the Pierid family. This is how a Cleopatra flying in a forest can identify a potential mate from a sea of apparently plain yellow butterflies of various species. Some butterflies have sexually dimorphic UV wing markings, i.e. the males look different from the females in the ultraviolet. This is probably an adaptation that helps male butterflies avoid trying to mate with other males.

Ultraviolet vision is found in marine animals as well. The underwater world looks very different in the near-ultraviolet waveband. Particulates in ocean water can scatter near-UV light to such an extent that the water looks foggy, and consequently marine life is thrown into sharp relief against a background such as the coral reef shown in the left-hand image in Fig. 1.36. This is a visible image taken through a filter that passes green light. The right-hand image in Fig. 1.36 is

¹¹W.R. Thompson et al. “Flavanols: pigments responsible for ultraviolet absorption in nectar guides of flowers,” *Science* **177**, 528–530 (1972).

¹²G. Horridge et al., *Journal of Comp. Phys.* **155**, 529–542 (1984).



Figure 1.35 Visible (left) and near-UV (right) images of *Goneopteryx cleopatra*. (Courtesy of Edward Aicken)

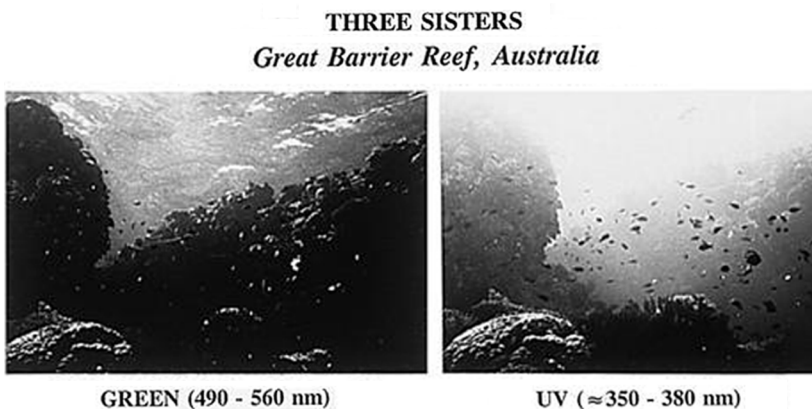


Figure 1.36 Visible (left) and near-UV (right) images of coral reefs and fish. (Courtesy of Prof. Thomas Cronin and the *Journal of Fish Biology*)

quite different: the water looks much brighter due to near-UV scattering, and the fish look dark. Ultraviolet vision may serve to make prey—particularly UV-opaque plankton—visible against a bright background illumination.

Many fish have UV-sensitive photoreceptors in their eyes.¹³ These receptors have peak sensitivity to light with a wavelength of 360 nm, which suggests that these fish perceive near-UV light as a distinct color, as butterflies and honeybees do. It is possible that ultraviolet vision may also help certain fish identify mates in the same manner as butterflies, and this theory is supported by the presence of a variety of pigments in fish skin that have reflectance peaks in the ultraviolet.

Optical Properties of Materials in the Near-IR and Near-UV

Why is it that materials like varnish and certain colors of oil paint are transparent to near-IR and SWIR light but not to visible or UV light? We have seen this phenomenon in the preceding examples of IR and UV imaging, and it is worth exploring the science behind it. UV light interacts with the electrons in molecules

¹³Losey et al., *J. Fish Biol.* **54**, 921–943 (1999).

in a different way from near-IR and SWIR light. The energy of UV photons is several times higher than near-IR and SWIR photons, and when these photons interact with a molecule, they tend to impart their energy to electrons in a single atom within the molecule rather than the molecule as a whole. There tend to be more excitation modes of molecules in the UV, which is why many molecular materials such as glass are opaque to certain wavelengths of UV light, yet they are transparent to visible, near-IR, and SWIR light. A very nice example of this UV absorption effect can be seen in Fig. 1.37, a comparison of two common optical materials in various bands of the spectrum. The figure shows a pair of seemingly identical 2-inch diameter windows imaged in three sub-bands of the UV. The window on the left is standard BK7 optical glass, while the one on the right is fused silica, which is transparent down to 180 nm.

These images illustrate why UV imaging below about 330 nm requires optical materials other than standard glass. However, the conventional wisdom that near-UV imaging requires fused silica lenses is wrong—BK7 works fine in the 340–400 nm near-UV band, especially if it is not antireflection coated.

Figure 1.38 presents an interesting example of how something commonly thought of as “white” does not always appear so white in invisible wavebands.

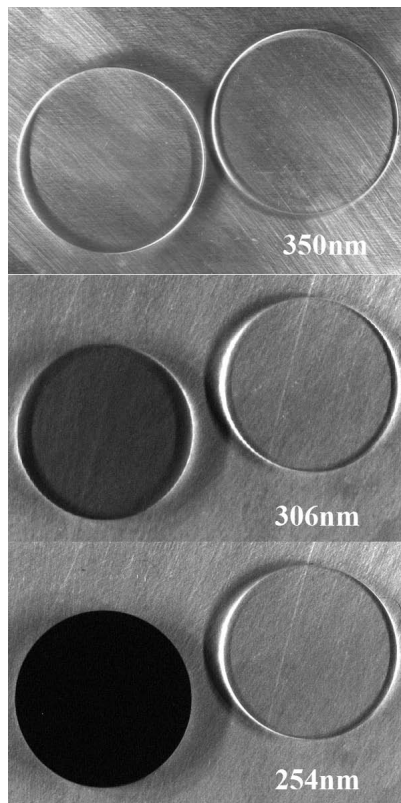


Figure 1.37 Images of BK7 glass and fused silica discs in three narrow UV bands. (Courtesy of David Hayes)

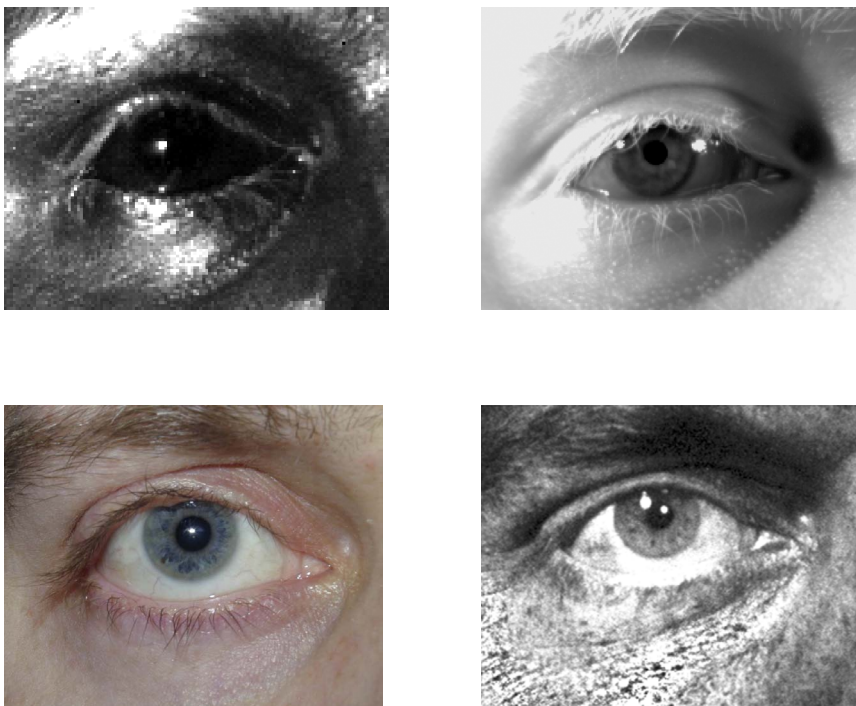


Figure 1.38 From upper left to bottom right: SWIR (2000–2500 nm), SWIR (950–1700 nm), visible (400–750 nm), and near-UV (350–380 nm) images of a human eye. (Courtesy of FLIR and Rand Molnar)

These four images of the same eye were taken with two different SWIR cameras, visible light and near-UV light, respectively.

The white of the eye, known as the sclera, is quite reflective in the visible and near-UV wavebands, as seen in the bottom images in Fig. 1.38; yet the water molecules in the sclera surface absorb light in the SWIR band, giving the eye a very unusual appearance when imaged in the 2000–2500 nm and 950–1700-nm wavebands. Note that the eyebrows and eyelashes appear white in the SWIR images, since the pigments that give these hairs their color hardly absorb SWIR light. Interestingly, all hair colors (even artificial ones) appear uniformly white in SWIR images, regardless of how dark they appear to the eye. The bottom-right image in Fig. 1.38 was made with near-UV light using black-and-white film in a standard 35 mm camera with a Wratten 18A filter that passes near-UV light in the 350–380-nm waveband but blocks visible light. The eye and the skin around it have reversed their appearance from the SWIR image. The white of the eye is quite reflective in the near-UV, while the hair is now quite absorbent. The skin shows a mottling—this is sun damage similar to that shown in Fig. 1.33.

Figure 1.39 contains three images of the author in many of the same wavebands as in Fig. 1.38. Note the change in the apparent shade of the blue shirt—the cotton and pigments in the dye respond differently as the waveband is shifted from long to short wavelengths. The skin in the near-UV image appears quite dark, almost



Figure 1.39 SWIR, visible, and near-UV images of the author. (*Courtesy of FLIR and Rand Molnar*)

like black makeup was applied. But it is just SPF15 sunblock! Sunblock absorbs near-UV light very strongly, protecting the skin underneath. Note the lighter skin around the eyes, on the chest, and in the right ear—these are places where I forgot to apply sunblock!

Atmospheric Effects in the IR and UV Wavebands

The atmosphere and sky have interesting optical properties in the near-IR and near-UV bands. These properties are highly influenced by aerosols and various gases in the air path, especially at ranges greater than several kilometers. Marine haze is an obscurant to visible light, as shown in Fig. 1.40, which are VIS and SWIR images of an oil rig at a range of 47 km. The droplets of water in this type of haze tend to be on the order of 500 nm across, which means that they scatter visible light quite strongly. The SWIR image shows much greater detail and contrast by comparison, and the flare flame on the rig can be seen clearly. This flare is a way to treat noxious gaseous by-products of the drilling process.

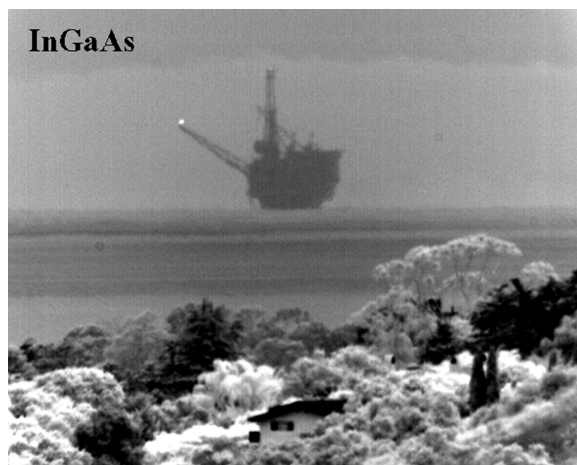
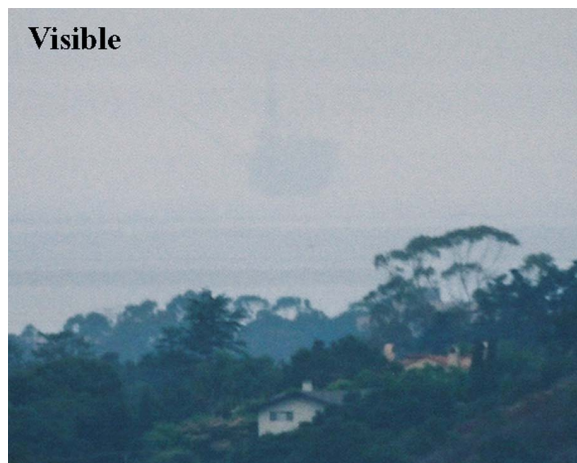


Figure 1.40 Top—VIS image of oil rig at 47 km range. Bottom—SWIR (950–1700 nm) image. (Courtesy of FLIR)

As you might expect, UV light is not transmitted through the atmosphere in the same way as visible light or NIW/SWIR light. Aerosols and particulates in the air tend to absorb and scatter UV. Certain types of air pollution absorb UV light and get converted to other chemicals. Every good film photographer has a 2A haze filter for their camera lenses. These filters protect the lens surface and also reduce UV haze that is especially apparent in landscape photography.

Figure 1.41 shows four images of the moon and the landscape around Nellis Air Force Base in Las Vegas. The UV image is highly affected by haze in the air that makes the mountains less distinct and by Rayleigh scattering of UV light by the atmosphere that completely obscures the moon. The visible image of the moon is hard to see against the bright blue sky. In the near-IR band, the moon is much more distinct, as the sky brightness diminishes and the effects of haze in the air become less substantial.

Infrared and Ultraviolet Light Sources

This chapter has included many examples of differences between near-IR, near-UV, and visible light in terms of their reflection by and transmission through materials, yet there can also be significant differences between the amounts of visible and infrared emissions by a luminous object such as a flame. The presence

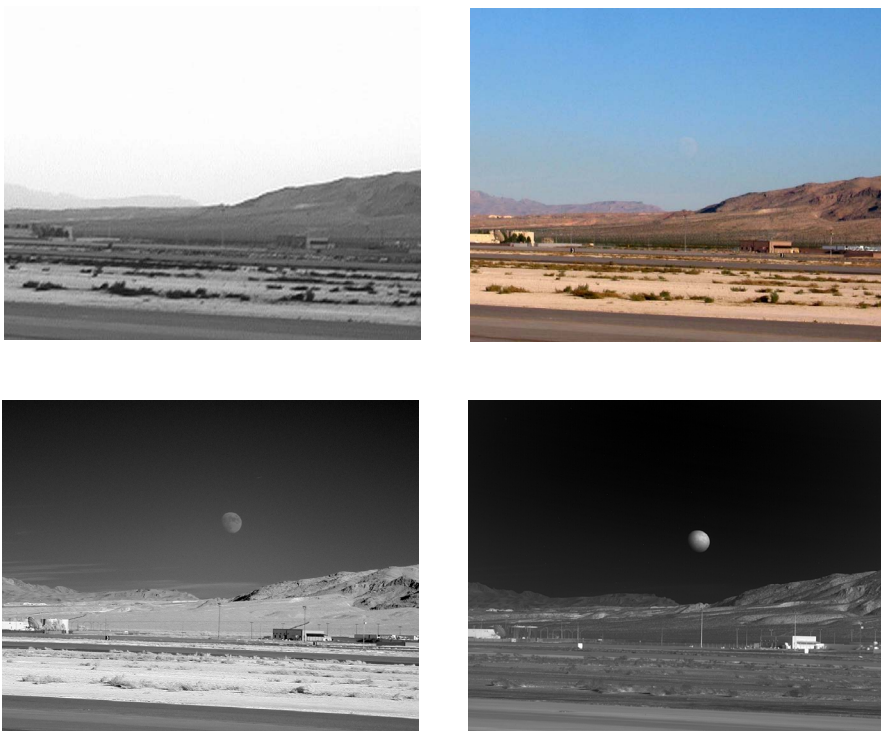


Figure 1.41 The setting moon over Nellis Air Force Base in near-UV, VIS, near-IR, and midwave IR wavebands. (*Midwave IR image courtesy of FLIR*)

of strong absorption bands in a material can also lead to strong emission of light at those same wavelengths when the material is heated. Many molecular compounds have most or all of their absorption bands in the infrared region of the spectrum. They are thus transparent to visible wavelengths of light and can only be seen in the infrared.

For instance, methanol and other alcohols burn with a flame that is quite hard to see during the day even when impurities are added to make the flames more visible. But there are a number of overlapping absorption bands present in alcohols in the infrared region of the spectrum, especially between 1600 and 1900 nm. These absorption bands correspond to various modes of vibrations between the bonded carbon and hydrogen atoms. Thus, burning alcohol glows very brightly in the near-IR and SWIR wavebands, and this characteristic can be used to detect invisible fires. Many motor sports involve alcohol-based fuels that are highly flammable and can produce invisible fires. Racecar drivers have been killed after crashes because no one could see that they were on fire, and small fires in refueling pits have grown out of control because the flames were invisible. Firefighters equipped with infrared imaging systems can see these fires and fight them more effectively. Compare the two views of burning methanol from a leaking fuel hose in Fig. 1.42. The visible image shows a dark patch where the alcohol has soaked into the metal deck, but the SWIR image shows bright white patches of flame around the hose.

Near-UV imaging is also useful for the detection of certain flames, rocket plumes, and hydrogen fires, all of which emit ultraviolet light. Methanol flames have a UV signature in the 240–280-nm waveband, and this makes it possible to detect methanol fires in broad daylight. Figure 1.43 shows a composite image of a pair of small methanol fires taken with a special camera system that consists of a visible-light camera mounted to a UV-sensitive camera with a solar-blind filter (solar blind is 240–280 nm). The visible-light channel is necessary because the solar-blind UV images alone would be nearly all black. The ozone layer of the Earth's atmosphere, which absorbs shortwave UV, prevents sunlight from reaching the ground with wavelengths shorter than about 300 nm. The filter passes 240–280-nm UV light emitted by the methanol fire but blocks longer-wavelength sunlight very effectively.

Because the UV sensor sees virtually no sunlight at all, it can be operated at an extremely high amplification factor, making it possible to pick up even weak



Figure 1.42 Visible (left) and SWIR (right) images of a methanol fire. (*Courtesy of FLIR*)



Figure 1.43 Composite visible and UV (240–280 nm) image of methanol fires. (*Courtesy of Ofil Ltd., Nes-Ziona, Israel*)

sources of solar-blind UV (UV in the 240–280 nm band). Both cameras are aimed in the same direction and see the same field of view. The UV component of the image is colored red for clarity. The red blobs cannot be reflected sunlight, since the UV channel is solar blind.

Corona is a phenomenon observed around sharp tips of electrical conductors in the presence of a strong electric field. The electric fields ionize gas in the vicinity of the tips. When the gas is air, a faint blue-violet glow emitted by nitrogen and other gases in our atmosphere can be seen. The name corona, which means “crown” in Latin, comes from the crown- or brush-like shape of the discharge from the end of conductors such as lightning rods during an electrical storm, faulty high-voltage transmission lines, or ship’s masts (sailors call it “Saint Elmo’s Fire”). Corona is an undesirable condition in the world of high-voltage power transmission—it usually indicates a broken wire or cracked insulator that is causing an intense electrical field to form and electrically overstress the air. Failure to remediate corona can have serious consequences, including fires and short circuits. Corona is hard to see with the unaided eye at night, and during the day it is nearly impossible to see, since most of the light is emitted in the ultraviolet band. Most power line inspections are carried out by helicopter, and thus must be done during the day for safety.

Fortunately, there is a way to overcome the visibility problem. Corona in air emits some light at UV wavelengths shorter than 300 nm. By blocking the sun’s rays with a filter that transmits UV wavelengths only shorter than 280 nm, corona is greatly enhanced even in bright sunlight, making it possible to detect faults on power lines before the problem becomes severe enough to cause heating. Figure 1.44 shows a picture of corona on an insulator stack. The white blobs of light are corona glow from surface leakage along the surfaces of the dirty insulators. As with the methanol image, the corona glow in the UV channel is overlaid on a visible-light image so that the observer can reference the corona glow to the points of emission in the scene.

An interesting source of UV light is radioactive material stored in water. Spent fuel rods from certain types of nuclear reactors are stored in deep “ponds” of water. This enriched uranium undergoes radioactive decay that releases gamma rays. The gamma rays interact with electrons in water and produce high-energy beta particles. The beta particles are electrons moving at relativistic speeds. Since the



Figure 1.44 Composite visible and UV (240–280 nm) image of power line corona. (Courtesy of Ofil Ltd., Nes-Ziona, Israel)

betas are moving faster than the local speed of light in water, electromagnetic shock waves are produced which lead to the emission of blue and UV light. Figure 1.45 shows the effect of this so-called Cherenkov radiation. UV cameras are used to image cassettes of spent fuel. This allows inspectors to verify the presence of fuel rods, since the rods glow with a distinctive spectrum heavily weighted towards the UV.

Infrared Photography and Heat Detection

Many people are under the impression that the infrared photographic film described earlier enables one to take photographs of people or other warm objects in total darkness. This is quite incorrect. In fact, people do radiate infrared light that can reveal them even in total darkness, but that light is known as **midwave or longwave infrared (MWIR and LWIR)**, which has wavelengths that are up to ten times longer than the wavelength of near-IR light. MWIR and LWIR light emissions are not detectable with conventional infrared film.

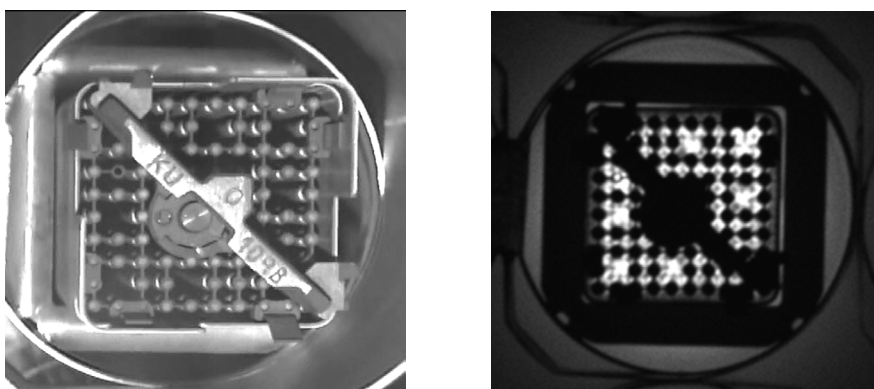


Figure 1.45 Visible (left) and near-UV (right) images of fuel rod assembly in a storage pond. The missing rods make the marked holes glow brighter because nothing is blocking the light paths. (Photo courtesy of Channel Systems)

Can conventional infrared film detect hot objects in total darkness? Yes, but only if the object is hot enough to emit near-IR light, which requires a temperature of hundreds of degrees centigrade. As an object is heated to increasingly higher temperatures, it glows with light of increasing photon energy and intensity. The intensity of the light emitted by an incandescent object can be a very strong function of wavelength. The glowing coal on the end of a cigarette is at a temperature of about $800\text{ }^{\circ}\text{C}$ ($1472\text{ }^{\circ}\text{F}$) when it is just sitting idle, as in Fig. 1.46. There is approximately 10,000 times more light emitted by that coal in the 900–1700 nm band than there is in the visible band!

When an electric stove burner is first turned on, the heating element appears black at first. Then it begins to glow with a dull red color, gradually becoming reddish-orange. If we could keep heating the element, it would glow with yellow light and then finally appear white-hot to our eyes (and then the kitchen would burn up). Reversing this process, the element returns to a dull red glow that gradually disappears as the burner cools. The burner would still be emitting near-IR light. Figure 1.47 contains two images of a pair of stove burners taken simultaneously, one with a visible-light camera, the other with a SWIR camera sensitive in the 950–1700-nm waveband.

The visible-light image on the left suggests that both gas burners are cold, but clearly the back burner is hot enough to glow with SWIR light, as shown in the SWIR image on the right. Also, the glowing burner is reflected in the stainless-steel splash panel behind it. That splash panel has a brushed finish, and is not very reflective to visible light, since the brush marks and ridges on the surface are larger than a wavelength of visible light. However, the surface is a much better reflector of the longer wavelengths of SWIR light emitted by the burner. As the burner cools further, the SWIR glow disappears. The light emitted by the burner becomes increasingly longer in wavelength as it cools. A different imaging system is needed to see the emitted mid-wave and long-wave infrared light. These wavebands of



Figure 1.46 Shortwave IR image of a lit cigarette illuminating a bathroom. (Courtesy of FLIR)



Figure 1.47 Visible (left) and SWIR (right) images of hot and cold stove burners. (*Courtesy of FLIR*)

thermal infrared light are discussed in the next chapter, along with a description of the special devices that enable us to see, among other things, body heat.

This chapter's exploration of the spectrum began with the near-infrared and near-ultraviolet wavebands, since these bands are very close to the visible waveband in wavelength, and the interaction between matter and visible, near-IR and near-UV light is similar. Many near-IR and near-UV images are essentially identical to visible-light images, but I purposely chose images that showed some interesting feature or property of an object not visible to the human eye. The following chapters will look at the world with wavelengths of light that are many times shorter or longer than visible-light wavelengths; then the difference in the appearance of things becomes very apparent.

Chapter 2

Thermal Imaging: We All Glow in the Dark

As we progress past the near-infrared and SWIR wavebands along the wavelength scale of the electromagnetic spectrum to longer wavelengths, we encounter the **midwave infrared band** (MWIR), which starts at 3 **micrometers** (abbreviated μm) and extends out to about 5 μm in wavelength; and the **longwave IR band** (LWIR), which is generally defined as light in the 7–14- μm waveband.¹ Figure 2.1 shows the relationships between the visible waveband and the infrared wavebands.

For the sake of simplicity, I will refer to the MWIR and LWIR bands as the thermal infrared waveband, and the corresponding imaging technology as **thermal imaging**. Though I am surely biased since I work in the industry, the thermal infrared band is currently *the* most fascinating region of the spectrum for invisible-light imaging because practically everything emits a substantial amount of light in this waveband. This makes it possible to see in total visible-light darkness because the scene is self-illuminated! The higher an object's temperature, the brighter it appears to a thermal imaging camera. For example, in a typical thermal image, a person standing in a room will appear to glow brightly against a darker, cooler background, as shown in Fig. 2.2. The child (shown here in pseudocolor) emits plenty of midwave IR light, while the TV emits almost none because the picture tube does not heat up in operation significantly and the color phosphors do not emit significant infrared light—they are designed for human eyes. Notice how the two objects reverse their appearance in the visible band—the TV is now bright, while the child is almost completely dark.

The presence or absence of visible light sources like incandescent light or sunlight does not significantly change the appearance of the thermal image, particularly in the LWIR band. Sunlight will heat up a scene, causing it to radiate

¹There is no strict definition of the ranges of wavelengths considered to be the MWIR and LWIR wavebands. Most thermal imaging technology is designed for 3–5 and 7–14 μm operation, since water vapor in the atmosphere is highly absorbing in various wavebands including those around 2 μm and 5–7 μm . Longer IR wavelengths in the VLWIR (Very Long Wave Infrared) waveband are used almost exclusively for astronomy applications by orbiting telescopes, because heavy absorption by molecules in the atmosphere prevents ground-based observation. The extreme end of the infrared waveband is around 100 μm .

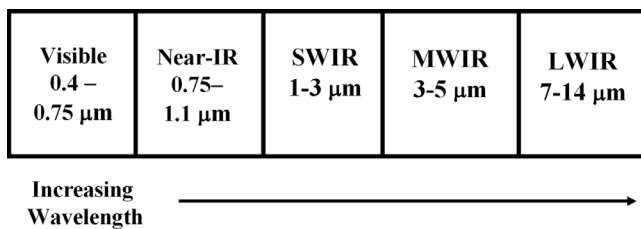


Figure 2.1 The infrared spectrum in relation to visible light.

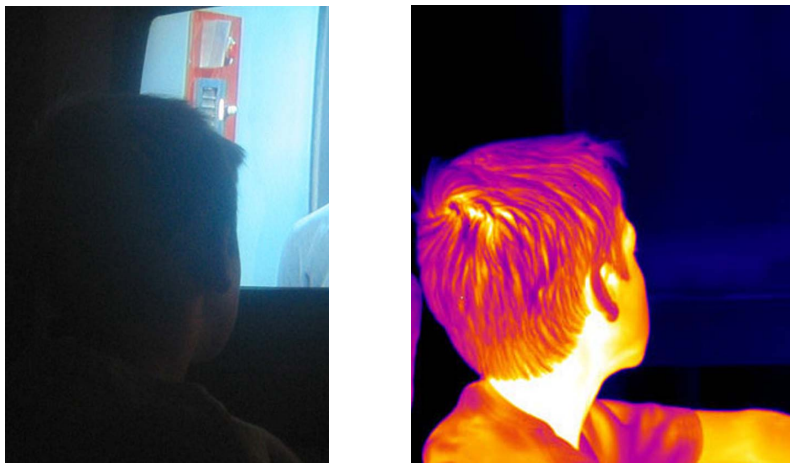


Figure 2.2 A child watching television: left–VIS; right–3–5 micrometers. (*Courtesy of FLIR*).

more thermal IR, but the sun itself is only noticeable when it reflects off shiny objects, and then only in the MWIR band. For this reason, thermal imaging technology facilitates the detection of many objects in total darkness and, in many cases, makes it possible to measure their surface temperatures. Midwave and longwave infrared light can also penetrate smoke, haze and mist, facilitating observation in conditions that make visible-light imaging impossible. For instance, a person lost on a moonless night in the woods without a flashlight or signal flare would be very difficult to find from the air with visible-light imaging. However, this person (or any warm-blooded animal) displays a natural infrared flare in the form of his or her body, a flare of thermal energy against a dark (cold) background. Outdoor backgrounds appear darker than any warm objects in the thermal wavebands, since trees and grass are much cooler than warm-blooded animals.

When we use technology to image the world in the thermal infrared waveband of the electromagnetic spectrum, we are exploring unknown territory, seeing things that no animal has ever seen. This is truly alien vision! Thermal images can look very different from visible-light images of the same scene. This is especially true in darkness, or what we call darkness because there is little or no visible light. The thermal infrared world is never really dark, and objects that are just slightly warmer

than the background around them can be detected with thermal imaging, provided they do not have shiny surfaces. Shiny surfaces such as polished aluminum emit much less IR light than the surfaces of organic materials (wood, skin, cloth) at the same temperature. Molecules emit and absorb infrared light readily—metals simply reflect it. Thermal imaging has found its way into the popular culture, especially into science fiction movies such as *Predator* and *Hollow Man*. The alien creature in *Predator* hunts a band of mercenaries led by Arnold Schwarzenegger through the jungles of Central America. This predatory and grotesque alien uses thermal imaging technology to see people and animals in the dense undergrowth. In the sequel, the Predator appears to use UV imaging as well, circumventing the thermal IR camouflage the human hunters employ (they apparently saw the first movie).

The IR world looks different than the visible world in bright sunlight. Conventional visible-light photographs taken in bright sunlight can be washed out by scattered visible light, which can reduce the sharpness of shadows. The sky looks blue because shorter wavelength blue light is scattered by the atmosphere more strongly than red light, and thus the blue component of sunlight lights up the air with a blue glow. This phenomenon is called Rayleigh scattering and it is caused by tiny density fluctuations in the air at the nanoscale level. Rayleigh scattering is a very strong function of wavelength, and it affects the propagation of infrared and ultraviolet light too. In the preceding chapter, we saw how the daytime sky appears bright white when imaged with a near-UV camera—this is scattered UV sunlight. Infrared light scatters even less than red light, and thus the sky appears nearly black when viewed in the IR wavebands. Near-IR images of a sunlit scene are reminiscent of visible-light photographs taken while on the surface of the moon: a black sky and harsh shadows. In both cases, scattering of light is absent: in one case because the long wavelength of IR light means little Rayleigh scattering, in the lunar case, because of the lack of an atmosphere. In a thermal image, the clear sky will appear black, but objects and scenery tend not to cast shadows. This is because every solid object in the scene emits thermal IR light.

This effect is very apparent in the following example. Figure 2.3 shows an IR image of one of the great pyramids and the Sphinx on a sunny day. Note the dark sky, which appears “cold” to the IR camera that imaged this scene in the 3–5 μm waveband (MWIR). The infrared intensities in the image are represented by pseudocolor, with white being the most intense and dark blue the least intense. The strongest infrared intensities represent the hottest temperatures within the scene. This particular pseudocolor scheme (called fusion in the IR camera industry) makes white the hottest pixels of the image, then yellow, then red, magenta, and finally blue as the coldest pixels. The addition of pseudocolor is a common technique used in thermal imaging to enhance slight temperature differences within a scene, as the eye is much more attuned to slight changes of color than to slight changes in grey level.

In this image, the sun is nearly overhead, and its rays strongly heat upward-facing surfaces such as the top of the pyramid (where the original facing is intact), the top of the Sphinx’s head, and the ground around them—as shown by the white and red pseudocolor. This heating is known as “**solar loading**,” an effect that can

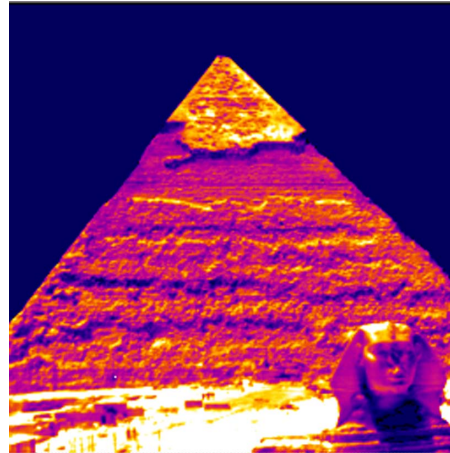


Figure 2.3 MWIR (3–5 mm) image of pyramid and Sphinx. (*Courtesy of Stan Laband*)

make objects buried at shallow depths visible to thermal imaging sensors, as we will see later in this chapter. The lower parts of the pyramid’s face that receive sunlight at a glancing angle are cooler and are represented by magenta color, while surfaces that are in shadow are cooler still and are represented by blue. The same heating patterns caused by solar loading are seen in the Sphinx. For example, the Sphinx’s neck and breast are cool, as they are well shaded from the sun by its head.

Solar loading can lead to an effect called **thermal scarring**. An object that shades the ground from the sun during the day will create a cooler area underneath it. Even after the object is moved, the cold spot persists, sometimes for hours, depending on the sun’s position when the object is moved. The black plastic plant pot shown in Fig. 2.4 was left in position for 30 minutes before it was removed. The visible image gives no indication that the pot was ever there, but the thermal scar persists for many minutes as shown in Fig. 2.5. This same technique is used to look for traces of military vehicles by reconnaissance satellites and surveillance UAVs—a transport jet can leave a thermal scar long after it has taken off, as can a ship moving through water.

Thermal imaging technology has advanced to the point where even very subtle surface temperature differences are quite easy to detect. Recall the example of the stove burner in the last chapter. It emitted SWIR light even when it appeared black to the eye. Turn off the burner, wait long enough, and the burner will cool to a temperature just a little above room temperature. It is then indistinguishable from the other burner if imaged in the SWIR waveband. Before the burner achieves thermal equilibrium with its surroundings, it will only be a few degrees hotter than the one that was never heated. It will not feel hotter than the other burner to the finger, and yet the temperature differences will be easy to see with a thermal imaging camera. In fact, the most sensitive cameras can see temperature changes of 0.01 °C or smaller. This is possible because the intensities of the MWIR and LWIR light emitted by “room temperature” objects vary sharply with their temperature. There can be a great deal of contrast (difference in brightness) between two

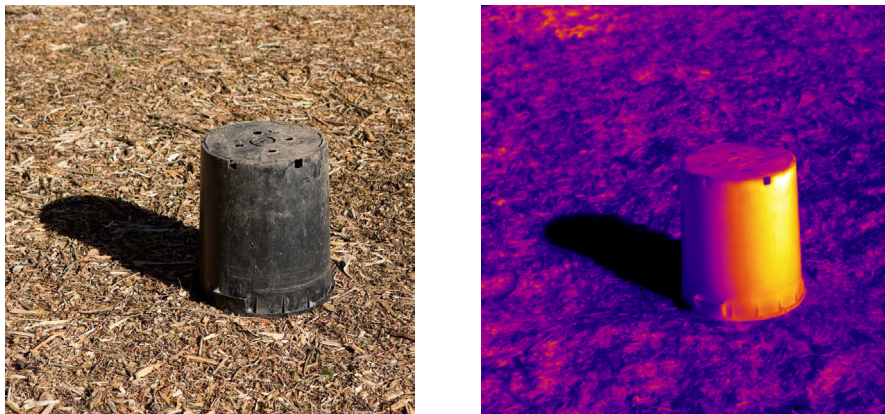


Figure 2.4 Plastic plant pot on wood chips in sunlight: left—VIS; right—MWIR (3–5 mm).

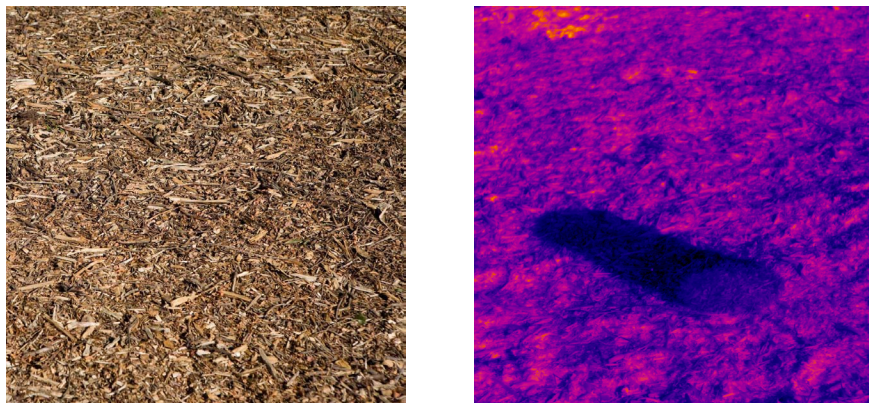


Figure 2.5 Thermal scar left by plant pot: left—VIS; right—MWIR (3–5 mm). (*Courtesy of FLIR [IR] and Patrick Stanbro [visible]*)

objects that are at slightly different temperatures. Figure 2.6 illustrates this contrast effect beautifully: a person walks barefoot into a kitchen and leaves behind heat footprints which are only a few hundredths of a degree centigrade above ambient temperature.

Another interesting effect one can see with MWIR imaging is the variations of skin temperature in a person's face. Figure 2.7 shows the author imaged in the MWIR waveband. I have particularly cold cheeks and a cold nose due to a case of Antarctic frostbite that permanently damaged the capillaries in my skin; therefore, those areas appear dark. Note the patchy hot spots on the neck and jaw. These hot spots change with time, and are caused by natural variations in blood flow. The eyes are the warmest spot on the face, warmed by the copious blood flow near the surface. The eye's surface is fairly isothermal (all at the same temperature), and only the surface layer emits MWIR light; all of the detail (iris, pupil) we see with visible light is hidden, as shown in Fig. 2.8, two images of my eye in visible and MWIR light. MWIR light is also absorbed by the surface layers of the eye, and thus

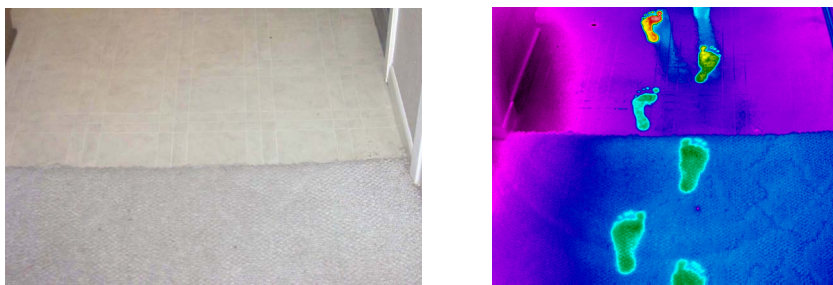


Figure 2.6 Visible and MWIR (3–5 mm) images of a floor with heat footprints. (*Courtesy of FLIR*)



Figure 2.7 MWIR (3–5 mm) image of the author. (*Courtesy of FLIR*)

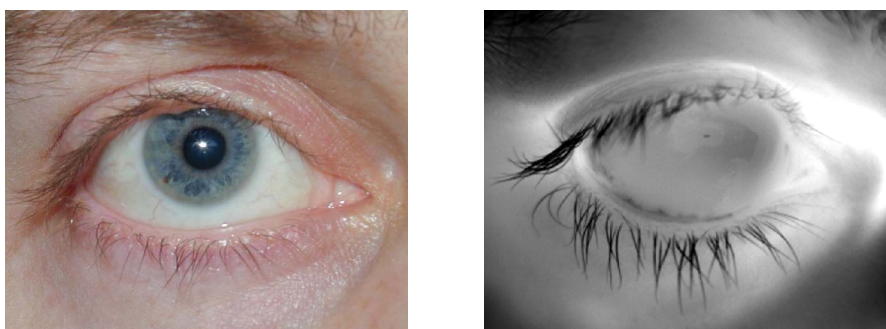


Figure 2.8 Visible (left) and MWIR (3–5 mm) (right) images of the author's eye. (*Courtesy of FLIR*)

it cannot enter the eye. So even if our retinas were somehow sensitive to MWIR light, it could not reach them. As discussed in the last chapter, our eyes cannot see light with a wavelength longer than about $0.75\text{ }\mu\text{m}$ (750 nm) because this light lacks the requisite energy to cause chemical changes in the retina that lead to visual perception.

The opacity and transparency of materials depend greatly on the waveband of light used to image the materials. Often, the optical properties of a material in the visible waveband are quite different in another waveband. This is particularly true in the MWIR and LWIR wavebands. In the last chapter, we saw that near-IR and SWIR light can penetrate through thin material that is opaque to visible light, reflect off what is underneath, and come back through the thin material to a near-IR imaging device. Thermal imaging can also see through certain thin materials that block the transmission of visible light. Figure 2.9 shows an example of an opaque material that transmits MWIR light; in this case, light emitted from the person in the black plastic garbage bag. There is little absorption in the $3\text{--}5\text{-}\mu\text{m}$ waveband in this black polyethylene, and the material is also quite thin, making it easier for longer wavelengths of light to pass through it. The walls behind the person appear dark, as they are colder than his skin, and therefore emit less MWIR light. The visible image was made with reflected overhead lighting, making the walls appear bright in the visible band.

Now let us consider the case of a material that is designed to be very transparent to visible light, yet blocks MWIR and LWIR light. Window glass is designed to be transparent to visible light, but its transparent properties do not carry over very

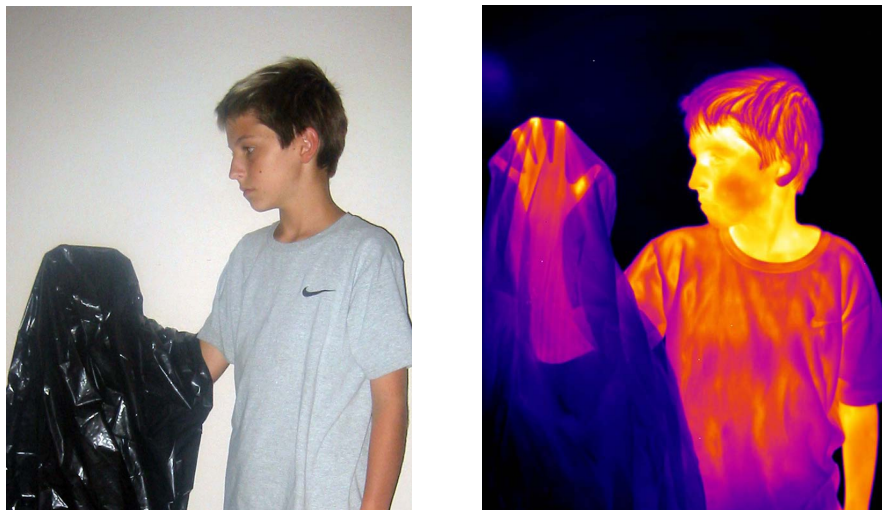


Figure 2.9 A boy with his arm inside a black polyethylene garbage bag: left—VIS; right—MWIR (3–5 mm). (*Courtesy of FLIR*)

far into either the ultraviolet or infrared bands.² Thermal infrared light strongly interacts with the silicon dioxide molecules in window glass, and thus we cannot see through glass windows with a MWIR or LWIR thermal imaging system.³ Figure 2.10 shows two views of a man sitting in a car, one in visible light and the other in MWIR light. These images illustrate a limitation of thermal imaging: the optical properties of glass place limits on thermal imaging for surveillance, which is a boon to privacy advocates everywhere!

Reflectivity of Materials

Some surfaces are good mirrors in the thermal IR band, but are not good mirrors in the visible band. For a metal surface, the surface texture determines the degree to which it will act as either a **diffuse reflector** or a **specular reflector** in different wavebands. A nice example of this is a stainless steel refrigerator door shown in Fig. 2.11. The surface finish is what machinists call “grained.” The grooves and texture have length scales on the order of 0.5 micrometers. Thus, visible light is highly scattered by the surface—it acts like a diffuse reflector. In the 3–5 micrometer band, the door becomes an excellent reflector, showing the person reflected in it. Many metal surfaces are excellent thermal IR mirrors.

Midwave and Longwave IR Imaging Systems

As we attempt to image the world around us with electromagnetic energy that departs significantly from the wavelength range of visible light, we can no longer use ordinary cameras with special films and filters to make images as we could in the near-infrared and near-ultraviolet bands. The imaging devices we need to make thermal images still use lenses, but they are made of special materials (such as silicon and germanium) that have very different optical properties from those of glass. Ordinary camera lenses, like the car windshield in Fig. 2.10 are opaque to MWIR and LWIR light. In addition, ordinary photographic film is not sensitive to these long wavelengths of light, so we need another means of detecting the focused image. There are different ways to accomplish this but all use very specialized detectors. Some of the original thermal imaging devices were developed for military use in the 1950s. They used single electronic detectors or linear arrays of detectors that were scanned (typically by a rapidly moving mirror) in such a way as to build up a two-dimensional image of a scene. Today, almost all thermal imaging systems are designed around focal plane arrays (FPAs), which are two-dimensional “mosaics” of electronic detectors. Each detector corresponds to a pixel, or picture element, in the final image. A lens focuses infrared energy onto the FPA, which then converts the energy into electronic signals that can be transmitted

²The American physicist Richard Feynman watched the first atomic bomb test through a car windshield, knowing that the glass would not transmit harmful UV light to his eyes.

³There are glass-like materials that are transparent to both visible light and infrared light, but they are expensive and hard to fabricate into large sheets.



Figure 2.10 Visible (left) and MWIR (3–5 mm) (right) images of a man sitting in a car. (Courtesy of FLIR and Patrick Stanbro)



Figure 2.11 Visible (left) and MWIR (3–5 mm) (right) images of a man reflected in a brushed stainless steel refrigerator door. (Courtesy of FLIR and Patrick Stanbro)

as a video signal to a display or recording device, just like a standard video camera. Because of the difficulty of building FPAs with the same number of pixels as conventional visible-light video cameras, thermal images taken with standard commercial FPA cameras have tended to be grainy in appearance compared to conventional video images. We now have commercially-available one-megapixel thermal imaging cameras that produce incredible imagery. Even bigger thermal IR FPAs have been built for satellite remote sensing and astronomical telescopes.

Figure 2.12 shows an infrared camera that is sensitive to energy in the MWIR waveband. The camera is about the size of a large loaf of bread. The FPA in this particular camera is made of the semiconductor material **indium antimonide**, which needs to be cooled to liquid nitrogen temperatures (77 K or -321.07°F) to reduce detector noise (which is very temperature dependent) to workable levels. A small **closed-cycle cooler** cools the FPA. Note the green color of the lens—this is an antireflection coating on a germanium lens. The lens is totally opaque to



Figure 2.12 Cooled MWIR (3–5 mm) camera. (Courtesy of FLIR)

visible light; it looks like a mirrored surface to the eye. Figure 2.13 shows a rough block diagram of the camera's insides; the image-processing electronics generates standard **analog video** signals as well as **digital video** data.

One of the most exciting developments in the history of thermal imaging camera technology was the uncooled IR FPA. These detector arrays do not need to be cooled to cryogenic temperatures to operate; they need only be stabilized at temperatures near ambient (25°C or 77°F) or, more recently, operated without any temperature control at all. Uncooled imaging cameras were an optional feature in Year 2000 Cadillac Sevilles as part of a night-driving system that projects a

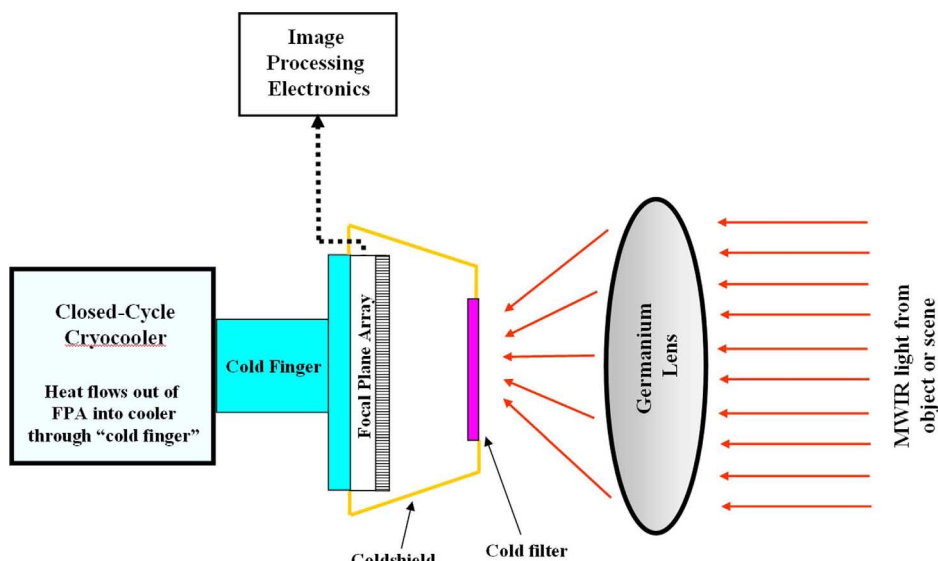


Figure 2.13 Block diagram of a cooled MWIR (3–5 mm) camera.

LWIR image onto the windshield to assist in low-light-level driving conditions. In recent years, BMW has installed thermal imaging cameras on their 7-series sedans as a must-have option for the tech crowd. Uncooled IR cameras can be extremely small and lightweight with low power requirements. Other applications for these miniature cameras include helmet-mounted imaging systems for firefighters and as a payload on unmanned aerial vehicles for military reconnaissance. Thermal imaging in the LWIR band gives a firefighter the ability to see through smoke, since smoke particles are too small to strongly scatter long-wavelength IR light. The firefighter observes a helmet-mounted video display of the thermal image, and can detect people from their body heat as well as hot spots in doors, walls, floors and ceilings that may indicate that a fire is still burning. Figure 2.14 shows a view of a person imaged through smoke by a miniature uncooled camera.

The ability to see through smoke is useful for long-range reconnaissance of forest fires. The Jesusita fire in Santa Barbara, California in 2009 was particularly destructive. The smoke was impenetrable to the eye from 10 km away, but the seats of the fires were easily visible with a MWIR camera, as shown in Fig. 2.15. MWIR light penetrates through smoke quite well, though generally not as well as LWIR light. The longer wavelengths of LWIR are less scattered by smoke particles for a typical bush fire like this.

Surveillance and Law Enforcement

Thermal imaging technology development has been driven mainly by the military, for the following reasons: infrared cameras can see objects that are well camouflaged in the visible band, and they can also image through smoke, haze and other battlefield obscurants. Initially, only the military could afford to buy high-speed FPA cameras, but as the cost of thermal imaging systems drops with the advent of new technologies and fabrication techniques, law enforcement is making increasing use of them for surveillance. Thermal imaging can detect a suspect hiding in the bushes; identify a car that just pulled into a parking garage late at night; or find recently fired weapons and other warm objects in darkness and in partially concealed places. Figure 2.16 shows two views of a warm handgun dropped into the bushes outside my house. The gun was in my waistband for an hour before the picture was taken, heating up to over 90 °F (32 °C). The gun is nearly invisible in the visible-light image even though it was illuminated with a flash, while the LWIR thermal image has high contrast between the gun and the vegetation in total darkness.

Figure 2.17 shows a man sneaking around the back of a house. Even though the scene is completely dark as viewed in visible light and the man is impossible to see in the shadows, he glows brightly in the MWIR band because he is about 10 °C (50 °F) hotter than the other objects in the scene. The rear windshield trim is reflective in the MWIR band, and since it is canted at an angle, it reflects the cold sky into the camera and thus appears black (cold) in this image.

Thermal imaging can also be used to detect density variations in materials, since differences in heating and cooling can create surface temperature differences.



Figure 2.14 Visible and LWIR images of person in smoke-filled building. (*Courtesy of FLIR*)

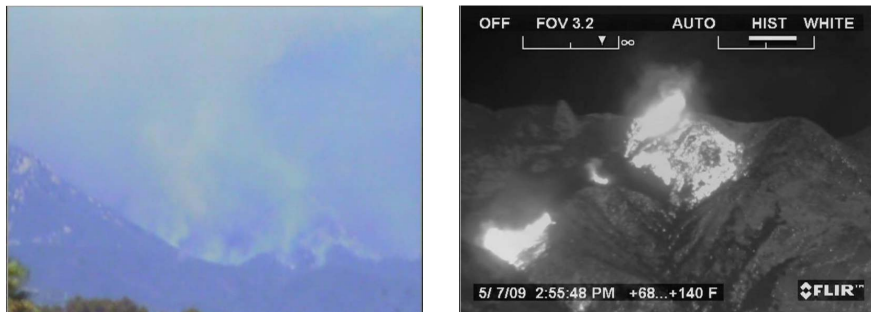


Figure 2.15 Jesusita fire at 10-km range in Santa Barbara, California: left—VIS; right—MWIR (3–5 mm). (*Courtesy of FLIR*)



Figure 2.16 Handgun in bushes at night: left—VIS; right—LWIR (8–13 μm). (*Courtesy of FLIR*)



Figure 2.17 Burglar sneaking in the dark: left—VIS; right—MWIR (3–5 mm). (*Courtesy of FLIR*)

Typically, denser materials will retain heat longer than less dense materials. Solar loading can supply the heat to a scene—once the sun sets, differential rates of cooling can lead to x-ray-like images. Figure 2.18 shows two views of a living room on a winter's day. The MWIR image shows that the studs behind the sheet rock are conducting the cold in from outside. The drywall screws are apparent as well—they are “probing” colder interior volumes of the studs and “conducting” the cold into the house. These volumes are closer to the exterior on the winter’s day. The ceiling is warm because of solar loading and the lack of decent insulation. Hidden compartments or contraband will also retain heat, making it possible for law enforcement to detect their presence with thermal imaging devices under certain conditions. Police have used thermal imaging to detect excess heat generated by lighting used for indoor marijuana cultivation. They would fly over a suspected building and image it from the air. The infrared evidence was then used to obtain search warrants for a physical search of the premises, though that is no longer allowed, since it is considered unreasonable search and seizure.

The phenomenon of differential heating and cooling also makes it possible to locate buried objects with thermal imaging. Figure 2.19 shows a LWIR image of unmarked shallow gravesites that are undetectable to the eye. The horizontal pseudocolor bar along the top edge of the image indicates IR intensity, with red being the highest intensity, followed by white, light blue and dark blue. The graves could be imaged by a thermal imaging camera because they contain voids (dead air spaces) caused by body cavities (in the case of burial without a coffin) or because the soil surrounding the coffins did not collapse as they deteriorated. The resulting air spaces act as insulation, thereby changing the surface temperatures above the voids as the flow of solar energy is blocked from entering the soil.⁴ This same process has been used to locate hidden contraband, terrorist explosives, landmines, buried storage tanks, and other objects that create a void or space underground that changes the way heat from solar loading flows.

Industrial Thermography

Industrial processes often require quick and precise measurements of the temperature of a surface at many different points without having to place a thermometer at each point. A thermometer works by thermal conduction, where thermal “vibrations” in a material are transmitted to a temperature probe. Heat is also transmitted by radiation, and the surface temperature of an object can be determined by observing the intensity of IR light radiated from the surface. A MWIR thermal imaging system is excellent for temperature measurement in the 0–200 degrees Celsius range. Temperature information can be displayed by assigning a temperature-dependent color value to each point in the image. This type of inspection is known as **thermography**. Some types of thermal cameras can be calibrated to measure temperatures to accuracies of around one degree centigrade.

⁴Gary Weil and Richard Graf, “Infrared Thermographic Detection of Buried Grave Sites,” *Thermosense XIV*, Vol. 1682, SPIE (1992).



Figure 2.18 Visible (left) and MWIR (3–5 mm) (right) images of a living room. (*Courtesy of FLIR and Patrick Stanbro*)



Figure 2.19 Thermal image of unmarked graves. (*Courtesy of Gary J. Weil, Entech Engineering, Inc.*)

Here are some examples of industrial applications for thermal imaging technology. Figure 2.20 has VIS and MWIR images of a car's heated seat. Thermal imaging is applied to a multitude of automotive systems evaluations, since many parts of an automobile operate at temperatures above or below the ambient temperature.

The top image in Fig. 2.21 is a visible-light image of a transformer bank. The bottom image in Fig. 2.21 is an MWIR image of a similar bank of transformers. The heating caused by an electrical load is apparent, as indicated by the rainbow pseudocolor. The right transformer is being loaded more than the other two, from the looks of it.

The transformers above are an example of a good application for thermal imaging for predictive maintenance, because, by design, they are hard to reach from the ground and are energized with high voltage on top, making noncontact temperature measurements from a distance safer and easier. If one of the transformers was malfunctioning, it would have a surface temperature that differed

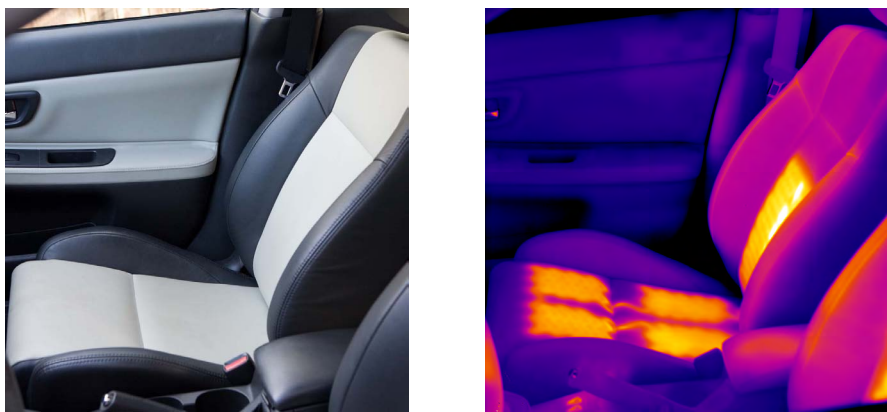


Figure 2.20 Heated seats in a car: left—VIS; right—MWIR (3–5 mm). (*Courtesy of FLIR and Patrick Stanbro*)



Figure 2.21 Visible (top) and MWIR (3–5 mm) (bottom) images of energized transformers. (*Courtesy of FLIR*)

from the others in the bank. Thermal imaging enables transformers and many other machines and components to be examined quickly and safely for thermal anomalies that are an indication of malfunction or imminent failure.

Small electrical circuits also lend themselves to the same kind of noncontact thermography as in the above example, since the electrical characteristics of a circuit can be changed by physical contact or even close proximity of a temperature probe (especially in high-speed circuits like those used in communications). Figure 2.22 shows visible and MWIR images of a high-speed electronic circuit board with overheating integrated circuits. The circuit performance is unaffected by the thermal imaging equipment, so the temperature measurements are a true indication of the thermal performance characteristics in operation.

Imaging Invisible Gases

Certain gases have strong resonances with infrared light at specific wavelengths. For example, hydrocarbon gases like methane and propane contain carbon-hydrogen or C-H bonds. The carbon and hydrogen atoms will move toward and away from each other like masses on a spring. The “spring constant” of the bond determines the resonant frequency which corresponds to the frequency of lightwaves with a wavelength of 3.3 micrometers. A midwave IR camera that is restricted to see only light right around 3.3 micrometers can image hydrocarbon gases in the air, gases that are normally quite invisible to the human eye. The wavelength restriction is accomplished with a bandpass filter that is placed inside the camera. Figure 2.23 shows an example of a propane leak out of a tank. To the eye, the leak is quite invisible. Within the narrow waveband of the camera, the cold gas absorbs light emitted by my skin behind it and looks like black smoke.

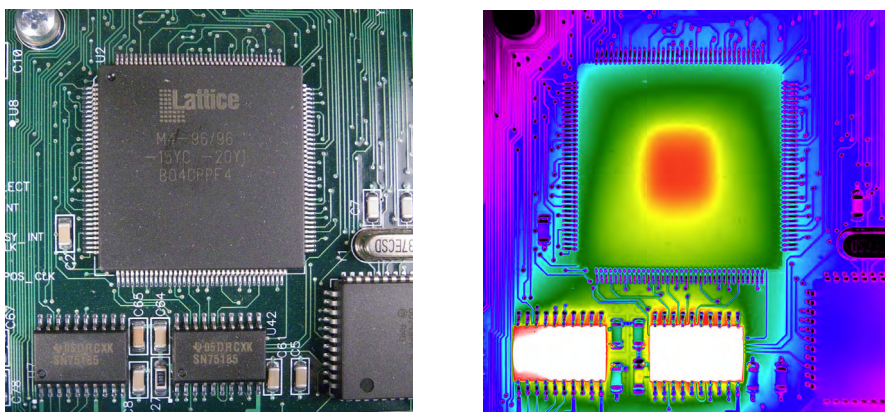


Figure 2.22 Visible (left) and MWIR (3–5 mm) (right) images of a high-speed circuit board. (Courtesy of FLIR)



Figure 2.23 Propane gas leak imaged with a special 3.3 micrometer midwave-IR camera. (Courtesy of FLIR)

Test Range Radiometry

Because thermal infrared camera systems are used extensively on the battlefield, it is crucial to characterize the appearance of military targets in the thermal IR band. This is known as **signature measurement**, and it is accomplished using special calibrated IR camera systems that perform **radiometric measurements**. The signature of an aircraft, for example, will consist of measurements of the shape of the exhaust plume, its **radiance**, and sometimes its **spectral signature**. Figure 2.24 shows a Harrier Jump Jet hovering in mid-air at Nellis Air Force Base in Nevada. The exhaust plume is barely visible in the first photo, but is very apparent in the MWIR image because the plume is loaded with hot water vapor and hot carbon dioxide. I happened to take a NIR image of the plane at the same time, and it shows the plume slightly more than the visible-light image, probably because the water vapor in the plume absorbs NIR light. The water vapor is hot enough to emit MWIR light, but cold enough to act as an absorber to NIR light.

Helicopters show various sources of heat in thermal infrared images, but by far the brightest part of the Chinook helicopter in the midwave IR band is the exhaust system in the back, as seen in the MWIR image in Fig. 2.25. The exhaust manifolds are not quite hot enough to glow with visible light; in fact, the IR images were taken in almost complete darkness. A reference image of another Chinook helicopter is included to illustrate the exhaust system.

High-Speed Thermography

Sometimes a scientist or engineer wants to measure the temperature of something that can't be touched or otherwise measured with a temperature probe. Bullets and cannon projectiles heat up as they move down a gun barrel due to friction. The frictional heating leads to barrel wear which is useful to characterize. Sniper detection systems will track bullets in flight by their thermal infrared signature. Figure 2.26 shows two ultrahigh speed pictures of a 30 caliber bullet in flight, about



Figure 2.24 Harrier jet hovering in place during an airshow: top—VIS; middle—MWIR (3–5 mm); bottom—NIR (0.78–1.1 μm). (*Courtesy of FLIR*)



Figure 2.25 Chinook helicopter taking off at night: left—VIS; right—MWIR (3–5 mm). (Courtesy of FLIR)

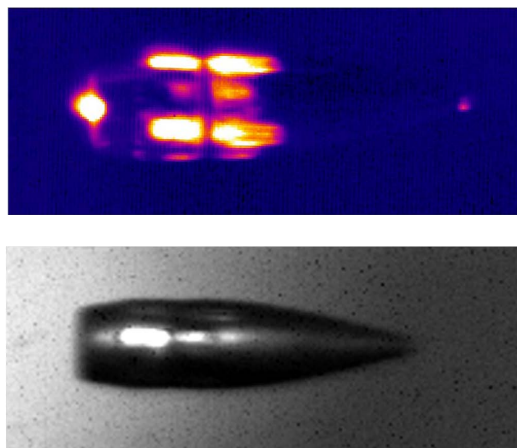


Figure 2.26 A 168 grain .30 caliber bullet in flight: top—MWIR (3–5 mm); bottom—VIS. (Courtesy of FLIR and Vision Research)

1 meter out of the muzzle of a military rifle. The bullet is moving at 840 meters/sec or about 1900 mph. Note the various hot parts—**aerothermal heating** makes the tip glow, friction makes the sides glow, and the tail of the bullet is reflecting the muzzle flash. The top image was made with a special ultrafast MWIR camera with a shutter speed of 1 microsecond, the bottom with an ultrafast visible-light video camera with a 2-microsecond shutter speed and external illumination.

Thermal Imaging and Biology

Seeing the infrared light emitted by objects that are only a little hotter than room temperature is a very useful ability for anything that hunts at night. Human eyes alone cannot see the infrared glow from another person or an animal. But a limited type of “thermal vision” does exist in the animal kingdom. Rattlesnakes and other pit vipers can locate their warm-blooded prey in total darkness by detecting heat

trails and the infrared light the prey emits. This is accomplished with specialized sensors located in the pits on either side of their heads, just below the eyes. The two pits are divided into two halves by a thin membrane stretched across the pit like a drum head. The membranes contain two large branches of the trigeminal nerve (one of the cranial nerves) that are fanned out across the surface of the membrane. These nerves respond to minute temperature changes of the membranes, which can be induced by the presence of a warm-blooded animal in front of the snake's head. The absolute temperature of the membranes is not sensed, only time-dependent changes, which is why the snake scans its head from side to side.⁵ The membranes serve as platforms for the nerves, and the platforms have a large surface area and low thermal mass, making them very sensitive to changes in infrared intensity. Each pit has a field of sensitivity that overlaps the other slightly, and the snake can tell when the prey is directly in front of its head because the two pits will generate approximately equal thermal signals in each pit. The infrared perception of the viper is not truly vision, since the snake only detects the existence and direction of a heat source, not its shape. This sense is akin to the heat sensitivity of one's skin, which can detect radiant energy in the IR band; though the pits are much more sensitive to IR light than our skin, being able to detect IR energy equivalent to that produced by a human hand at a distance of 30 cm.⁶

Most mammals show their highest surface temperature around their eyes because of the high degree of blood flow and the lack of any insulating layer over the living eye tissue. Extremities such as the ears and nose tend to have the lowest surface temperature because they don't receive as much blood flow as the eyes, or in the case of the nose, they may be wet, cooling the nose by evaporation. Cats and dogs tend to have hot eyes and cold noses as seen in Fig. 2.27.

Thermal energy is a vital aspect of biological processes, and infrared imaging allows us to monitor the flow of thermal energy within living tissue. Thermal imaging can be used in medical applications to detect anomalies in skin and tissue surface temperatures, anomalies that can often reveal damage or abnormalities in underlying tissue. Figure 2.28 shows a normal forearm imaged in the visible and MWIR bands. The surface of the skin is warmed up slightly by blood flow, and thus one can see the arteries and veins from their heat signature. If there were vascular damage to an area of the arm, then the skin there would appear colder than surrounding undamaged areas.

Now consider a vascular abnormality that results in a thermal anomaly. Figure 2.29 shows a MWIR image of a hand missing an index finger. The finger was lost in a shotgun accident, and as a result the stump is colder than the other digits as a result of vascular damage. This image is rendered with pseudocolor indicated by the color bar to the right of the image: white or red pixels are the hottest temperatures in the scene, and purple or black is coldest. Thermal images such as this could be used to indicate surgery to restore blood flow to tissue.

⁵Gamow et al., "The infrared receptors of snakes," *Scientific American*, **228**(5) 94–99 (May 1973).

⁶Angus Bellairs, "The Life of Reptiles," p. 388, Universe Natural History Series, Universe Books (1970).

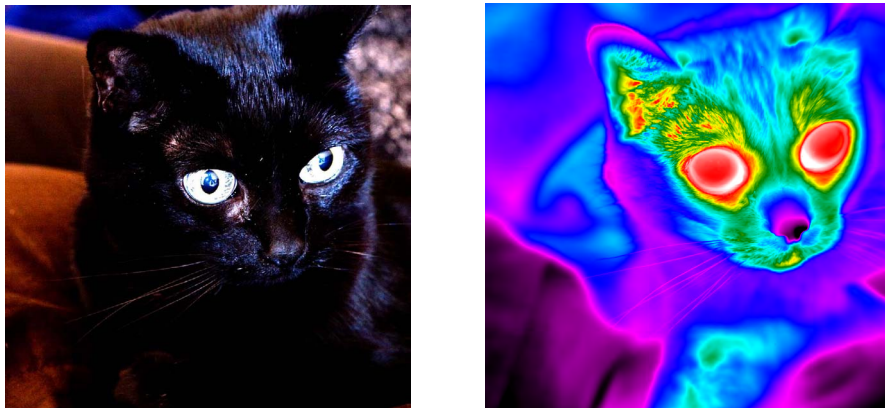


Figure 2.27 VIS and MWIR (3–5 mm) images of a cat. (*Courtesy of FLIR*)



Figure 2.28 Visible (left) and MWIR (3–5 mm) (right) images of blood flow in a forearm. (*Courtesy of FLIR*)

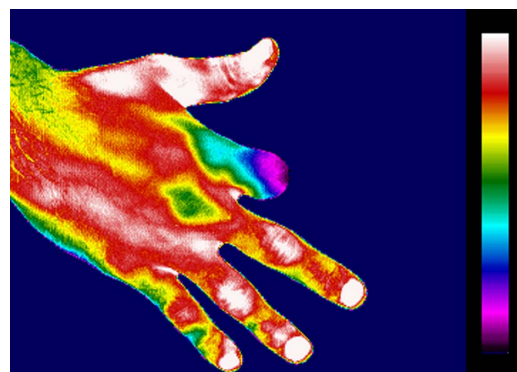


Figure 2.29 MWIR (3–5 mm) image of hand with a missing finger. (*Courtesy of FLIR*)

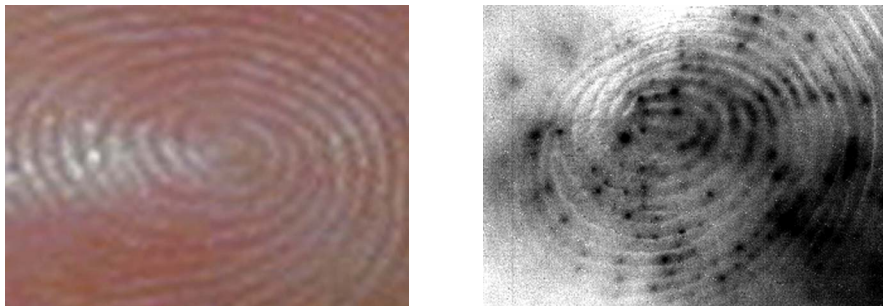


Figure 2.30 Visible (left) and MWIR (3–5 mm) (right) images of a fingertip. (Courtesy of FLIR)

Stress injuries such as repetitive motion injury can also be diagnosed with thermal imaging—the affected limb or digit will show excessive surface temperatures.

Figure 2.30 is an MWIR image of a fingertip taken with a close-up lens. The sweat glands cool the skin through evaporation and thus show up as small cold dark spots, corresponding to a cooler temperature. Thermal imaging is used to study the mechanism of perspiration and the distribution of sweat glands in skin.

Biological systems, like industrial machines, have to manage thermal energy in order to function properly. The chemical reactions that govern the functioning of biological systems are quite sensitive to temperature, and most organisms will die if their internal temperature fails to stay within a particular range. A failure to properly regulate the temperature of living tissue may be due to environmental causes, disease, injury or some other condition, and the detection of thermal anomalies in tissue is often a vital part of biological and medical research. Scientists use thermal imaging to measure temperature, since it makes it possible to monitor the surface temperature of organisms at many points simultaneously without physical contact. Surface temperatures can sometimes be used to determine the internal temperature of an organism, especially in cases where the organism is fairly small, as is the case with hummingbirds, shrews and insects, for example. This hummingbird in Fig. 2.31 shows a peak surface temperature around the eyes of 31.6°C (88.88°F), as measured by a calibrated MWIR camera.

An interesting case of an insect's failure to maintain body temperature is found in Japan. The Japanese honeybee *Apis japonica* has developed a novel defense against predatory hornets. When a hornet approaches a hive, the bees will often sense its chemical odor. They will mass around the hornet in a ball and begin shivering their muscles rapidly, creating a hot blanket around the hornet. The temperature inside the ball reaches 47°C (116.6°F), which is one degree hotter than the maximum temperature that the hornet can withstand, but only one degree cooler than the maximum temperature the bees can withstand. The bees are right at the edge of survival and are just barely able to kill the hornets without killing

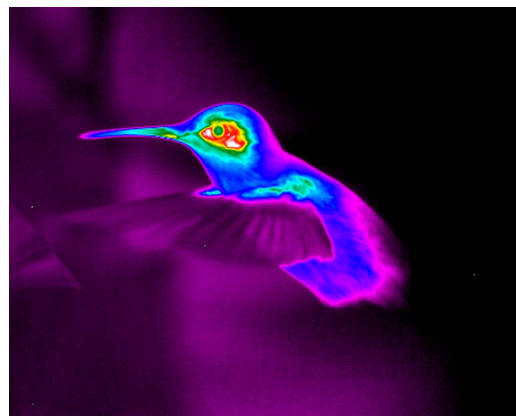


Figure 2.31 Hummingbird in flight—MWIR (3–5 mm). (Courtesy of FLIR)



Figure 2.32 LWIR image of a bee ball (left) and visible image of a dead hornet dragged by bees (right). (Courtesy of Dr. Masato Ono, Tamagawa University, Tokyo)

themselves, a close match in a thermal “arms race.”⁷ The left image in Fig. 2.32 shows a LWIR image of a ball of bees taken with an uncooled microbolometer camera. Note the maximum temperature of the ball’s surface is about 43 °C (109.4 °F), according to the pseudocolor bar along the top of the image (white is equivalent to 48 °C [118.4 °F], pink is just a bit colder). The right image in Fig. 2.32 shows a dead hornet being dragged out of the hive by worker bees that have just killed it with a ball.

Thermal Imaging in Astronomy

As mentioned in the introduction, astronomers have used imaging technology to extend celestial observation over a large range of the electromagnetic spectrum. Infrared telescopes are part of this modern family of instruments. They are able to see thermal phenomena that are not apparent to visible-light instruments. Some of these infrared telescopes are ground-based, usually on mountaintops or

⁷Ono et al, “Unusual thermal defence by a honeybee against mass attack by hornets,” *Nature*, **377**, 334–336 (1995).

other locations that reduce the effects of the atmosphere on observation. Other instruments are flown on orbiting platforms, eliminating the effects of atmospheric absorption. We have seen some interesting effects on terrestrial objects caused by solar loading, and the same effects are seen on other objects warmed by the sun. For example, during a lunar eclipse, the Earth blocks sunlight from reaching the moon for as much as 70 minutes. Right before the eclipse, the moon's surface has been heated to very high temperatures by the sunlight. When the sunlight is blocked, the moon no longer shines with reflected light, but it glows with its own heat.

Figure 2.33 is an image of the moon made by the SPIRIT III telescope on the MSX (Midcourse Space Experiment) satellite during the total lunar eclipse in September of 1996. The image has red pseudocolor added, where the lighter the shade of red, the higher the surface temperature. SPIRIT stands for SPatial InfraRed Imaging Telescope, an instrument that has, among other sensors, an infrared imager consisting of a scanned array of silicon detectors in a **cryostat** cooled with solid hydrogen. These cooled detectors can image in six wavebands between 4.2 and 26 μm .⁸ This particular image was made through a passband filter with a center wavelength of 4.29 μm . Note the white circular "hot spots" on the surface. These are impact craters, where denser, subcrustal rock material was exposed by meteor impacts. The dense rock on the crater floors retains heat longer than the powdery crust material, and thus the crater floor glows brighter in IR light for a longer time during an eclipse, when the solar loading is interrupted by the earth's shadow. The **cooling curves** obtained from a time series of images like this one can be used to obtain information about the physical properties of the surface.

The brightest spot in this image is the crater Tycho, the youngest of the large impact craters on the moon. Tycho can be easily seen through binoculars when the moon is full. It has a dramatic pattern of radial lines, known as rays, which are remnants of the rock ejecta blown out of the moon's surface during the meteor impact that created the crater. The rock on the bottom of the crater is fairly fresh, i.e. it has not been exposed long enough to pulverization by micrometeor impacts. When we look at Tycho, we are seeing the dense rock beneath the crust of the moon that holds heat longer than the lower-density crust outside the impact area.

Thermal imaging is a powerful tool that enables us to see objects in the absence of visible light without having to provide illumination, and to see through certain thin materials that absorb visible light. But thermal imaging requires temperature differences: it is very hard to discern an object that is at the same temperature as its surroundings. Seeing through material is fairly limited, since thermal infrared light cannot penetrate more than a few millimeters of material before it is completely absorbed. If we want to see objects through greater thicknesses of material, we need to image with much longer or shorter wavelengths of light. The next chapter travels to the long-wavelength region of the spectrum, a region where light can

⁸Bartschi et al., "The spatial infrared imaging telescope III," *Johns Hopkins APL Technical Digest*, 17(2), 215–225 (1996).

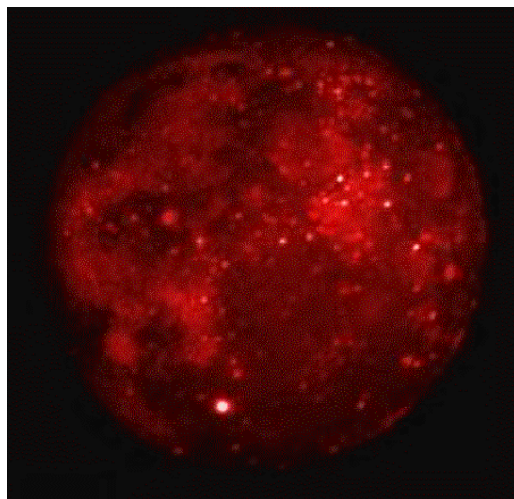


Figure 2.33 Eclipsed Moon imaged in 4.29- μm waveband. (*Courtesy of DCATT Team, MSX Project, and BMDO*)

be highly penetrating and temperature differences are not required, enabling the production of images completely unlike anything seen so far in this tour of the electromagnetic spectrum.

Chapter 3

Microwave and Millimeter-Wave Imaging: Piercing the Veil

The appearance of the world changes dramatically when we image using light wavelengths radically different from the wavelengths of visible light. Infrared and ultraviolet images of familiar objects such as people and butterflies are often different from their corresponding visible-light images (as seen in the last two chapters), but the objects or scenes are nearly always recognizable, and most materials that are opaque in visible light are also opaque in these wavebands. These similarities in the general appearance of objects in both visible and invisible light break down sharply at both ends of the electromagnetic spectrum. As seen in the introduction, visible light falls roughly in the middle of the spectrum plotted in a **logarithmic scale**—for the purposes of this discussion, think of infrared, visible and ultraviolet wavebands of light as medium-wavelength wavebands, or **medium light**, to coin a term. Medium light is strongly emitted and absorbed by the atoms and molecules in matter, and thus is not able to penetrate through more than a few millimeters of solid material. Very short and very long wavelengths of light (which one could call **extreme light**) tend to penetrate much deeper into the surface of materials that are absorbent to medium light, and therefore the surface one actually ends up imaging is often quite different from the surface that is apparent to visible-light imaging.

A good example of this property is x-ray imaging. We cannot see the bones in our hand with visible light—the skin is all we see. But x rays (light with very short wavelengths) pass through the skin with very little absorption, until they encounter the bones beneath. The reason for this is that x rays have such high energy that they tend not to interact with the outer electrons in atoms and molecules—instead they transfer energy to the inner electrons, which they are much less likely to encounter: the outer electrons in atoms and molecules give matter its physical volume—the inner electrons are localized within a tiny region near the core of atoms. Extreme light at the other end of the spectrum (the long wavelength end) interacts with matter in a very different way from x rays, but with some of the same effect—materials become transparent. Microwaves (light with very long wavelengths) can pass through many meters of dry sand or kilometers of water ice before they reflect off what lies buried beneath. Microwaves have such long wavelengths and their photons have such corresponding lower energy that they tend to transfer energy to

matter very gently, over much longer distance scales than is the case with medium light. Examples of these phenomena appear in this chapter, which explores the long-wavelength end of spectrum, and in the next chapter, which explores the short-wavelength end of the spectrum.

The long wavelength end of the spectrum is, for the purposes of this discussion, light with wavelengths on the long side of the extreme infrared band. This region of the spectrum covers wavelengths from about $100\text{ }\mu\text{m}$ to 1 mm (the **sub-millimeter, or sub-mmW band**), wavelengths around several millimeters (**millimeter-wave, or mmW band**) and the 10 mm to 1 m region (the **microwave band**). Figure 3.1 illustrates this part of the spectrum. Beyond microwaves lies the **radiowave band**, which most people associate with wireless transmission of information rather than imaging technology. The farthest this visual exploration will venture in the long wavelength direction of the spectrum is a wavelength of $\sim 73\text{ cm}$, which lies in the microwave band. At wavelengths longer than about 1 m , imaging becomes problematic. We can certainly *detect* radio waves with wavelengths longer than a meter with a simple antenna, but making a highly directional sensor (like a dish antenna) that can generate what we consider to be images (distinguishing objects and representing their shape) is quite difficult to do.¹

The images we will examine are generated by both passive and active imaging systems. Millimeter-wave energy is emitted naturally from objects at terrestrial temperatures in much the same way as long-wave infrared energy, though at a much lower intensity. This natural emission rapidly becomes weaker at increasingly longer wavelengths; as a result, microwave energy emissions from terrestrial objects cannot easily be used for imaging, since any signal tends to get buried in the inherent noise of the imaging sensor. Microwave imaging of terrestrial objects requires active illumination: the technique of **radar** (radio detection and ranging).

The discovery of the long-wavelength region of the electromagnetic spectrum happened about the same time as the discovery of x rays. Heinrich Hertz was a professor of physics in Germany in the late 19th century. He is credited with discovering radio waves with a simple experiment involving a spark gap to generate radio waves and a loop antenna to detect them. Hertz correctly surmised that the waves were light waves with very long wavelengths (on the order of a meter), having observed many of the wave-like properties of visible light in these waves, including reflection and refraction. The Hertz is a unit of frequency (cycles per second) named in his honor.

The sub-millimeter, millimeter-wave and microwave bands are remarkably useful for scientific and industrial imaging applications, since they can be used to see through material that is opaque to more conventional imaging wavebands (visible, IR, and UV). For instance, microwave imaging has been used to see through the permanent and visibly-opaque cloud cover on the planet Venus. Millimeter-wave imaging technology can see through clothing and other thin

¹This is due to the wave-like properties of light; **diffraction** effects drive the requirement that a highly directional sensor be many wavelengths in diameter. There are ways to synthesize a large antenna out of an array of smaller, interconnected antennae.

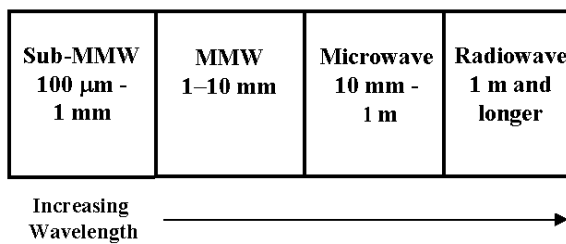


Figure 3.1 The long-wavelength region of the electromagnetic spectrum.

materials, enabling detection of explosives and drugs concealed on a person. In both cases, the materials (clouds or cloth) appear opaque in the visible waveband (or IR and UV) because the size of the “scatterers” (clouds or cotton fibers, in these two examples) is similar to the wavelength of the light. Much shorter wavelength visible light is scattered so many times as it traverses the material that the original direction of the light wave (and thus any image) is lost. We can regain our ability to image through these materials by going to increasingly longer wavelengths where the waves we use average over the scatterers and so suffer only slight deflections in their path. If the wavelength of the energy is sufficiently long, we can even use it to image through materials as opaque as many meters of dry sand in the desert, like Superman’s famous “x-ray vision.” All the above examples are presented in this chapter.

Sub-Millimeter-Wave Imaging: T-Rays

The sub-millimeter waveband is one of the newest wavebands to be used for imaging. This region of the spectrum falls into a technology gap between the photodetectors used in the LWIR waveband and antenna-type detectors for millimeter-wave and microwave imaging. Detectors based on tiny thermometer elements working in the submillimeter waveband have to be cooled to very low temperatures and suffer from low sensitivity, while conventional thermal sources and special lasers used for active illumination are low in brightness. Recent technology developments in solid state device physics have now made it possible to generate and detect extremely short pulses of light with wavelengths of a fraction of a millimeter. Sub-millimeter imaging is also known as T-ray imaging, since the frequency corresponding to lightwaves with sub-millimeter wavelengths is in the terahertz range.²

This imaging technology has interesting applications in packaging and materials inspection, and it is in the early phases of commercialization for this purpose and others.³ Extremely short pulses of sub-millimeter light are transmitted through a sample and detected on the other side by a tiny antenna. The detected signal contains both density and composition information, since the chemical properties

²1 Terahertz = 1 trillion cycles per second.

³David Zimdars and J.V. Rudd, “Opening the terahertz window,” *Photonics Spectra* (May 2000).

of the material can change the pulse shape, making it possible to determine what is inside packages without opening them.

Figure 3.2 shows a T-ray image of an integrated circuit inside a plastic package. The plastic absorbs very little T-ray energy, and thus the interior components (circuit and conductive traces) are revealed. Figure 3.3 shows two T-ray views of a leaf: one after it has been freshly picked and one after 48 hours. Water in the leaf absorbs T-rays, and the right image shows that water has selectively evaporated from the leaf. The color bar indicates the relative water concentration inside the leaf. The edges of the leaf have dried out, but there is still water contained in the center of the leaf and in the veins. Figure 3.4 shows a milk chocolate bar with almonds in both visible and T-ray light. The T-ray image is a map of the time it takes for a T-ray pulse to reach the receiver. Changes in the thickness of the bar change the pulse arrival time, since the T-rays slow down in the chocolate. The letters on the bar are visible because they change the thickness of the bar—the letters are molded into the surface. The almonds produce a sharp increase in the pulse arrival time, since the T-rays are slowed down even more than in the chocolate.

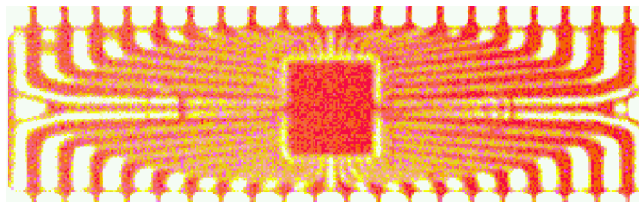


Figure 3.2 T-Ray image of an integrated circuit. (*Courtesy of Prof. Daniel Mittleman and Prof. Martin Nuss*).

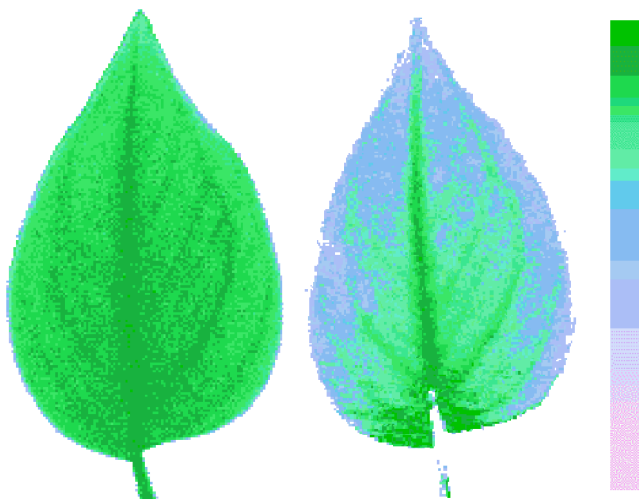


Figure 3.3 T-ray image of a leaf at 48-hour interval. (*Courtesy of Prof. Daniel Mittleman and Prof. Martin Nuss*).



Figure 3.4 Visible (top) and T-ray (bottom) images of a milk chocolate bar with almonds. (Courtesy of Picometrix, Inc.)

Millimeter-Wave Imaging: Seeing Through Clothing and Fog

The region of the spectrum known as the millimeter-wave (abbreviated mmW) is located in the wavelength range between 1 and 10 mm. Millimeter-wave images are radically different from what our eye sees, since one millimeter is about 2,000 times the wavelength of visible light. Millimeter-wave imaging is only just beginning to be used for practical purposes, as the technology that makes it possible to synthesize vision with reasonable frame rates in the mmW band is a fairly recent development. Early imaging work in this waveband during the 1960s and 1970s utilized a single detector scanned over a scene with a moving mirror. This scanning technique could take many minutes to generate an image, making it suitable for static scenes only.

Applications such as covert imaging for security purposes or aeronautical navigation require a fast frame rate (20–30 frames per second). For example, airports, courthouses and other areas have devices to control the entry of contraband materials, but there are limitations to their effectiveness. Metal detectors are employed to scan people, but this does not prevent the introduction of nonmetallic contraband (drugs, explosives, etc.) carried in under clothing. It is not always practical or desirable to pat down everyone that comes through a security checkpoint, and there are health and safety concerns associated with x-ray imaging of people, although x rays of luggage are fairly useful in finding contraband.⁴ A waveband of electromagnetic energy is needed that penetrates clothing to image what is underneath without any health risk. Ideally, the person being scanned would emit these lightwaves naturally, eliminating the need to illuminate the subject.

⁴I say fairly, since it can be difficult to interpret luggage x-ray images, and there is a large probability for human error.

Electromagnetic energy in the 3-mm waveband fulfills this requirement. It is naturally emitted by skin in sufficient amounts to produce a passive image (like thermal infrared), and it freely penetrates thick clothing (unlike thermal infrared).⁵ Cloth is composed of molecules that absorb strongly in the visible, ultraviolet and infrared wavebands, and most cloth is thick enough to absorb all or most of the light in these wavebands. If we want to see through clothing, we need to use a waveband like mmW that can image through clothing with enough spatial resolution to image some small concealed object like a plastic bag full of cocaine. Figure 3.5 shows a schematic diagram of this phenomenon. The contraband becomes a dark blob on the skin, because it emits less millimeter-wave light than skin. X-ray imaging can certainly see through clothing (and denser materials), but it requires a source of x-ray light to illuminate the target.

Figure 3.6 shows two views of a man. The left image, made with visible light, shows a man who does not have the appearance of being armed, but the mmW image on the right reveals that he is concealing two handguns under his sweater. This striking image is the weak glow from his body in the 3-mm waveband. The high degree of contrast in the mmW image is due to the optical properties of the dissimilar materials present. The person appears much brighter than the guns because of differences in **emissivity**. Human skin emits more mmW energy than metal or plastic at the same temperature, so the guns appear darker in the image than the skin, and stand out in sharp relief in the mmW image. Clothing is thin and passes the skin's emission of mmW light easily, but the thick metal of the guns completely blocks the emissions, creating a shadow. Plastic explosives and drug packets have similarly lower emissivities relative to human skin, and are usually thick enough to block mmW light from the skin, making them easy to detect as well.

Millimeter-wave imaging is also known in military circles as all-weather imaging, since it has the ability to produce picture-like images in conditions that defeat other imaging systems. Radar imaging, which will be discussed shortly, can “see” through weather and atmospheric conditions, but the imaging technology does not easily allow for high-resolution imaging at high frame rates, which is what one needs to land a plane in heavy fog.

Many plane crashes have resulted from poor visibility due to inclement weather conditions during landing. A pilot running low on fuel has little choice but to attempt a landing in fog or drizzle; these conditions are very difficult to see through with visible or IR sensors. Visible light has a wavelength around 500 nm, or 0.0005 mm, which is comparable to the size of water droplets in fog. When light waves pass through a medium with scattering particles that are comparable in size to the wavelength of the light waves, there is strong scattering, which is why fog appears as a uniformly white substance to our eyes. In the case of mmW imaging systems, the wavelength of light detected is several millimeters. There is very little

⁵The 3-mm waveband is widely used because it corresponds to a “window” in the atmosphere, with little absorption by water compared to wavelengths on either side of the 3-mm waveband. This region of the spectrum is also known as the W band.

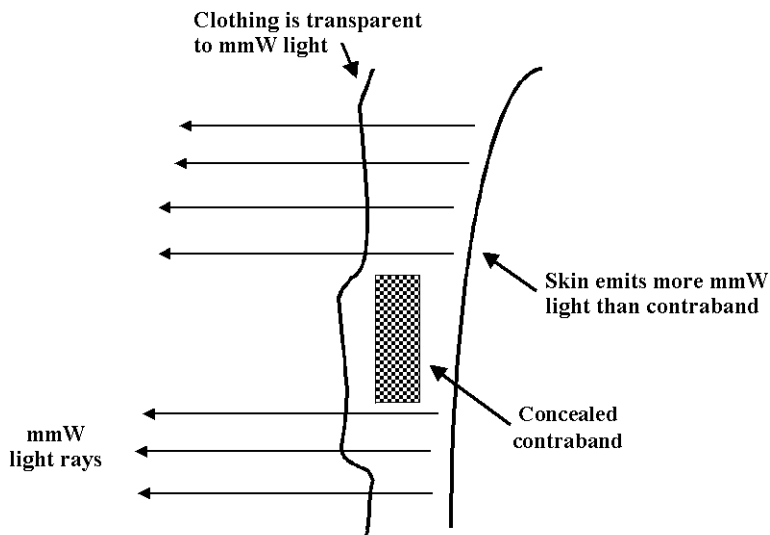


Figure 3.5 Side view of concealed contraband under clothing.

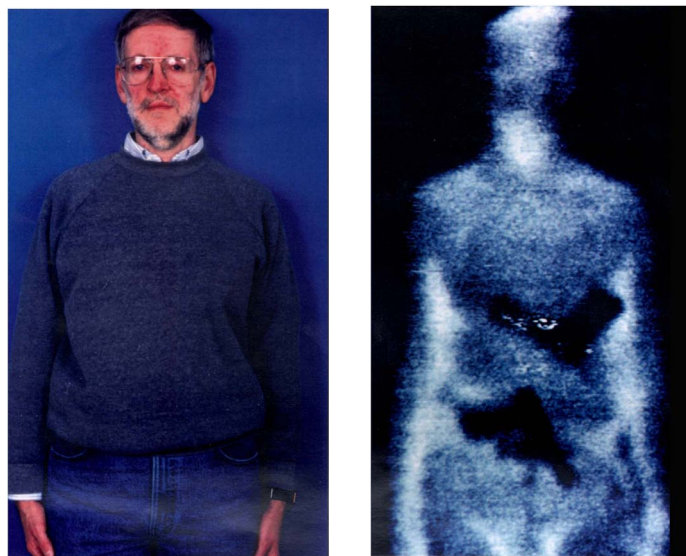


Figure 3.6 Visible (left) and mmW (right) images of a man with concealed guns. (*Courtesy of Millivision Corporation*)

scattering of this light off of water droplets that are thousands of times smaller than the wavelength of visible light.

Commercial millimeter-wave imaging cameras may soon help pilots land in zero-visibility weather, in cases where the unaided eye and infrared imaging systems are effectively blind. Figure 3.7 shows two views of a runway at Shafter

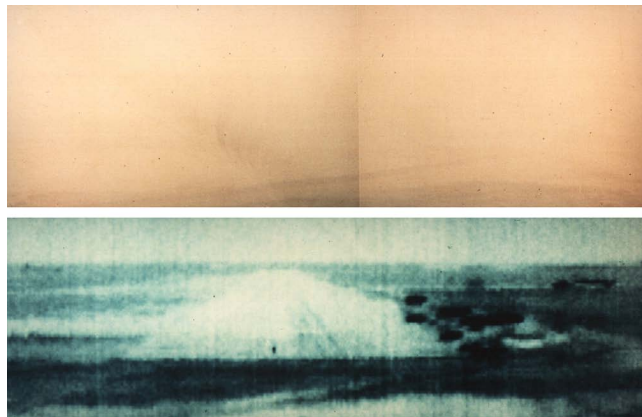


Figure 3.7 Visible (top) and mmW (bottom) images of a runway in zero-visibility fog. (Courtesy of Northrup Grumman Corporation)

Airport in Bakersfield, California. The visible-light image shows nothing but white fog, common early in the morning at this particular airport. The mmW image (3-mm waveband) reveals the runway and control tower at a resolution on the order of 60 by 60 pixels. This resolution is limited by the size of the imaging system, which is set by the space available in the nose of a typical aircraft. This imaging system uses a 46-cm-diameter plastic lens that focuses mmW light onto a focal plane array of miniature mmW receivers. These convert the mmW image into electrical signals that are processed into video that drives a visual display in front of the pilot's face.⁶ Figure 3.8 shows a mmW camera developed by TRW mounted on the nose of an aircraft with the aerodynamic nose shroud removed. The white plastic lens is visible in the front.

Radio Astronomy: The Foundations of Radio-Wave Imaging

For thousands of years, astronomers were limited to visible-light bands of the EM spectrum by the physiology of the human eye. The 20th century brought the development of instruments that could view planets, stars, galaxies and other more exotic celestial objects over much larger regions of the electromagnetic spectrum than the visible band. Today, astronomers have observed the heavens over a spectrum that is 20 powers of 10 wide in wavelength of the electromagnetic spectrum, from radio waves to gamma rays—an amazing achievement that is largely unknown outside of astronomy circles. One important branch of “invisible-light” astronomy is radio astronomy, the observation of celestial objects in the 1-cm to 10-m region of the electromagnetic spectrum.⁷

Our ability to image celestial objects with light from the radio portion of the electromagnetic spectrum has its roots in the 1932 discovery of radio waves of

⁶Yujiri et al., “Passive millimeter-wave camera,” *SPIE Proc.*, **3064**, p. 15, 21–22 April 1997 [doi: 10.1117/12.277080].

⁷John Krause, *Radio Astronomy*, Cygnus-Quasar Books, Powell, Ohio (1986).



Figure 3.8 Passive millimeter-wave camera on aircraft nose. (*Courtesy of Northrup Grumman Corporation*)

unknown origin coming from outer space. Karl Jansky was an American radio engineer studying thunderstorm interference of radio transmissions. He noticed that his experimental directional antenna (shown in Fig. 3.9) received signals in the 14.6-m waveband—signals that could not be linked to any terrestrial radio sources. The apparent position of the source was a point in the sky; this source moved around in the sky and reached peak strength every 24 hours. This suggested that the source's position was fixed with respect to the stars, rising and setting like a star, which meant that it had to be extraterrestrial.

Today we know that this object is a powerful celestial radio source located at the center of our galaxy. The object is located in the portion of the sky nearest the constellation Sagittarius, and since it is the brightest radio source in Sagittarius, it is known as **Sagittarius A**. In fact, Sagittarius A is one of the most powerful radio sources in the sky as seen from Earth. It is believed to be a massive rotating **black hole** that generates intense radio waves through the interaction of electric and magnetic fields with matter that is being sucked into the hole.⁸ Radio astronomers have built on Jansky's pioneering work, creating large, highly directional **dish antenna** systems that can scan images of the sky in the radio band of the electromagnetic spectrum. This technology has led to the discovery of many unexpected types of celestial objects such as **pulsars**, **quasars**, and vast **molecular clouds**, all of which emit radio waves.

⁸Ibid.

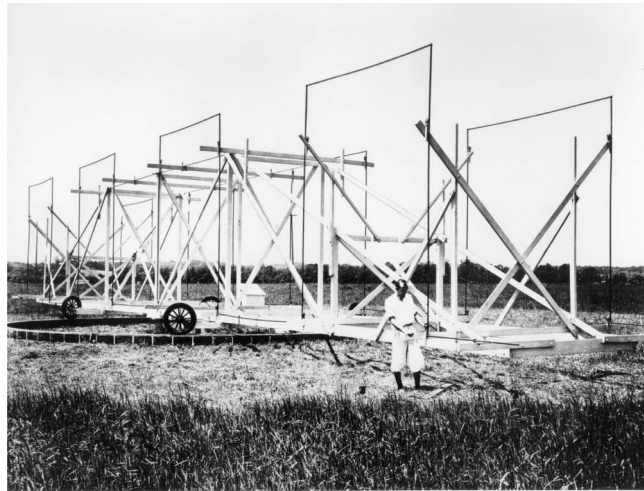


Figure 3.9 Karl Jansky and his steerable 14.6-m wavelength radio antenna. (*Courtesy of NRAO/AUI*)

Figure 3.10 shows an image of the entire sky as seen with lightwaves in the microwave band. The elliptical shape of the sky image is a projection of the spherical surface of the sky called an **Aitoff projection**. The pseudocolor bar on the right side of the image indicates the relative intensity of microwaves, white being the strongest intensity and black the weakest. The light used to form this image has a wavelength of 73 cm, and is emitted by sources such as pulsars, **supernova remnants**, and gas-filled, star-forming regions of space. Stars emit very little energy at this wavelength, therefore this radio image of the sky is essentially devoid of stars! The light we see in this image is generated by mechanisms that are nonthermal in nature, meaning that the objects that emit light

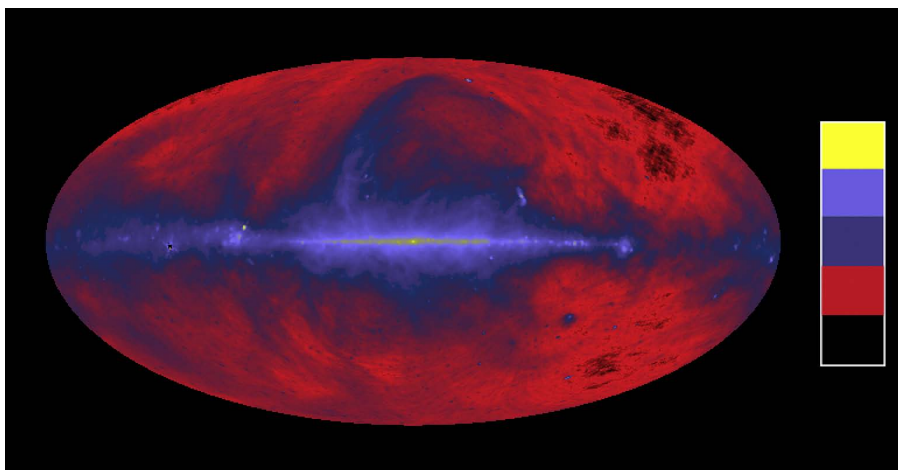


Figure 3.10 Microwave sky in the 73-cm waveband. (*Courtesy of NASA*)

are not generating it through heating (as, for example, is the case with a light bulb filament). Because stars generate most of their light by glowing incandescently at a very high temperature, most of the light they emit is at much shorter wavelengths than the radio band. They are weak radio emitters (except in special cases where they “flare,” in which case the interaction of the flare’s magnetic field and the hot gas of the star results in powerful bursts of nonthermal radio emissions.)

This image of the radio sky is in galactic coordinates, which puts the center of the **Milky Way** (our galaxy) at the center of the image, and aligns the plane of the Milky Way with the “equator” of the image. The horizontal band through the center is radio emission from objects within the plane of the Milky Way and the intense white blob in the center is Sagittarius A, the compact radio source mentioned earlier. The large looping structures represented by light blue pseudocolor are remnants of “bubbles” blown by star-forming processes within vast molecular clouds of gas. If we could see light with a wavelength of 73 cm with our eyes, the dominant structures in the sky would be these large bubbles and structures, all having an apparent size much greater than either the full moon or the sun. The image was made by combining data taken in the 1970s from three large radio telescopes: Jodrell Bank in England, the Effelsberg 100-meter in Germany, and the Parkes 64-meter in Australia. As the last two names imply, all of these telescopes are massive dish antennae tens of meters across that can be steered around to scan the sky. The first two antennae are in the Northern Hemisphere, the last in the Southern, making it possible to obtain a data set of the entire sky.

For comparison, consider the sky we see with our eyes, as seen in Fig. 3.11. This image, like Fig. 3.10, is made up of many small color photographs that are “stitched” together by a computer algorithm into an Aitoff projection. The broad band of stars is an edge view of the plane of our galaxy, what we call the Milky Way. The Milky Way contains many radio sources, which is why Figs. 3.10 and 3.11 look similar along the “equator”; yet there are important differences. Sagittarius A, located at the very center of this image, is not visible to our eyes, since intervening dust clouds scatter and absorb the visible light emitted by it. Since the wavelength of microwaves is much longer than the size of interstellar dust particles, the microwave light used to make Fig. 3.10 propagates freely through the dust.⁹ The large loops and swirls of microwave-emitting hydrogen gas are too cold to glow with visible light, and thus are absent from the visible sky.

Devices such as radio telescopes that “see” with microwaves and radio waves (1 cm to 10 m or more) do not work on the same principle as human eyes and standard photographic cameras. Figure 3.12 is a schematic of a typical radio telescope. Instead of a lens, these imaging systems have directional antennae that are sensitive in a cone-shaped or fan-shaped beam pattern. Instead of an FPA of sensors similar in function to the human retina, many radio astronomy imaging systems have a

⁹As mentioned earlier, the scattering of waves by objects depends on the size of the objects relative to the wavelength of the wave. Visible light is highly scattered by dust particles, which are typically the order of a wavelength in size. Conversely, radio waves pass freely through dust, as they are many times longer in wavelength than the size of the dust particles.

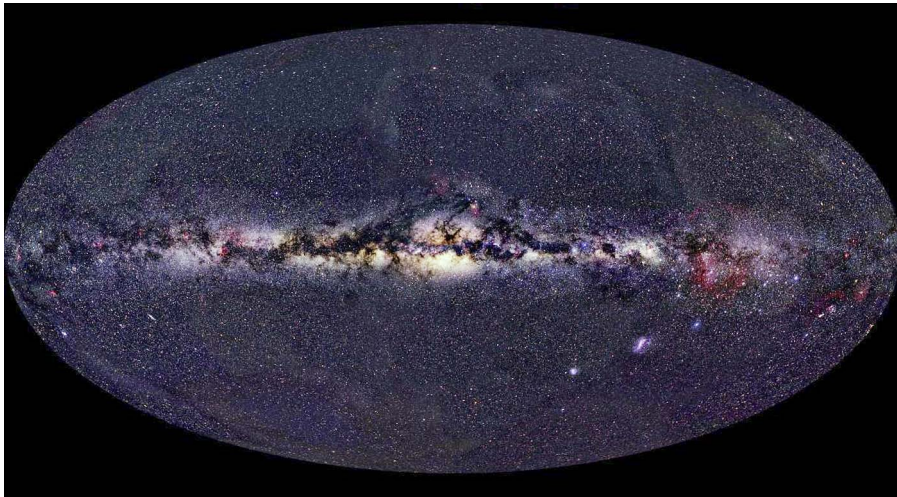


Figure 3.11 Aitoff projection of the visible sky. (Courtesy of Axel Mellinger)

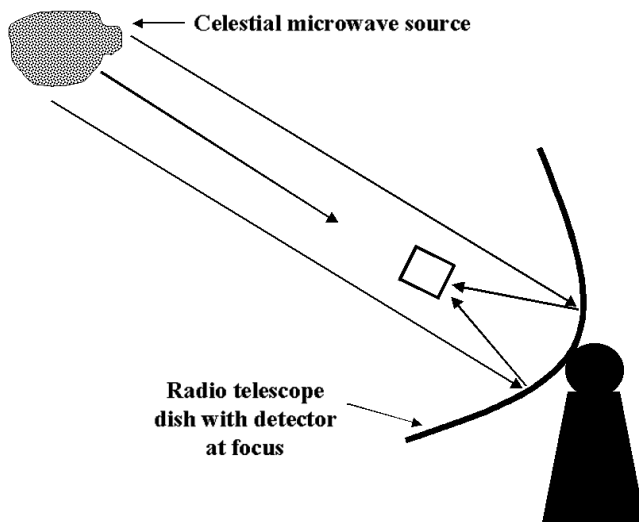


Figure 3.12 Block diagram of radio telescope and celestial source. The telescope has a narrow field of view (the “beam”) that scans the source.

single detection element, since the scenes they image do not change on the time scales of a scan; and therefore a multielement detector is unnecessary. The antenna assembly is scanned back and forth across the target to build up an image, much as an inkjet printer builds up an image by scanning back and forth across a piece of paper, forming an image line by line.

The disadvantage of scanning an image pixel-by-pixel is that the scene has to stay still during the scan; but this is not a serious problem when recording astronomical image data, since the scene is unchanging over very long time scales.

High-resolution radio telescopes have to be enormously large for two reasons: the phenomenon of wave **diffraction** means that as an antenna gets smaller, its spatial resolution or beamwidth grows larger, which effectively blurs the resulting image. This effect is proportional to wavelength, and in the case of microwaves with wavelengths of ~ 10 cm, antennae have to be tens of meters in diameter to achieve sufficient resolution to study many compact radio objects in the sky. Radio telescopes must also have large collection areas in order to be able to detect distant sources, since more electromagnetic energy is concentrated on the detector. Figure 3.13 shows the Parkes Observatory radio telescope in Australia. This 64-m diameter dish weighs 1000 metric tons, and it images in the microwave band.

Radar Imaging: A Microwave Searchlight

This chapter has thus far presented applications for radio imaging that are passive, i.e., relying on radio emissions from the source or scene, rather than on active illumination. Passive radio imaging of terrestrial objects such as buildings, people, and mountains is possible in the millimeter-wave band, but becomes much more problematic in the microwave band because the intensity of thermally generated radio emissions is extremely low. We need active imaging technology to see terrestrial objects in the microwave band (unless they happen to be microwave transmitters). Active imaging of terrestrial objects with energy from the radio band of the spectrum dates from the 1940s, when **radar** was invented to detect enemy aircraft. Radar stands as one of the most significant advances in imaging technology, and the inventors of radar are often credited with being the people who won World War II for the Allies. Indeed, radar is an extremely powerful imaging tool that makes it possible to see objects at long range, day or night, and in any weather. Radar systems use multiple pulses of radio energy that reflect off of a target and back to a receiver. The amplitude and frequency of the returning echoes contain information about both the geometry and reflecting properties of the reflecting object or material, as shown in Fig. 3.14. Radar on an aircraft or



Figure 3.13 Parkes Observatory. (Courtesy of David McClenaghan, CSIRO)

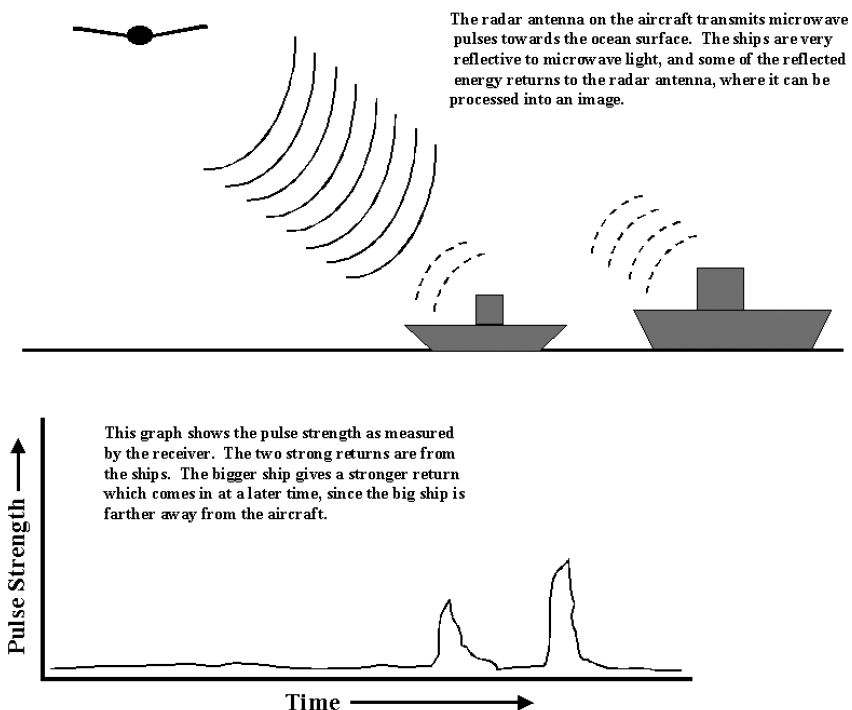


Figure 3.14 Airborne radar system schematic.

spacecraft can create images of Earth's surface (or other planets) by data processing millions of return pulses. The movement of the platform carrying the radar system defines one axis of scan; the image builds up along the direction of flight.

Military radar systems development has resulted in many commercial and scientific applications for radar, and the recent advent of small, high-speed computers has made it possible to generate three-dimensional radar images that require sophisticated image processing. Early radar images tended to be difficult for untrained observers to interpret, largely owing to the unavoidable presence of noise in the radar image caused by scattering of the radar signal by atmospheric phenomena or flocks of birds. It is now possible to eliminate a great deal of this "clutter," as it is called, by using advanced data processing techniques and special antenna hardware.

Recall from the last chapter that electromagnetic waves are scattered weakly when they pass through a non-conductive material that consists of particles that are much smaller than the wavelength of the electromagnetic waves. Because of this property of waves, imaging radar can penetrate through jungle vegetation, ice, snow, and dry sand and soil, revealing concealed or buried objects hidden to our eyes, and in many cases also hidden to infrared and ultraviolet imaging systems. This has led to the use of imaging radar in the field of archaeology. Large-scale archaeological sites are often obscured by windblown sand or vegetation, making them very difficult to study with conventional aerial photography. Imaging radar

flown on the Space Shuttle *Endeavour* in 1994 penetrated through cloud cover and heavy vegetation to reveal the existence of previously unknown temple ruins in the ancient city of Angkor in Cambodia. This system, known as **SIR-C/X-SAR**, illuminated the earth's surface from an orbital altitude of about 160 km. Figure 3.15 is a model of the radar antenna array. This assembly, which measures 4 m by 12 m, fits into the Shuttle's cargo bay. When the bay doors are opened, the antenna can scan the Earth's surface, sending thousands of pulses per second of microwave light that bounce off the Earth's surface 160 km below and back to the antenna.

The complex irrigation system of canals and reservoirs around Angkor is revealed in Fig. 3.16, along with the main temple structures. Archaeologists had only been able to study remnants of the system from the ground, and were unable to "get the big picture" as to how water was distributed. Studying the city from the air with visible or infrared imaging is nearly impossible, as much of the previously cleared area is now hidden by dense rainforest canopy, and the whole region is often covered with clouds. Years of civil war made flying over the Cambodian jungle dangerous, as aircraft sometimes drew ground fire. Radar imaging effectively "sees through" the clouds and much of the rainforest covering, giving a sense of what the city must have looked like in antiquity. The temple structures show up in Fig. 3.16 as rectangular shapes long known to archaeologists. But just above those shapes in the image are subtle, rectilinear patterns that are the ruins of a previously unknown city that predates Angkor.

The SIR-C/X-SAR imaging system flown on *Endeavour* also imaged objects through layers of dry sand. The Sahara desert regions of Northeast Africa were not always as devoid of water as they are today. Approximately 7000 years ago rainfall in the region was sufficient to support the existence of rivers that have long since been buried under several meters of windblown sand. Figure 3.17 shows one of these ancient drainage systems near the Kufra Oasis in southeast Libya. The

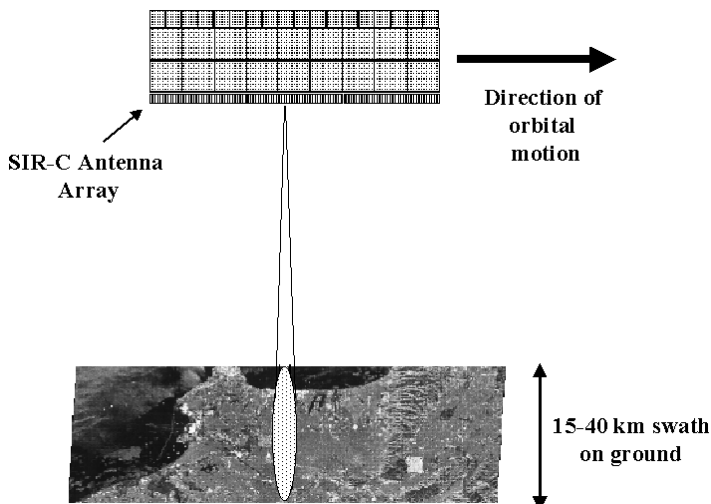


Figure 3.15 Model of SIR-C/X-SAR imaging radar antenna array.



Figure 3.16 Radar image of Angkor in Cambodia. (*Courtesy of NASA*)

ancient drainage system, known as Wadi Kufra, has two branches radiating from the settlements in the top center part of the image. The east branch of the river, which is on the right side of the image, is completely buried in sand and was unknown until SIR-C/X-SAR imaged the area. This information has been used as a “road map” by archaeologists searching for stone-age implements along ancient riverbanks.

Imaging radar has also been used to discover some interesting geological features on Earth. The Antarctic continent is covered with a vast sheet of thick ice that contains 70% of the world’s fresh water. This massive amount of ice is the result of millions of years of snowfall without any melting. The ice sheet is over 4 km deep in places, and contains geologic information such as atmospheric composition and average temperature locked into the layers of ice. There are a number of subglacial lakes: liquid water trapped underneath the layers of ice and warmed from below by geothermal heat.

The largest of these lakes is Lake Vostok. Vostok is Russian for “east,” and Lake Vostok is situated in East Antarctica, near the Russian base Vostok. It is 50 km by 240 km (about the size of Lake Ontario) and lies beneath about 3.5 km of ice. Its maximum depth is 500 m, making it one of the largest lakes in the world. Lake Vostok was unknown until aircraft with radar altimeters flew over the area in the

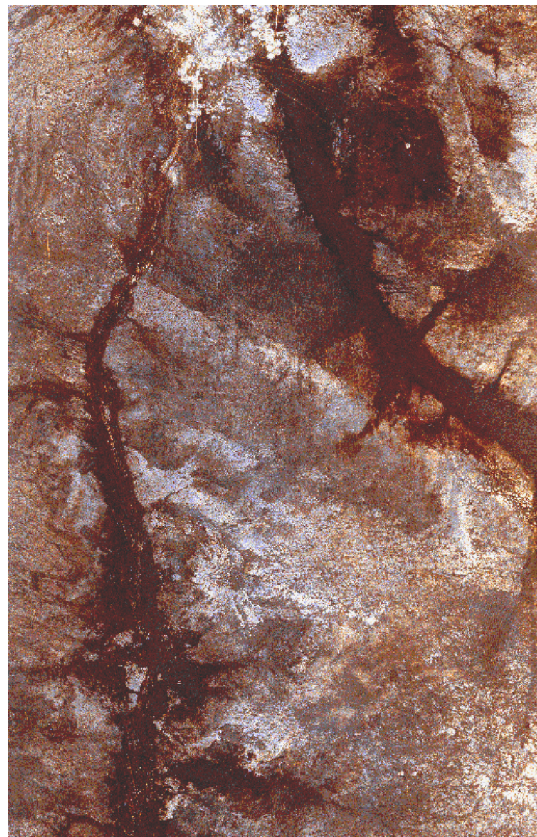


Figure 3.17 Radar image of Wadi Kufra, Libya. (*Courtesy of NASA*)

1970s and discovered regions of ice that had what appeared to be very flat, smooth terrain underneath, which was consistent with the radar signature one would expect to see from liquid water under the ice. Seismic data and satellite imagery later confirmed the existence of the lake and its full extent.¹⁰ Imaging through the ice is possible only in the microwave band of the electromagnetic spectrum, as shorter wavelengths of light are highly absorbed. Microwaves travel through the ice of Antarctica and reflect off the material underneath, mapping the topology of whatever lies beneath; it is as though the ice were removed completely. Figure 3.18 shows a 6-cm-wavelength microwave image of the lake taken by *Radarsat*, a Canadian satellite equipped with imaging radar that flies in a circumpolar orbit, enabling it to scan both the Arctic and Antarctic regions. The image is made of multiple rectangular images that are overlaid. The images are from the **swaths** defined by the orbital path of the satellite. Note the rough terrain surrounding the lake; this is the mountainous topology of the rock beneath the ice sheet. The lake's "surface" appears smooth, since we cannot see the rock beneath the lake, which is effectively shielded by the reflective properties of the liquid water.

¹⁰Oliver Morton, "Ice Station Vostok," *Wired* 8(4), 121–146 (April 2000).

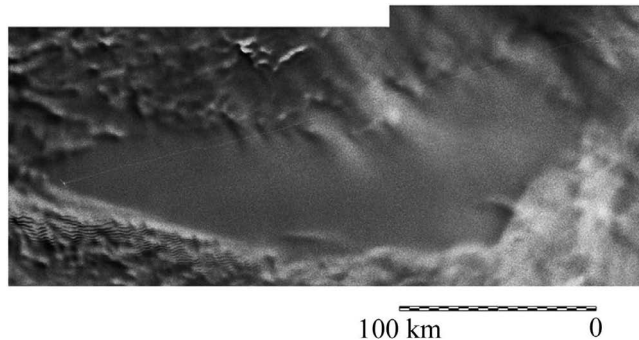


Figure 3.18 Lake Vostok imaged by Radarsat with 6-cm microwaves. (Courtesy of Canadian Space Agency)

Lake Vostok generated tremendous excitement because scientists theorized that there may be a unique ecosystem within the waters that has been cut off from any contact with the outside world for geologic time scales. Plans are being made to drill into the lake and introduce remote sensing devices without contaminating the water inside.

Spacecraft carrying active radar imaging have voyaged to other places in the solar system. The most famous mission of this type is that of the *Magellan* spacecraft, which carried an 8-cm-wavelength **synthetic aperture radar** system to Venus. Venus is a most inhospitable planet, with a surface temperature of 500 °C (932 °F) and a highly poisonous atmosphere of sulfuric acid clouds at a pressure 92 times that of the sea-level pressure on Earth. The entire surface is covered with this thick cloud cover, and no one knew what the planet's surface actually looked like until the *Magellan* spacecraft imaged it between 1990 and 1994. Like the SIR-C radar on the space shuttle, the orbital motion of *Magellan* defines the scan axis. Nearly the entire planet's surface was imaged during hundreds of orbits around the planet.

Figure 3.19 shows two views of Venus. The visible-light image, taken by the *Galileo* spacecraft, reveals nothing about the surface of the planet, only dense white clouds of sulfuric acid droplets. But the microwave image generated from *Magellan* data shows a rugged terrain of meteorite impact craters, valleys, and mountains. The coloration is a simulation of how the surface of the planet might appear to a human eye, based on color video information transmitted by the Soviet *Venera* landers, the only spacecraft to land on the surface of Venus.¹¹ The shading is an indicator of surface relief, where the lighter shading indicates the higher altitudes and the darker colors the lower altitudes, respectively. The lighter areas are highlands, the Venusian equivalent of continents on earth. The white patch in the middle of the image is an area known as Maxwell Montes, where the

¹¹The four successful Soviet *Venera* landers only operated for a few hours at most before succumbing to the incredibly hostile atmosphere. Barring some very sophisticated advances in spacecraft and spacesuit technology, astronauts will likely never walk upon the surface of Venus.

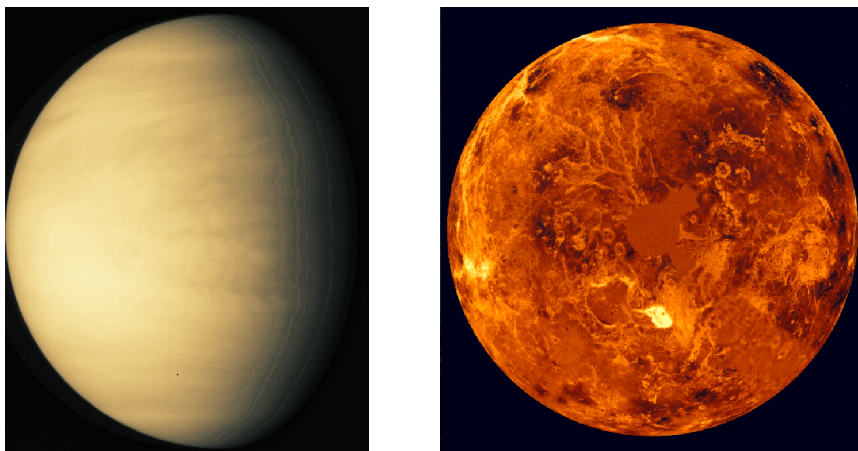


Figure 3.19 Visible and microwave images of Venus. (Left image courtesy of Calvin J. Hamilton, right image courtesy of NASA)

highest mountains on the planet are grouped together. This radar image of Venus demonstrated for the first time that the geology of Venus has some similarity to the geology of earth, as the **trough-and-ridge** structure seen on many parts of Venus looks exactly like trough-and-ridge structures seen on the Pacific and Atlantic Ocean floors. Note that the surface of Venus is only partially illuminated by the sun in the *Galileo* image, while the entire surface of Venus is illuminated and imaged by microwaves in the *Magellan* image.

Magellan was able to image small surface features of Venus in addition to large-scale formations. Figure 3.20 is a radar image of Maat Mons, a volcano 8 kilometers in height imaged at an oblique angle to the surface. Note the variations in the brightness of the image—these are caused by differences in the surface texture. Texture has a strong effect on the reflectivity of a surface to microwaves. As with Fig. 3.19, the choice of colors was suggested by the *Venera* color video data, although here the brightness is proportional to the signal return strength rather than the relative altitude of the surface.

Small-Scale Imaging Radar

Radar imaging can also be applied to imaging applications involving everyday objects and distance scales. Developments in high-speed data acquisition electronics at Lawrence Livermore National Laboratory have led to a novel type of radar called MIR, an acronym that stands for micro-power impulse radar. This short-range radar, which operates in the 15-cm microwave band, can see through opaque materials like soil and concrete, and can create high-resolution images of buried objects. MIR technology forms the heart of a new type of portable mine-sensing device that can detect plastic landmines that elude conventional metal detectors.

The radar uses ultrashort pulses of radio waves to detect boundaries between materials. A small amount of radio light is reflected at the boundary between



Figure 3.20 Radar image of Maat Mons. (*Courtesy of NASA*)

two dissimilar materials (dirt and a mine's plastic casing, for example). The radar receiver records the strength of the return echo and the round-trip time (the time for the signal to be emitted, reflect off a boundary, and return). Because the pulses are extremely short, the radar can be used at very close range and is ideal for imaging landmines buried several centimeters deep in soil.

The left image in Fig. 3.21 is a photograph of an antitank mine prior to burying at the Nevada Test Site. MIR imaging enables a mine sweeper to image "slices" of the mine, corresponding to different depths under the soil surface. This slicing method makes it much easier to discriminate between a mine and a square piece of buried metal debris, as the internal structure of the mine has a distinctive shape or "signature," as shown in the right image in Fig. 3.21. The mine is the large square object with a roughly circular opening in the middle, with a bright square object within the circle. This circular opening is the pressure plate that triggers the mine when a tank drives over it, and the bright object within is the detonator. MIR imaging has many potential uses in the fields of law enforcement and archaeology for the detection of objects hidden inside concrete, within stone, or behind brick walls. Figure 3.22 are visible-light and MIR views of a 30-cm-thick concrete slab

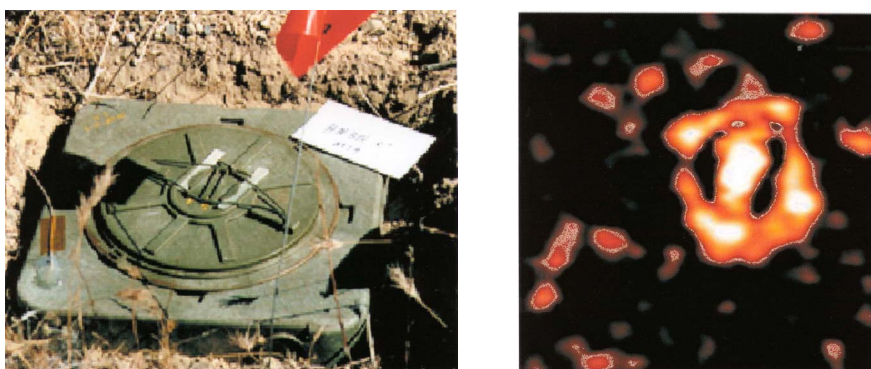


Figure 3.21 Visible (left) and MIR (right) images of an antitank mine. (*Courtesy of Lawrence Livermore National Laboratory*)

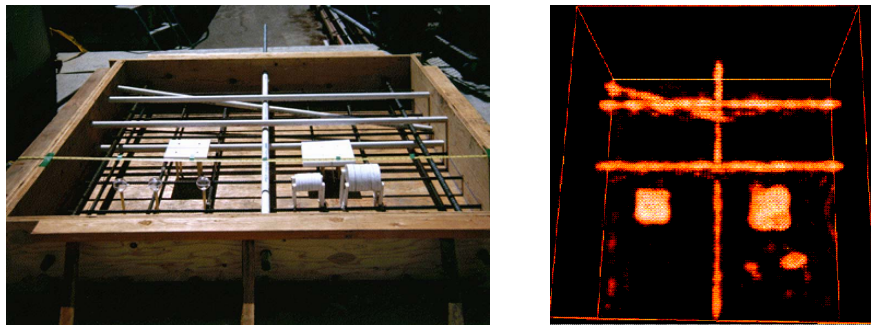


Figure 3.22 Visible (left) and MIR (right) images of metal structures in concrete slab. (Courtesy of Lawrence Livermore National Laboratory)

containing metal rods and plates. The concrete has yet to be poured in the visible image.

Light in the long-wavelength region of the electromagnetic spectrum has the ability to penetrate through certain non-conductive materials that are very opaque to visible, infrared and ultraviolet light. This penetrating power is most apparent at the longest wavelengths, in the radio and microwave bands, and is a consequence of its gentle interaction with matter—the photons impart very little energy to the material they encounter. The shorter wavelengths in this region of the spectrum (sub-mmW, mmW) are not as penetrating, but they can be used to generate images with much higher resolution than radar images. Millimeter-wave imaging has some of the penetrating power of radar combined with the advantage of much higher frame rates, making real-time, long-wavelength synthetic vision available. Sub-millimeter-wave imaging gives us the ability to see through thin, low-density materials and, in some cases actually determine the chemical composition of the material. Astronomers use microwave light to detect and image celestial material too cold to emit at shorter wavelengths. The penetrating power of microwaves also gives us the ability to see exotic celestial bodies invisible to conventional visible-light imaging due to the obscuring effects of intervening matter.

The next chapter will consider extreme light at the other end of the spectrum—lightwaves with wavelengths so short and frequencies so high that they interact with matter more like particles, an interaction characterized by deep penetration of matter combined with abrupt transfers of energy.

Chapter 4

X Rays and Gamma Rays: Crookes Tubes and Nuclear Light

Light becomes something quite strange and powerful in the region of the electromagnetic spectrum in which wavelengths are shorter than in the near-UV ultraviolet waveband. This region, shown in Fig. 4.1, includes the **extreme ultraviolet**, x-ray and gamma-ray wavebands. X rays and gamma rays are electromagnetic waves with such short wavelengths (and correspondingly high energies) that they interact with matter very differently than do the longer wavelengths discussed previously. For the purposes of the following discussion I shall describe x rays and gamma rays in the context of **photons**, which are particles of light. Light has a dual nature: it can behave as a wave sometimes and a particle at other times. When it is a particle, or photon, it is best described by its energy; that is more appropriate than describing this light as a wave of a particular wavelength.

This method of description reflects the way these high-energy photons interact with matter: when an x ray or a gamma ray does interact with an electron or a nucleus in material, there is a significant amount of energy transferred to a very localized area, like a bullet hitting a metal target. That is why x rays and gamma rays are considered radiation and are dangerous to living beings—the energy transfer often produces permanent chemical changes, which can lead to cellular mutation in living tissue. At the same time, when x rays and gamma rays traverse matter, the probability that they will interact with the matter is fairly low, and if the material is thin or has a low **atomic number**, then a significant fraction of the light can pass through with little or no loss. The thicker or denser the material, the more reduction in the intensity of a transmitted beam of x rays or gamma rays. This is the principle behind **radiography**: the film or detector receives more radiation along a path of lower density or thickness through the material being imaged, and less along a thicker or denser path. Thus, the bones of the hand appear darker in a radiograph than the surrounding flesh, since the photographic film is less exposed.

X rays and gamma rays were not initially recognized to be electromagnetic waves at all. Their wave-like properties were hard to detect because their wavelength (~ 10 nm and smaller) is very short, and it was not until some years after the discovery of x rays that it was conclusively shown that they are electromagnetic waves, producing **diffraction patterns** on a screen after passing through a narrow metal slit or a crystal.

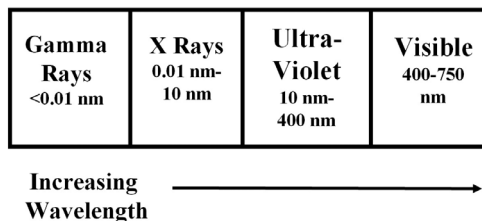


Figure 4.1 The short-wavelength region of the electromagnetic spectrum.

X rays and gamma rays are best known for their ability to enable imaging through opaque material, since they are not absorbed by matter nearly as much as is light with longer wavelength. While microwave light can be used to image through certain materials such as dry dirt or sand quite well, it cannot penetrate effectively through conductive materials such as water or metal. X rays and gamma rays, however, can penetrate all known materials. While visible light may only penetrate a few millimeters deep into human tissue, x rays at modest energies will easily pass all the way through a person's chest, and a person could easily look nearly transparent in a gamma-ray image – bones and all. Electromagnetic waves at these high energies are generally not encountered in daily life except when generated by medical or scientific instrumentation, or (in the case of gamma rays) by radioactive isotopes such as **Cobalt-60**. Luckily for us, the atmosphere blocks nearly all x-ray and gamma-ray light impinging on Earth from extraterrestrial sources.¹

We can imagine what it would be like for a hypothetical creature that could see only in the x-ray or gamma-ray wavebands to be on Earth. Such a creature would have a very hard time passively imaging anything in our atmosphere at sea level, since there would be virtually no available x-ray or gamma-ray illumination from the sun or other celestial sources, and none at all from ordinary (non-radioactive) objects. This situation is quite different from what a creature with thermal infrared vision (like the Predator in the movie of the same name) would encounter, for example. People, animals, trees and machines all emit thermal infrared light and can be observed without any active illumination being present. Observing people or trees or other objects using light in the x-ray and gamma-ray bands would require active illumination of a very specialized nature. Ordinary light sources such as lightbulbs emit invisible light (infrared and ultraviolet), but they do not emit x rays or gamma rays because the filaments in lightbulbs are simply not hot enough. A lightbulb filament would have to be heated to *millions* of degrees to glow incandescently with x-ray light. Making incandescent x rays with even modest energies in a terrestrial laboratory is very hard to do.² It takes extreme conditions such as those encountered in a nuclear explosion or nuclear fusion reactor to achieve these temperatures.

¹X-ray and gamma-ray astronomy requires detectors mounted on high-altitude platforms such as rockets or satellites.

²Incandescent means that the material producing the x rays is doing so by heating alone; this requires enormously high temperatures (>1 million degrees centigrade).

How, then, are x rays made? For the most part, they are made the same way they were made by their discoverer, Prof. Wilhelm Konrad Roentgen (1845–1923), a German physicist. Roentgen's method is not incandescent—rather it uses electrons as x-ray generating “bullets.” Roentgen used an evacuated tube with two metal electrodes inside connected to a high voltage power supply. The electric field generated by the power supply accelerates electrons emitted from a hot wire filament inside the tube and smashes them into a metal plate. The electrons penetrate into atoms in the metal surface and are sharply deflected by the electric fields near the nuclei of the atoms. This deflection produces x rays. The energy of the resulting x rays is described in units that include the acceleration voltage of the x-ray tube. We thus speak of x rays as having energies of kilo-electron volts, or keV. One keV is the kinetic energy of an electron that has dropped through a potential difference of 1000 volts (1 kV). This same method of generating x rays is still used today. Typical medical x-ray tube voltages are 100 kV; we would describe the resulting x rays as having energies of 100 keV, corresponding to a wavelength of about 0.01 nm (10^{-11} m), or about a tenth of the radius of an atom. Electron-volt units are a convenient way to describe their energy, even when the source has nothing to do with voltage, as in the case of thermal x rays. In fact, this descriptive convention applies to all sorts of high-energy particles produced by particle accelerators, radioactive decay, or astrophysical sources.

Gamma Rays

Gamma rays are electromagnetic waves with extremely short wavelengths, shorter than x rays, and with correspondingly higher photon energies. They are not caused by the rearrangement of electrons within an atom; rather, they are generated by changes in the nuclei of atoms, changes due to nuclear decay processes where a nucleus changes internally and releases energy. Their energies correspond to binding energies of **nucleons** in the nucleus. We can generate gamma rays by assembling concentrated masses of radioactive material or by using powerful particle accelerators to accelerate electrons to very high energies and then smash them into a target material, causing nuclear processes to occur. The gamma-ray band encompasses all photons with energies above about 100 keV, corresponding to wavelengths of 0.01 nm (10^{-11} m) and shorter. What is the difference between x rays and gamma rays? There is no particular boundary between the two (since the naming convention is somewhat arbitrary), but most scientists consider x rays to be produced by electron-atom interactions, whereas gamma rays are in the million electron-volt or higher energy range and are produced by nuclear processes such as radioactive decay.

X-ray and gamma-ray imaging technology is quite different from imaging technology described in previous chapters. The wavelike properties of light at medium wavelengths (visible, UV and IR) make it possible to image this light onto detectors, much like our own eye, which like a standard film camera consist of a detector material in a focal-plane array (the retina) and an imaging optic (the crystalline lens) that focuses a scene onto the retina. X rays and gamma rays do

not lend themselves well to being focused by lenses or mirrors — they pass right through the material of the optics without deflection. But lenses and focal-plane arrays are not the only way to make an image from electromagnetic waves. As seen in the last chapter, microwave imaging systems create images through precise timing of return pulses of microwave energy, or, in the case of passive imaging, by scanning a reflective parabolic antenna with a single detector at the focal point back and forth over a scene. Most x-ray and gamma-ray images are made an entirely different way, by a method that does not require a lens. The images we traditionally associate with x rays are what are known as shadowgrams; that is, a recording of an object's shadow projected onto a detector material, which could be a piece of film or a sheet of glass coated with phosphor. Thus, the object under investigation has to be placed between the x-ray source and the detector, as shown in Fig. 4.2. It should be noted that there are techniques for focusing x rays—there will be an astronomical example later.

The discovery of x rays was one of the last great scientific achievements of the 19th century, and heralded a new age of physics. Wilhelm Roentgen was awarded the first Nobel Prize in physics for a discovery he made in 1895: he found that a Hittorf tube (a special evacuated tube with metal electrodes and a high-voltage current) produced penetrating rays that fogged photographic film and made fluorescent materials glow even when the tube was covered with black paper to block the ultraviolet light that was also emitted by the tube.³ Figure 4.3 shows a schematic drawing of a Crookes tube, an x-ray tube similar to the Hittorf tube used by Roentgen. The low-voltage power supply heats a filament called a cathode, causing electrons to “boil off”—a process known as thermionic emission. The 100 kV supply accelerates the electrons towards the metal target, known as the anode. These high-voltage electrons strike the target, causing electrons in the metal atoms to emit x rays.

Roentgen’s system produced x rays with sufficient energy (about 40 keV) to image the bones in his hand using a fluorescent screen. He soon discovered that photographic film is also sensitive to x-ray light. Figure 4.4 shows the first x-ray image made with film; it is a picture of the hand of Roentgen’s wife Bertha with her wedding band clearly visible. X-ray images are also known as radiographs.

Doctors began using x rays as part of diagnosis and treatment of patients almost immediately after Roentgen announced his discoveries. The exploitation of x-ray imaging technology by the medical establishment raced far ahead of any understanding of their effects, particularly on living tissue. The publicity blitz that followed the initial discovery engendered a great deal of quackery and misinformation, some of it with tragic consequences. Some writers in the early 1900s claimed that x rays could raise the dead, cure blindness, or treat skin conditions, and many people were injured permanently with large, uncontrolled doses of x rays. X rays (and gamma rays) are dangerous in high doses because

³A translation of Roentgen’s original paper can be found in E.C. Watson, “The Discovery of X Rays,” *American Journal of Physics* **13**, 284 (1945).

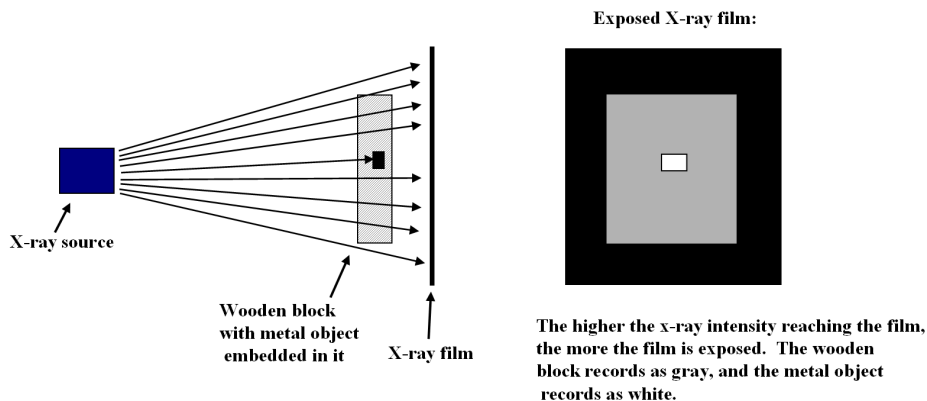


Figure 4.2 Schematic of an x-ray shadowgram.

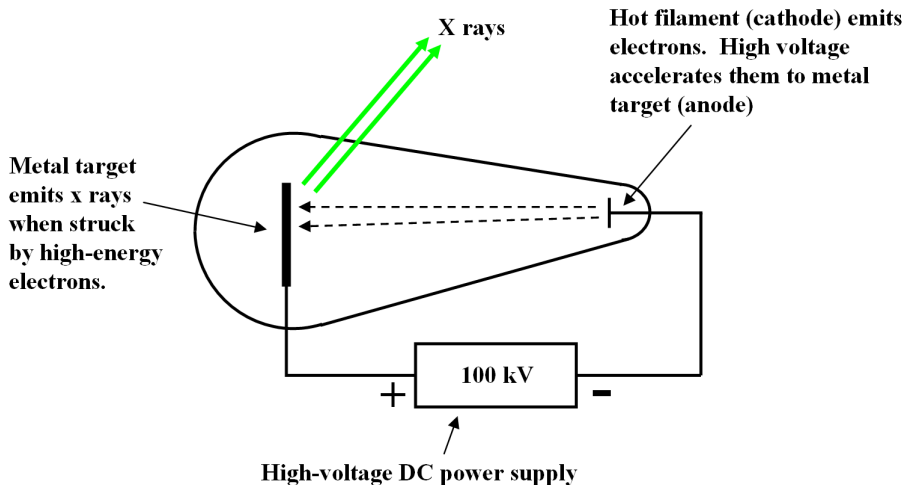


Figure 4.3 Crookes tube schematic.

they cause powerful chemical reactions deep within tissue. Ultraviolet light is dangerous for the same reasons, but it can only penetrate a few millimeters into the skin, in contrast to X rays and gamma rays, which can easily travel all the way through a person's body. These rays can damage cells deep within tissues by causing ionization, a process whereby electrons are knocked off atoms and molecules, making the ionized material much more chemically reactive than it would be in an un-ionized state. The first indications that x rays were harmful to tissue were damaged hands, since early x-ray technicians often used their hands as test objects for medical x-ray equipment. After repeated exposure, they often developed basal-cell skin cancer and other serious conditions. Figure 4.5 shows the hands of Mihran Kassabian (1870–1910), an early x-ray researcher who died of cancer that was almost certainly due to his high occupational x-ray dosage. His condition required numerous amputations of fingers as the necrosis progressed. Kassabian's laboratory is shown in Fig. 4.6. Note the numerous x-ray images on the



Figure 4.4 The first radiograph. (*Courtesy of the American College of Radiology*)



Figure 4.5 Hand of Mihran Kassabian, x-ray martyr. (*Courtesy of American College of Radiology*)

wall and the handheld fluoroscope he is using to examine the chest of a gentleman, and that neither Kassabian nor the subject is wearing any kind of shielding or protection from the x-ray source.

Doctors were not the only people with an intense interest in x rays. In contrast to every other waveband of invisible light, x rays were brought to the public's attention immediately after their discovery. Within a year of Roentgen's discovery, x-ray studios were popping up that sold bone portraits for home display. An advertisement for an x-ray studio is shown in Fig. 4.7. These studios were like

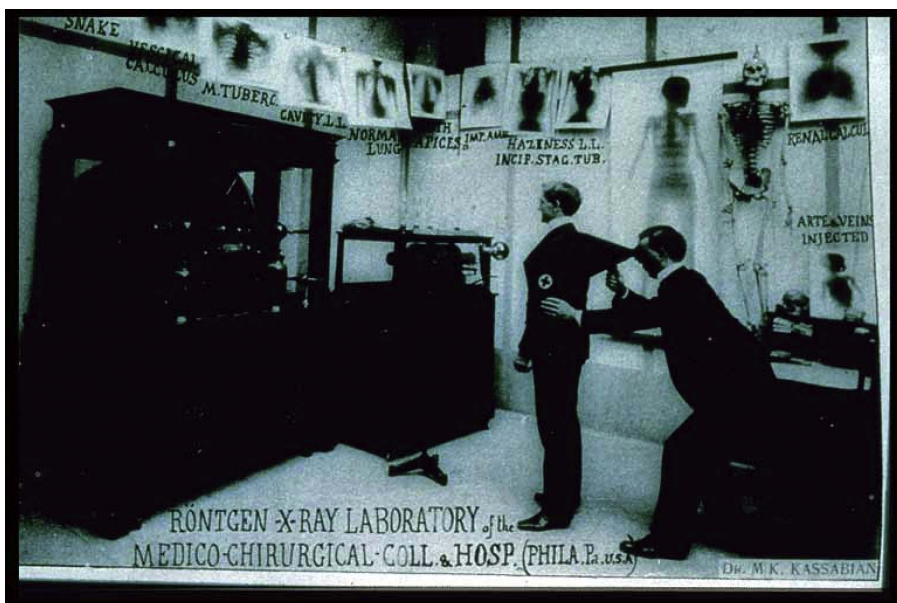


Figure 4.6 Kassabian's x-ray laboratory. (Courtesy of American College of Radiology)

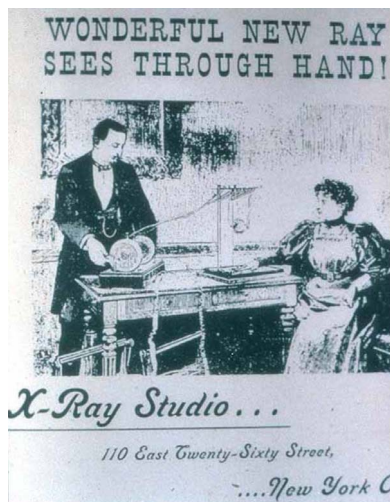


Figure 4.7 X-ray studio advertisement. (Courtesy of American College of Radiology)

regular photographic studios of the period, a far cry from modern radiology laboratories. In keeping with the décor of *fin-de-siècle* parlors, some commercial x-ray power supplies were built into beautiful wooden cabinets. Figure 4.8 shows an advertisement from the early 1900s for the massive and expensive Nelson machine, an electrostatic generator powered by a hand crank that was used to power x-ray tubes.

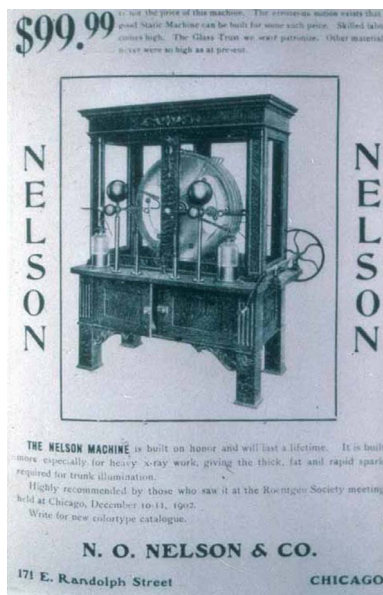


Figure 4.8 Nelson x-ray power supply. (*Courtesy of American College of Radiology*)

Before public awareness brought legislation and regulations to control x-ray apparatuses, the systems were fairly common and were often operated by untrained workers. The infamous Tricho machine was used in beauty salons to remove unwanted hair from women. Many Tricho patients suffered permanent injury (including ulceration, carcinoma and death) from x-ray exposure, injury that sometimes did not present symptoms for many years. Another well-known unregulated x-ray device is the shoe-fitting fluoroscope used in many shoe stores all over America until the 1950s. Some of these machines were still in use until the 1970s and 80s, their owners apparently unaware of federal regulations prohibiting them. These machines would show the shoe salesman and the customer the relative position of the bones of the foot inside the shoe. Many people would play with the machines and subject their feet to extended doses of x rays. An example of such a machine is shown in Fig. 4.9.

There are several viewing ports to enable the shoe salesman and the customer to see the fluoroscope screen simultaneously. On one model called the Foot-O-Scope, there were three different buttons for men, women and children, but all gave the same intensity of x rays! Figure 4.10 shows an early radiograph of a foot inside a shoe. Note the many nails in the heel of the shoe.

The “x-ray craze” happened as it did because there are few technical challenges to making x-ray images. The only implements needed to make live x-ray images are a Crookes tube, a high-voltage power supply, and a phosphor-coated glass screen. Objects placed between the Crookes tube and the screen cast an x-ray shadow onto the phosphor, which converts the x rays striking it into a visible green glow. These components are relatively easy to make, and many amateurs have built x-ray sources this way, although this is no longer a very popular activity because of



Figure 4.9 Shoe-fitting fluoroscope. (*Courtesy of Dr. Paul Frame*)

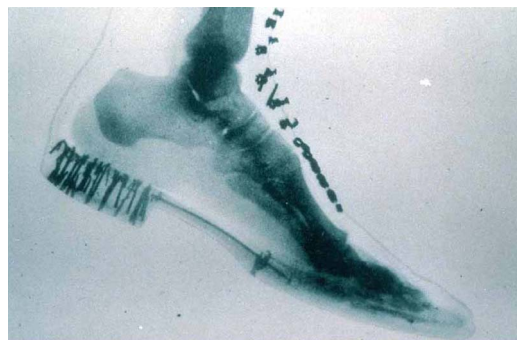


Figure 4.10 Radiograph of a foot in a shoe. (*Courtesy of American College of Radiology*)

the inherent or perceived hazard of an unshielded x-ray source. Some professional radiographers have used x-ray imaging for artistic purposes. Figure 4.11 shows a lily imaged via x rays onto a fine-grain radiographic film used for mammograms. The energy of the x-ray photons is chosen to give a pleasing contrast in the image. X-ray photons with too high an energy would pass through the flower with very little reduction in intensity, making the image very weak. For aesthetic reasons, the image is a positive one: dark shades of gray represent the densest regions of the flower, the opposite of how most medical x-ray images are presented.

Today, x-ray imaging and x-ray vision are part of our cultural vernacular, more than any other invisible-waveband imaging technology (although thermal infrared imaging has now penetrated the collective consciousness of the public). *X: The Man with X-ray Eyes* was a popular movie in the 1950s about a scientist who



Figure 4.11 X-ray shadowgram of a lily. (Courtesy of Steve Meyers)

develops a serum that enables him to see through objects. This ability becomes uncontrollable and makes his life a nightmare.

Superman was equipped with x-ray vision that could only be stopped by lead barriers. Figure 4.13 shows an image from *Destination Moon*, a comic book in the *Tintin* adventure series. Two detectives (named Thomson and Thompson) are trying to find a skulking skeleton, not realizing that they have been seeing each other imaged with x rays in a fluoroscope screen.

Just as infrared energy can penetrate materials used in artwork to reveal information about hidden material, so x rays are often used to examine old paintings and other works of art. Figure 4.14 shows two views of an oil painting called *An Old Man in Military Costume*, by Rembrandt. The radiograph shows that there is only one painting on the canvas. Any other oil painting underneath would almost certainly be revealed in the radiograph, since many oil-based pigments contain lead and other metals that absorb x rays and cast shadows in diagnostic radiographs. The x-ray diagnosis of paintings is often used to verify their authenticity, since many art forgers paint forgeries over paintings on old canvases.

Art conservationists and archaeologists also use a variety of other x-ray imaging systems originally developed for medical applications. Conventional medical and industrial radiography only yields 2D information about the interior of objects. The x-ray CAT scan is a method of capturing 3D x-ray images that has been applied in some interesting non-medical applications. CAT scanning technology has been a boon to modern medicine since its invention by Sir Godfrey Hounsfield in 1972. CAT stands for computer-aided tomography, the process of building an image up from many small “slices” through an object. The slices are made by measuring the absorption of a thin beam of x rays projected through the object along a particular path. The amount of x-ray absorption is a measure of “column density” along that path. The CAT scan machine measures the column density along thousands of paths through the body, paths that intersect each other in defined ways. The computer determines the x-ray density of each intersecting point in space within the

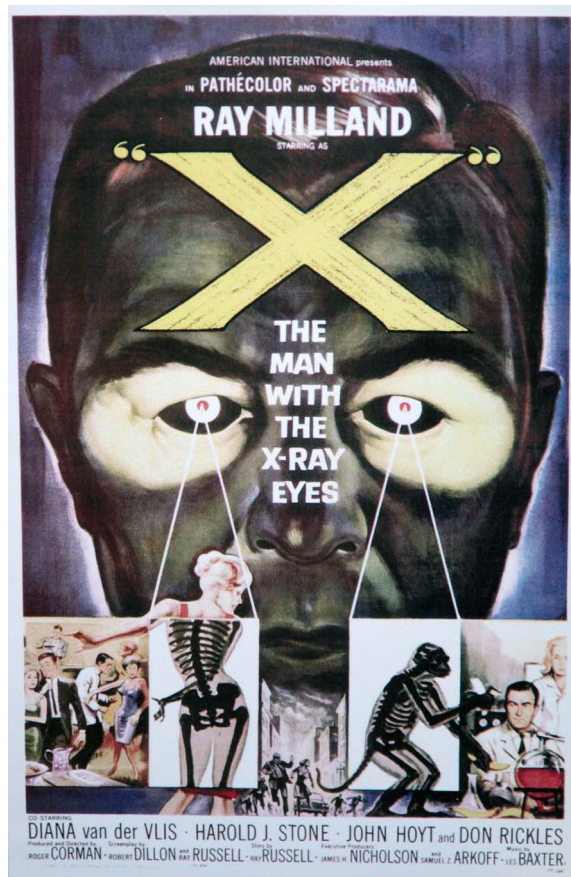


Figure 4.12 Movie poster from *X: The Man with the X-ray Eyes*. (Courtesy of MGM)

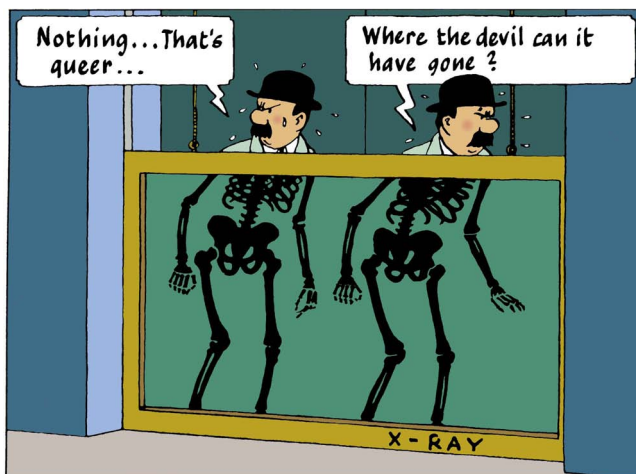


Figure 4.13 Thomson Twins imaged by a fluoroscope. (Courtesy of Hergé/Moulinsart) © Hergé/Moulinsart 2010.



Figure 4.14 Visible and x-ray images of a painting. (*Courtesy of the J. Paul Getty Museum, Los Angeles*)

object from the thousands of column density measurements. By comparing x-ray density values (known as CT numbers) of material samples to the CT number of a hidden object in the scan, it is possible to identify the actual material of a particular feature of the CAT scan. For example, a medical CAT scan of a human torso with a bullet lodged within would return a CT number equivalent to that of lead for the volume elements in the scan corresponding to the location of the bullet, effectively locating the bullet's position. The 3D image of the bullet's location would guide a surgeon's decisions about how best to extract it.

A beautiful example of x-ray CAT scanning technology put to novel use is in the field of archaeology and the examination of mummified remains.⁴ Figure 4.15 shows an Egyptian mummy from the 22nd dynasty (945–715 BCE) being loaded into a CAT scanner at St. Thomas' Hospital in London. The mummy, a priestess by the name of Tjentmutengebtu, currently resides in the British Museum. The curators there chose her as the subject of a CAT-scan analysis because she was mummified at a time when the mummification process was at its technical prime. Also, her *cartonnage*⁵ casket is tightly sealed and cannot be opened without damage, requiring non-invasive techniques to study the mummy inside.

Figure 4.16 shows a frontal CAT-scan image of the mummy. Several amulets are visible: a hawk at the breastbone and a winged figure (possibly a vulture) at the pubis. A winged goddess was placed over the front surface of the neck, and an unidentified object was attached to the left arm. A small object is visible over

⁴Baldock et al., “3-D reconstruction of an ancient Egyptian mummy using x-ray computer tomography,” *Journal of the Royal Society of Medicine* 87, 806–808 (1994).

⁵Cartonnage is made of linen glued together in many layers with a stucco or gesso coating on top. It is strong and has an excellent surface for painting.



Figure 4.15 Mummy being loaded into CAT scanner. (*Courtesy of Prof. Clive Baldock*)



Figure 4.16 CAT-scan front view of a mummy. (*Courtesy of Prof. Clive Baldock*)

the umbilicus, and a winged scarab is over the feet. A four-sided plate covers the abdominal left flank incision where the liver, stomach, lungs, and intestines had been removed.

Figure 4.17 is a side view of the mummy showing a cross section of the casket and the mummy's skull. Special image-processing software reconstructed the shape of the head and precisely imaged the molars; the software computed the location of boundaries in three dimensions and generated a surface model. A forensic odontologist determined Tjentmutengebtu's age at death as being between 19 and 23, based on the degree of wear in the molars.



Figure 4.17 CAT-scan cross section of a mummy. (*Courtesy of Prof. Clive Baldwin*)

A more recent CAT scan of a mummy is shown in Fig. 4.18. This mummy, a man named Nesperennub, is also on display at the British Museum.

X-ray inspection of cargo is commonplace in airports and seaports today, and large-scale x-ray machines can scan trucks, trains, containers, and palettes, looking for contraband. Occasionally, these scans reveal hidden items inside of trucks, as shown in Fig. 4.21, an image made with **backscatter x-ray** technology.⁶ This type of x-ray imaging is based on a scanned beam of x rays that scatter off of atoms in the object back to an imaging detector, rather than on a detector placed on the far side of the object that records transmitted x rays. The system preferentially detects the presence of light chemical elements, such as carbon, oxygen and nitrogen. Heavier atoms also backscatter x rays, but they then absorb them, reducing the signal from metals, for example. Light atoms are found in explosives, drugs and people, all of which are routinely smuggled across borders. The brightest objects in Fig. 4.21 are those that backscatter x-ray light with the least absorption, and they are all made of low atomic number atoms: the marijuana concealed behind a false wall at the front of the trailer, the wooden support structure for the secret compartment, the tires, and the fuel in the tank.

X-ray searches of living people are problematic on many levels, though the health risk is essentially nil. Years of negative press and misinformation has generated a strong public perception that ionizing radiation at any dose is potentially lethal, even though people are constantly exposed to radiation in their daily lives, whether they like it or not. People will not easily consent to having their bodies x rayed, even though the dose administered by modern x-ray equipment is generally only a fraction of the natural radiation from outer space that one is exposed to during an airplane flight at 30,000 feet, for example. The backscatter x-ray imaging technology used to make the truck image also offers a way to image through clothing to detect contraband. Only minimal radiation is deposited deep within living tissue, since the x rays only have to penetrate clothing and not the

⁶W. Sapp et al., “A mobile x-ray system for non-intrusive inspection of vehicles,” *Proceedings: Harnessing Technology to Support the National Drug Control Strategy, ONDCP International Technology Symposium*, 14-19-14-25 (Chicago, 1997).



Figure 4.18 X-ray CAT scan of the mummy Nesperennub, an Egyptian priest who was mummified in approximately 800 BCE. (*Photo courtesy of SGI*)



Figure 4.19 A color image of Nesperrenub's cartonnage casket, which has remained sealed for almost 3000 years. (*Photo courtesy of the British Museum*)



Figure 4.20 A close-up x-ray CAT scan of Nesperrenub's hands showing various ornamental rings. (*Image courtesy of SGI*)

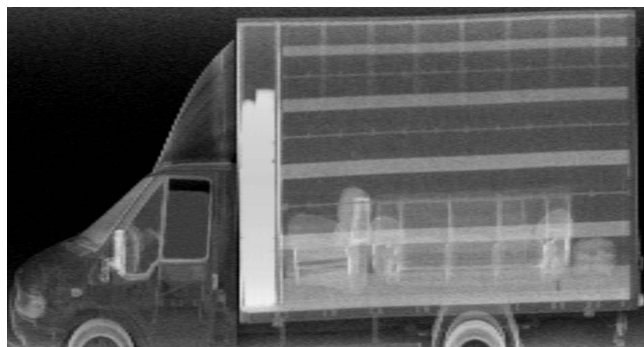


Figure 4.21 Marijuana concealed behind a false wall in a truck. (*Courtesy of American Science and Engineering*)

whole body. Figure 4.22 shows a backscatter x-ray image of a man with multiple concealed weapons under his clothing. Weapons or other contraband concealed inside the body cannot be detected by this method. Note that a slight shadow of the folds of his trouser legs can be seen. Hair is completely absent from this image—its very low density does not produce a strong backscatter signal. At this time, these machines are gaining greater adoption for airport security because of problems in the last few years with terrorists smuggling bombs and explosive materials onto planes. The real danger is surgically implanted bombs that would be virtually impossible to detect without a full body transmission x ray of the suspect.

High-Energy Astronomy

The sky contains many remarkable objects that emit x-ray light through processes that are extremely dynamic, and many of the more exotic objects in the sky

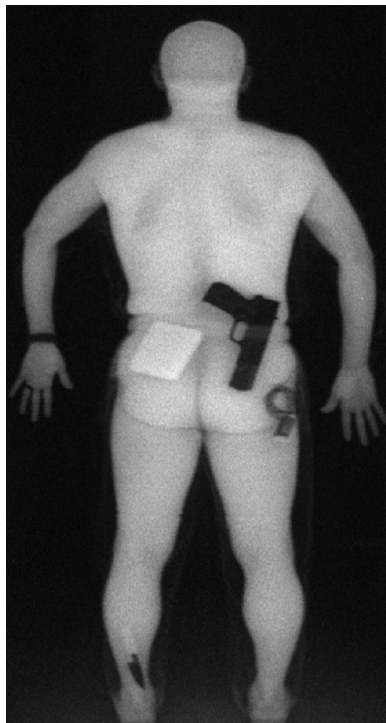


Figure 4.22 Backscatter x-ray image of a man. (*Courtesy of American Science and Engineering*)

were unknown to science until we observed them with orbiting telescopes. X-ray telescopes must be located above the atmosphere, since the air mass above us absorbs nearly all of the dangerous UV, x-ray, and gamma-ray light that shines down on Earth. Some of these celestial objects such as black holes or **gamma-ray bursters** are very bright in the x-ray or gamma-ray bands but are hardly noticeable at other electromagnetic wavelengths. Other objects, such as our own sun, are much brighter in the visible band than in the x-ray or gamma-ray bands.

As with radio astronomy, celestial objects can look markedly different in the x-ray and gamma-ray bands from the way they appear in visible light. For example, the Sun, imaged in the x-ray region of the spectrum, normally appears quite black, as shown in Fig. 4.23.

This image was made using x rays at the low-energy end of the x-ray waveband. These are called **soft x rays**, and they are lower in energy than the x rays used for medical imaging. The apparent darkness of the Sun in the x-ray band is remarkable, since the Sun is so bright we can hardly stand to look at it with our eyes for even a fraction of a second. Yet the outer layer of the Sun that emits visible light is simply too cold to radiate much light in the x-ray band. It takes magnetic phenomena to heat the Sun's surface material up hot enough to emit x rays. The bright loop-shaped structures shown in the image are solar flares. Solar flares are episodic events that occur when the Sun's magnetic field pops out of the surface in localized

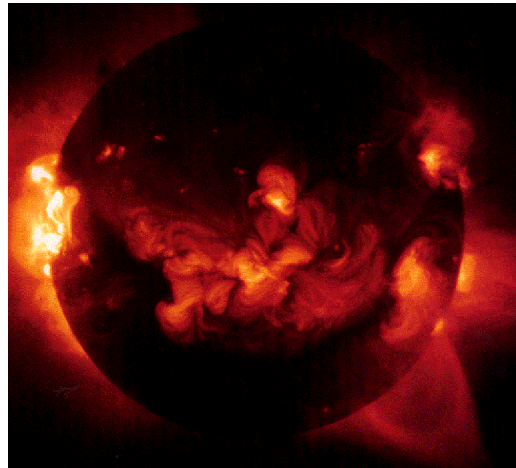


Figure 4.23 The Sun imaged with soft x rays. (*Courtesy of Yohkoh/SXT*)

regions (sunspots) and heats gas in the solar atmosphere to several million degrees by virtue of powerful electric and magnetic fields within the flare. The magnetic field pops out of the surface owing to the differential rotation of the Sun—the material at the Sun’s equator rotates faster than the material at the poles. The Sun’s magnetic field is locked to the dense solar material, and the differential rotation stretches and tangles the magnetic field like rubber bands, causing it to pop out of the surface in loops. The hot gas contained in the loops then glows with x-ray light.

Another interesting feature of the x-ray emission from the Sun is its variability, which can be as much as a factor of 100, in contrast to the extreme stability of the Sun’s brightness in the visible waveband (it varies by about 0.1% in an 11-year cycle.). How can this be? This is because we are observing very different aspects of the Sun in these two regions of the electromagnetic spectrum. When we observe the Sun in the visible waveband, we are seeing light emitted by the outer layer that maintains a very steady temperature. In contrast, x-ray emissions from the Sun are all from solar flares, where there is little stability and large changes can happen over a period of days or hours.

The soft x-ray telescope on the Yohkoh satellite, which carries two x-ray imaging sensors aboard it, produced Fig. 4.23.⁷ One is sensitive to **hard x rays**, in the 20–80-keV range, and the other to soft x rays in the 0.1–4 keV range. The detectors are silicon devices that convert the x rays into electrical signals. In this particular design, the x rays are imaged onto the detector array with grazing-incidence optics. The x rays strike a ring-like metal shape at a grazing incidence (like stones skipping off the surface of a lake) and are deflected onto the detector elements. The efficiency of this type of optic is fairly low, since the collection area is a small fraction of the total aperture.

⁷*Yohkoh* is the Japanese word for “sunbeam.”

Gamma-ray Imaging

Next comes the final frontier of the electromagnetic spectrum: the gamma-ray waveband. The term “gamma-ray” denotes the highest energy waveband of the electromagnetic spectrum, essentially x rays in or above the MeV (million electron volt) energy range. Gamma rays are generated by a number of mechanisms, including annihilation of **antimatter** and matter, acceleration of charged particles by strong magnetic fields, and radioactive decay of the nucleus of an atom.

Gamma-ray imaging has its roots in experiments done in the 1890s. The scientist Henri Becquerel discovered the phenomenon of radioactive decay in a serendipitous experiment performed in 1896. He had recently learned of Roentgen’s discovery, and intended to see if fluorescent materials emitted x rays. One of the fluorescent materials in his laboratory was a salt of uranium called uranyl potassium sulfate, and he found that the salt caused a photographic plate wrapped in black paper to darken after several hours of sunlight exposure. Becquerel mistakenly thought that the sunlight caused the salt to emit x rays. When he tried to repeat his experiment, the sky in Paris was overcast, so he put the package away in a drawer for about a week. He then decided to develop the film anyway, expecting to find the images very weak. But, as he observed: “On the contrary, the silhouettes appeared with great intensity. I thought at once that the action might be able to go on in the dark.”⁸ This was a clear demonstration of the phenomenon of radioactive decay that produced penetrating radiation without any external stimulus. The film was fogged by gamma rays passing through the paper wrapping.

Later work by the physicist Ernest Rutherford and P.V. Villard established that radioactive decay gives rise to three distinct types of radiation now named alpha, beta and gamma radiation after the first three letters of the Greek alphabet. The first two types are helium nuclei and electrons, respectively, while gamma rays are electromagnetic waves of a very high energy, so high that it was not known for some time that these very penetrating rays were in fact electromagnetic waves. It is quite difficult to observe the wave-like properties of gamma rays since their wavelength is extremely short, and conclusive proof of their wave-like properties came many years after their discovery.

Gamma rays are very useful in certain imaging applications. Their highly penetrating properties make them one of the only means of optically imaging the interior of particularly thick or dense objects, and they can produce images in situations where x-ray imaging cannot. Examples of hard-to-image objects include steel shipping containers or marble statues, where even very hard x rays fail to produce a usable image. Radioactive gamma-ray emitters such as Cobalt-60 are used to produce gamma rays at energies of approximately 1 MeV (1 million electron-volts). The gamma-ray source can be very compact and does not require external power, making it particularly convenient in applications where access is difficult, such as inspection of welded joints in pipelines. It is very inconvenient to

⁸Emilio Segre, *From X Rays to Quarks*, W.H. Freeman (1980).

place an x-ray tube inside a pipe and supply it with high voltage, but a gamma-ray source can be easily pushed or dragged through even a small pipe. One common gamma-ray source design consists of a small titanium capsule that contains the isotope. The capsule is kept in a lead container with thick walls when not in use, to protect people from gamma-ray exposure; unlike an x-ray tube, one cannot turn off a radioactive source. The gamma-ray images are made with x-ray film in light-tight packages placed on the other side of the target from the gamma-ray source. This technique can be used to image through several inches of steel, as shown in Fig. 4.24.

The examples of mummies in sealed caskets demonstrate how useful x-ray imaging is in non-invasive applications. Gamma-ray imaging has similar uses in archaeology and art conservation, especially when it is used on particularly thick, dense materials. Figure 4.25 shows a marble statue named *Crouching Aphrodite* imaged in visible light and with gamma rays from a radioactive source made of an isotope of the element iridium. The gamma-ray image shows that the head of the statue fell off and was repaired with metal rods. This shadowgram was recorded on film and is a negative image like most medical x-ray images: the lightest regions correspond to the greatest thickness of material, particularly the combined thickness of the arm around the elbow and the head directly behind it.

PET Scans: Observing Living Tissue with Gamma Rays

Gamma-ray imaging has proven to be as useful in medical research as x-ray imaging, but it is used rather differently. X-ray imaging of tissue is active, that is, there needs to be an external x-ray source to illuminate the subject. The gamma-ray

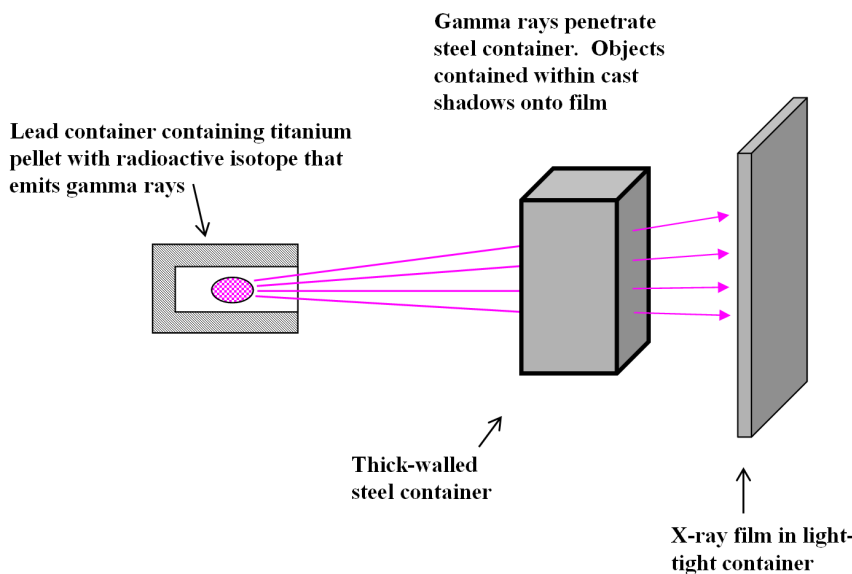


Figure 4.24 Gamma-ray imaging with radioactive source and film.

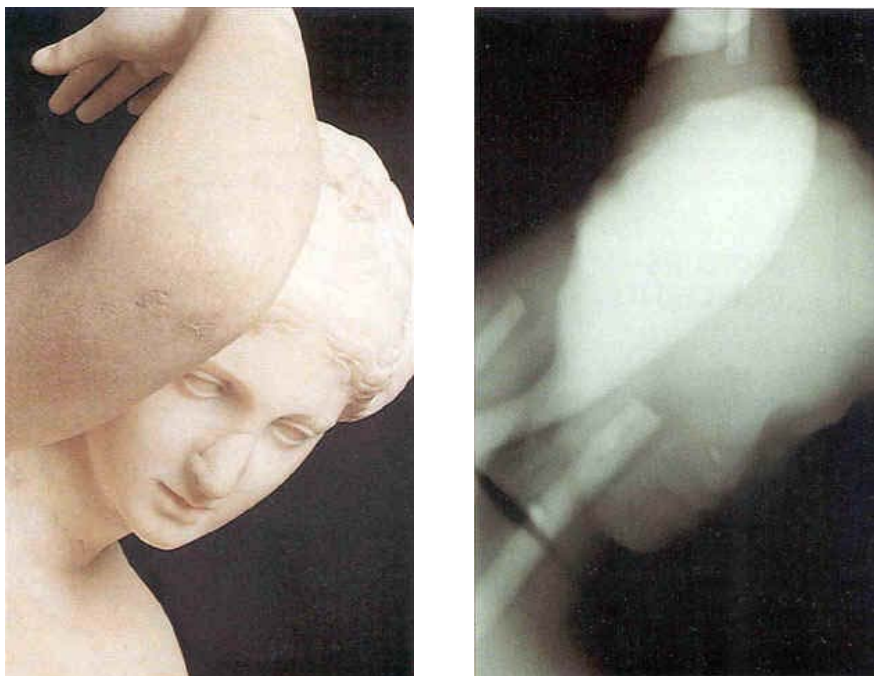


Figure 4.25 Visible (left) and gamma-ray (right) images of a marble statue. (*Courtesy of CEA*)

imaging technique known as the PET scan does not require an external gamma-ray source. Instead, the subject is made to emit gamma rays. PET stands for positron emission tomography, a method of imaging chemical processes within living tissue. It works in the following way: special **tracer** molecules are ingested, inhaled, or injected into living tissue in the form of a drug “cocktail.” They are then selectively concentrated in tissue via processes (such as metabolism) that are normally not directly observable. The tracers can be compounds such as simple sugars that are specially prepared to contain one or more radioactive atoms that spontaneously emit **positrons**. The positrons are antimatter: positively charged electrons that rapidly collide with electrons in neighboring atoms. The collision results in the annihilation of both the positron and electron and the creation of two gamma rays with energies of 511 keV (equal to the energy of a positron or electron). This powerful technique allows physicians to observe biochemical processes directly and compare them with clinical data in order to detect some abnormality noninvasively.

The PET scanner detects gamma rays with a ring of gamma-ray detectors placed around the subject, as shown in Fig. 4.26. The gamma-ray detectors, known as scintillation crystals, convert the gamma rays into visible light, which is then detected by a high-speed light detector. A computer analyzes the electrical signals from the light detectors and generates a 3D image. The physics of the annihilation process dictates that the two gamma rays are emitted in exactly opposite directions.

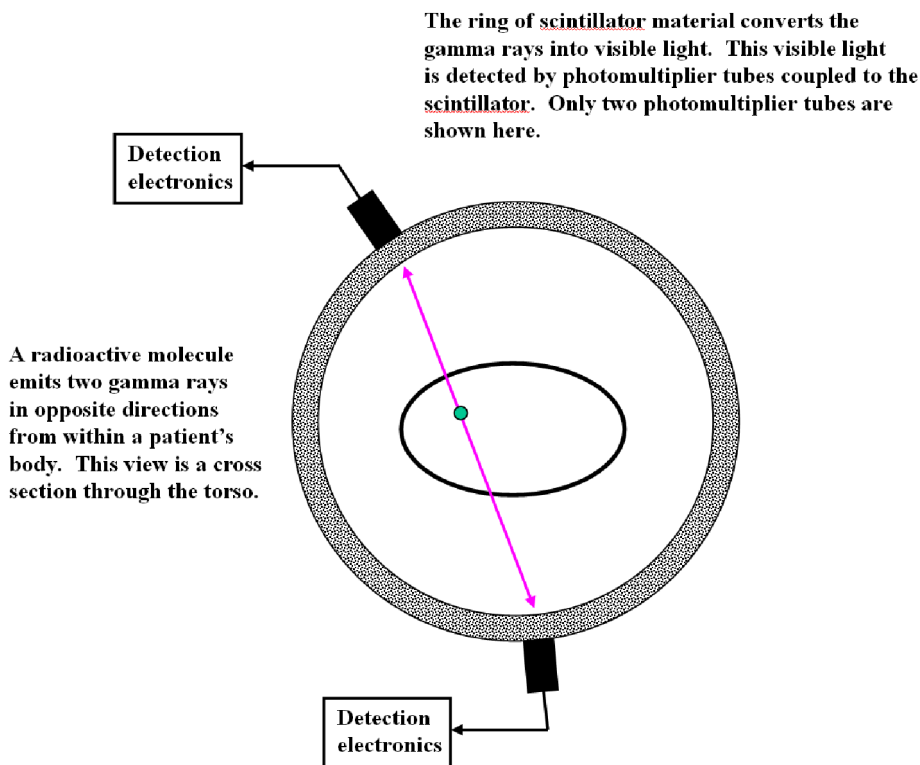


Figure 4.26 Schematic diagram of a PET scan.

This characteristic is used to discriminate between positron-induced gamma-ray signals and unwanted “background” signals produced by naturally occurring radiation. The computer only counts pairs of signals that come very close in time to one another from opposing detectors in the detector ring. A large number of gamma-ray detections are sufficient to create a picture of the concentration of the tracer as a function of position within the tissue, just as thin x-ray beams can be used to recreate a 3D map of density within a person (or mummy).

Figure 4.27 shows two different PET scans of a human heart in a person with a history of heart attacks. The left image shows blood flow in muscle using a radioactive ammonia tracer. Arrows point to tissue that has been rendered inactive by a loss of blood flow. The question is whether a heart bypass could restore heart function in the damaged area. This question can be answered with a PET scan using a different tracer to indicate a different biochemical process, in this case metabolic activity, using radioactive glucose. The right image shows the presence of metabolic activity in the areas that appear dark (inactive) in the left image. This indicates that the heart muscle in the area is in “metabolic hibernation” and could possibly be restored to nearly normal function with a bypass. The color bar between the two images indicates the relationship between the pseudocolor in the image and the relative intensity of gamma-ray signals.

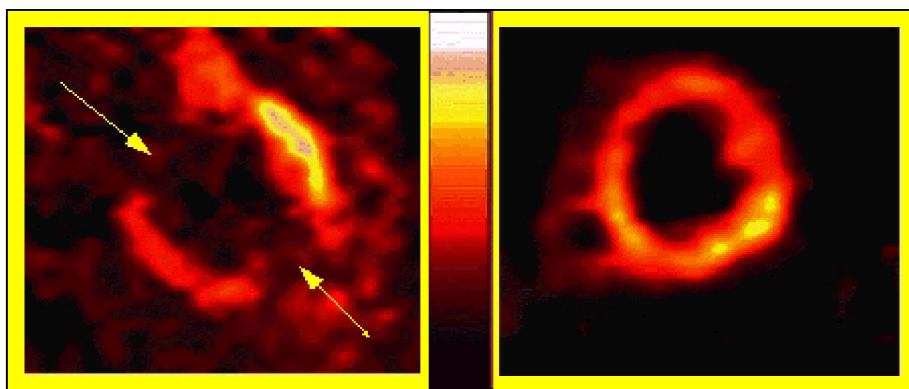


Figure 4.27 Heart muscle viability indicated by PET scans: left image shows loss of blood flow in regions, right image shows metabolic activity. (*Courtesy of Dr. David Lilien, Biomedical Research Foundation of Northwest Louisiana*)

The brain of a person with Alzheimer's disease exhibits decreased metabolic activity, which can be imaged with PET techniques. Figure 4.28 shows pairs of images of two different brains: one normal, the other of a person with Alzheimer's disease. The two images of each brain are tomographic "slices"; i.e., images of a thin cross-section at two different positions, which is why they differ in size (like two slices from a pineapple, one near the end, the other in the middle). The pseudocolor indicates levels of metabolic activity, with red being the strongest and blue being the weakest. The arrows indicate regions of the diseased brain that show reduced metabolic activity. PET can serve as an early indicator of the disease, as much as several years before other clinical methods would result in a similar diagnosis. Figure 4.29 shows two slices of an epileptic child's brain. The arrows indicate regions of the brain in the right hemisphere where glucose metabolism is decreased. Removing this tissue with surgery cures the seizures about 80% of the time.

Radioactive materials that emit gamma rays through nuclear decay processes do so at discrete energies. A gamma-ray detector that is sensitive to the energy of the gamma-ray photons can be used to identify these radioactive materials. One can incorporate energy-sensitive detectors into an imaging system known as an imaging spectrometer. It is in some ways like color television, in that the color (wavelength or equivalently, energy) information is preserved and can be quantified, unlike a black and white television system that only displays intensity information. Scientists at Lawrence Livermore National Laboratory devised a gamma-ray imaging spectrometer, or GRIS, that allows one to determine not only the intensity of gamma rays from radioactive decay, but also the precise radioactive element that gave rise to them in the first place.⁹ Imaging gamma rays onto an array of detectors is difficult, since conventional lens designs will not work. A pinhole

⁹K. Ziock, "Gamma-ray imaging spectrometry," *LLNL Science and Technology Review*, (October 1995).

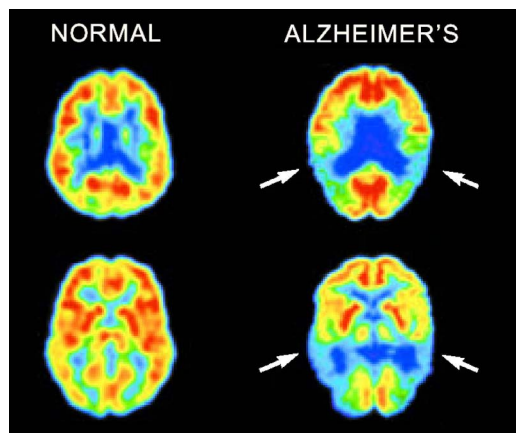


Figure 4.28 Normal brain (left) and brain with Alzheimer's disease (right) PET scans. (Courtesy of Dr. Michael E. Phelps, UCLA School of Medicine)

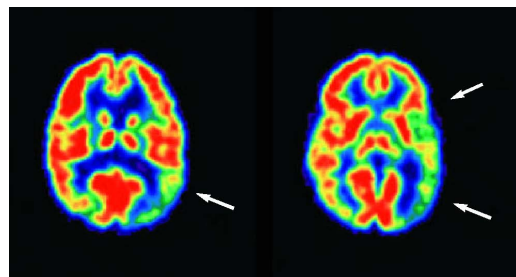


Figure 4.29 Epileptic brain PET scan. (Courtesy of Dr. Michael E. Phelps, UCLA School of Medicine)

will act as a lens for gamma rays, but a single pinhole gives very low light-gathering efficiency. The gamma-ray imaging spectrometer has a **coded-aperture mask** that consists of hundreds of pinholes stamped in a special pattern on a sheet of metal. Having hundreds of pinholes greatly increases the light gathering power of the imager over what it would be with a single pinhole. Behind the coded-aperture mask is a position-sensitive detector that converts the gamma rays into electrical signals on a grid of wires. The signals are then read out by a computer that uses the coded aperture mask pattern to calculate a real image.

The measurement of gamma-ray photon energy in an image has some interesting applications in the handling of nuclear material. As discussed earlier, radioactive elements that emit gamma rays do so at particular energies. It is possible to identify nuclear materials by the gamma rays they emit. For example, Fig. 4.30 shows two false-color images of a 1/8-inch thick sheet of **depleted uranium** with **plutonium** rods behind it. The color bars are maps of gamma-ray intensity, where white and green correspond to the lowest intensity, up through red to blue for the highest intensity. In the top image, the energy sensitivity is set to 100 keV, corresponding to the energy of gamma rays from depleted uranium. In the bottom image, the energy

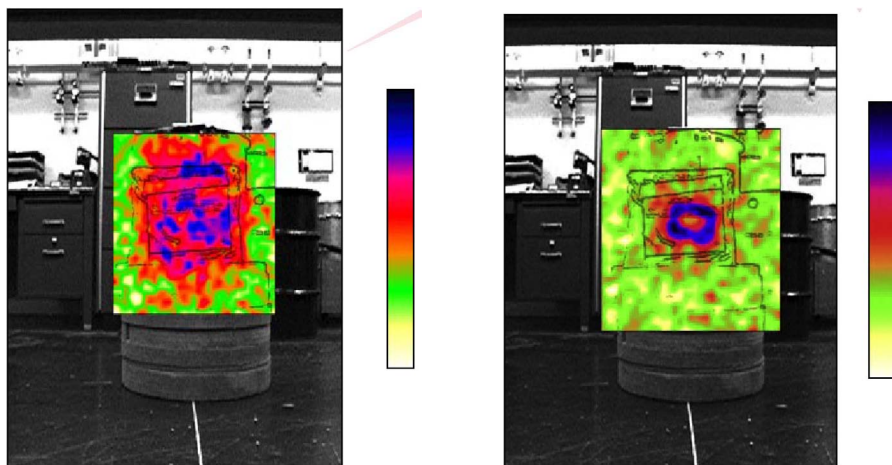


Figure 4.30 GRIS images of depleted uranium (left) and plutonium fuel rods (right). (Courtesy of Lawrence Livermore National Laboratory)

range is centered around 400 keV, which eliminates the lower-energy uranium-induced gamma rays, and shows the plutonium radiating through the uranium shielding. The gamma-ray images are overlaid onto a visible-light image of the room containing the nuclear material. A lightly traced outline of the container is overlaid onto the gamma-ray images.

This technique can be applied to problems of contamination and container contents verification, since the gamma rays can carry information about the contents of a container through its walls. This system can also be used for on-site inspection and characterization of nuclear weapons and nuclear materials for arms-control purposes, as shown in the illustration in Fig. 4.31. Figure 4.32 shows a GRIS image of a Peacekeeper missile with its 10 warheads contained within. The image was made without having to move the missile out of its silo or remove the nose cone, which would compromise the readiness of the missile.

The x-ray and gamma-ray wavebands are the shortest-wavelength, highest-energy wavebands in the electromagnetic spectrum as we presently know it. Perhaps in the future, scientists will create a name for a new band of light beyond gamma rays, associated with some undiscovered set of phenomena. The penetrating power of this high-energy light makes it extremely useful for imaging through material that is opaque to lower-energy light. X-ray and gamma-ray imaging also yields information about the workings of nuclear reactions and magnetic phenomena that generate high-energy light through nonthermal processes, both on Earth and in the cosmos.

The next chapter explores acoustic imaging, an alternative to imaging with light. Scientists frequently encounter situations where they cannot image objects with light at any wavelength, either because it would be dangerous to the subject being imaged, or because material between the imaging system and the object being imaged is too thick or dense to allow the passage of light. Acoustic imaging offers an alternative to lightwave imaging that overcomes some of these difficulties. It



Figure 4.31 Rendering of GRIS inspection of a Peacekeeper missile in its silo. (*Courtesy of Lawrence Livermore National Laboratory*)

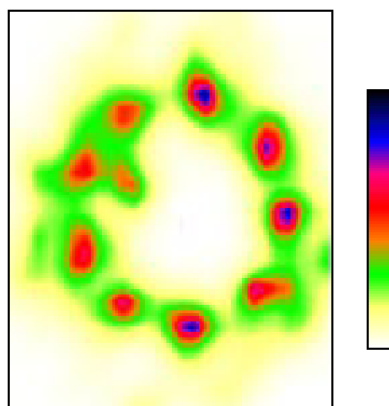


Figure 4.32 GRIS image of a Peacekeeper missile warhead package. (*Courtesy of Lawrence Livermore National Laboratory*)

can make hidden objects or acoustic phenomena visible—synthetic vision based on acoustic waves rather than lightwaves. Also, state-of-the-art acoustic imaging technology can generate spectacular images with resolution that rivals that of imagery generated with light. For this reason, I have included acoustic imaging in this book, even though acoustic waves are not part of the electromagnetic spectrum.

Chapter 5

Acoustic Imaging: Seeing with Sound

By imaging with the appropriate wavelength of electromagnetic energy, materials considered completely opaque become transparent, revealing hidden wonders. Objects the human eye perceives as dark look light, and light objects look dark; indeed the whole notion of dark and light becomes very subjective, as it depends on the wavelength response of the imaging technology used and not what the human eye sees. However, imaging with light waves is not always possible or desirable because of basic imaging limitations imposed by the optical properties of matter between the object and the imaging system. As we turn the imaginary knob on our head and sweep the response of our eyes through the electromagnetic spectrum, we may never find a waveband of light capable of imaging through a particular obstacle. For instance, we cannot see through even the purest ocean water for more than about 100 m at any wavelength of light, yet the ocean floor is full of interesting things worth imaging.¹ Imaging with light is not always desirable because sometimes the light we need to see through intervening matter may be harmful. Imaging of a fetus can be done with x rays—in fact doctors used to x ray pregnant mothers as a means of diagnosing prenatal conditions—but this practice is now discouraged due to the potentially harmful effects of x rays on the developing child.

Acoustic or sonic imaging is an alternate way to see through intervening matter. This is literally “seeing with sound,” made possible because sound waves are very similar to electromagnetic waves in their properties, yet they travel freely through fresh or salt water, tissue, and a variety of other materials that are opaque at many or all wavelengths of electromagnetic energy. Acoustic pictures are different from pictures made from light in that they are essentially maps of density variations. Sound waves will reflect from boundaries between different materials and carry back information about changes in density and object shape to a sensor. There are several different ways to image with acoustic waves, and these methods are all analogous to techniques used to image with light. For instance, some acoustic

¹Very long wavelength radio waves can penetrate through ocean water, but building an imaging system that would operate in the kilometer-scale waveband is extremely impractical and would have very limited resolution, i.e., the image would be blurry.

imaging systems use special lenses and mirrors which reflect or refract acoustic waves in order to focus them onto sensor arrays, just like the human eye or a conventional photographic camera. Other systems include the acoustic equivalents of radar systems discussed in Chapter 3. These acoustic radar systems transmit pulses of sound toward a target in a beam pattern, detect the reflected pulses, and process them into a visual image.

Like ultraviolet vision, acoustic imaging is an ability that humans do not naturally have but that exists in the animal kingdom. Animals such as bats and dolphins live in conditions where available visible-light levels are often so low as to be insignificant, making acoustic imaging an alternative means of navigating the environment and locating prey.² This particular ability, known as echolocation, is an active imaging behavior involving specialized organs for the transmission and reception of sound and neural processing within the animal's brain. Echolocating animals emit short pulses of acoustic energy from specialized organs. These waves propagate through air or water, strike objects, and are reflected back to the animal's ears. The brain processes these perceived echoes into something like a picture of the environment in ways that are not well understood. The "picture" that bats perceive must be fairly detailed, since bats can fly around in a completely dark room and avoid obstacles such as thin wires with uncanny ability.³

Underwater Acoustic Imaging

Water is transparent to light only within a very narrow range of wavelength, which (not coincidentally) corresponds to our visual spectral range. But even within that range, water is nowhere near as transparent as air. Even the purest natural waters absorb light to such an extent that it is difficult to see an object more than 50 m away even under ideal conditions. Often water is much more turbid, cutting visibility to zero or near zero. It can be almost impossible to see submerged objects when the surface is choppy or even slightly disturbed by waves and wind. Yet the need to see what lies beneath bodies of water is great, since many things get lost in oceans, lakes, and rivers—things like ships, cars, planes, bodies, and cargo. **Sonar** imaging offers a solution to this problem. It is the acoustic counterpart of radar, standing for "sonic navigation and ranging."

Sonar has its roots in the invention of the underwater microphone or hydrophone during World War I. Multiple hydrophones lowered from ships enabled the detection of submarines by their engine noise. This passive sonar evolved into systems that rely on active illumination of an underwater target with short pulses

²Recall that all known animal species that have eyes cannot see light with wavelengths that are longer than about 750 nm. The photoreceptors in the eye are insensitive to longer wavelengths (infrared) so the eyes of cave-dwelling animals cannot utilize thermal infrared energy that is naturally emitted by materials at terrestrial temperatures.

³For more information on bat echolocation, see Kunz, T.H. and P.A. Racey (Eds.), *Bat Biology and Conservation*, Smithsonian Institution Press, Washington, D.C. (1998). For dolphin echolocation information, see W.W.L. Au, *The Sonar of Dolphins*, Springer-Verlag, New York (1993).

of sonic energy. Originally these pulses were generated mechanically; modern systems use an electronic device called a transducer. The transducer also serves as a sound detector; it is like a speaker and microphone in one. Underwater objects reflect some of the energy in the sonic pulses back to the transducer, yielding information about them. A simple case of sonar imaging is a depth finder. A narrow beam of sound pulses is directed straight down from a transducer. The pulses reflect off the bottom (or any object with a density that differs from water) and travel back to the transducer. An electronic circuit measures the time difference between the emission of the outgoing pulse and the reception of the reflected pulse and converts this time difference into a distance. That distance is twice the depth of the water.

Imagine a wreck lying on the bottom of the ocean, 200 m below the surface, as shown in Fig. 5.1. The height of the wreck is 20 m. If depth measurements are made in the vicinity of the ship, they find that the sonar distance will vary between 180 m and 200 m. The 180 m measurement is the 200 m ocean depth minus the height of the ship above the ocean floor. If the boat were driven around and depth measurements taken at many different points on the ocean surface, the readings will generate a crude sonar image of the submerged ship. It will appear as a 20-m high feature on the ocean floor.

High-resolution sonar imaging is an extension of the depth finder, with the addition of sophisticated data processing and a data collection system that measures the shape and strength of the return pulses in addition to their round-trip times. The shapes of the return pulses are modified by the geometry of

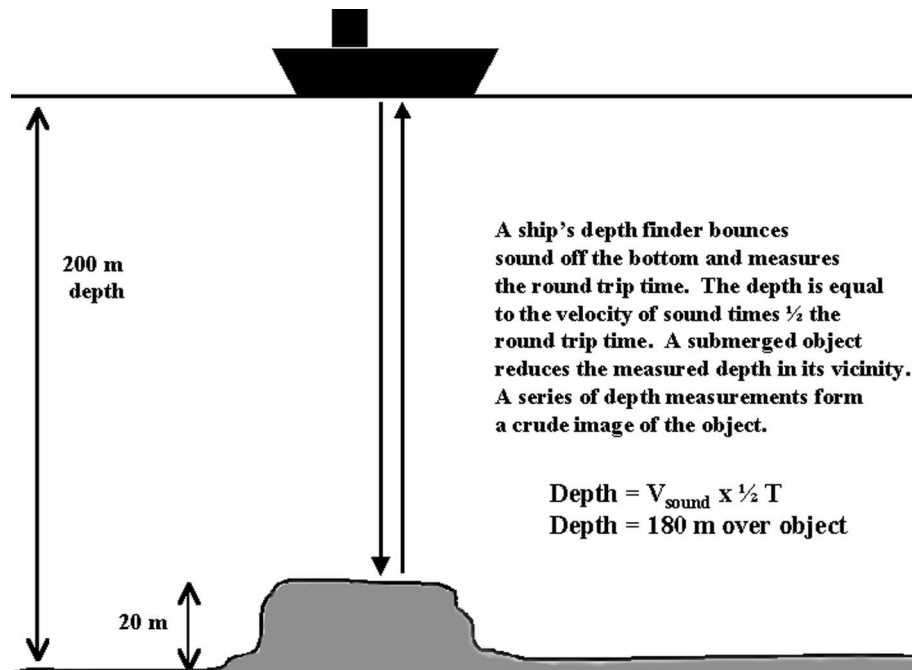


Figure 5.1 Schematic of ship's depth finder.

the target, while the strengths of the return pulses depends on the density of the target (higher density equals stronger return pulse) and the distance to the target. The strength, shape, and timing information about the return pulses is processed by a computer and turned into a visual image on a computer screen. One commonly-used imaging sonar system works in the following manner: An ultrasonic transducer and electronics for transmitting and receiving ultrasound pulses are housed in a torpedo-shaped float known as a towfish. A fan-shaped beam of sound emanates from the sonar transducer in a direction perpendicular to the towfish direction of motion. Figure 5.2 shows an advanced towfish design with its underwater cable attached. Figures 5.3(a) and 5.3(b) show the acoustic beam pattern emitted by a typical towfish.

The transducer detects reflected portions of the sonar pulse and measures their arrival time, shape and strength. As the towfish moves along, the data it receives are used to generate a sonar picture of the bottom, building up an image line by line. The smallest feature that can be resolved by imaging sonar depends on the wavelength of the sonar pulse. Sonar that uses sound with wavelengths of a few millimeters can detect features as small as 20 cm at an imaging range of about 100 m. The price one pays for this resolution is its effective range.

Sonar imaging has come a long way since its inception in the 1950s, and modern sonar images are often very striking, as though they were actual photographs. Figures 5.4 and 5.5 are images of the *Empire Knight*, a British freighter that sunk in 90 feet of water off the coast of Maine during World War II. The viewer is looking straight down at the sea bottom. The color saturation corresponds to the strength of the return signal—white pseudocolor indicates the strongest return and black the weakest return. Note the black streak that runs from top to bottom along the middle and the sonar “shadows” thrown by the ship. These are artifacts of the towfish sonar pattern, which scans to the side and therefore cannot “see” objects directly below the swath or behind objects with height above the bottom. The length of the shadow is directly related to the height of the object and can be used to give such information; the same shadowing effect is seen in radar images of mountainous terrain, since the imaging technique is very similar.



Figure 5.2 Sonar towfish with undersea cable. (Courtesy of Garry Kozak, L-3 Klein)

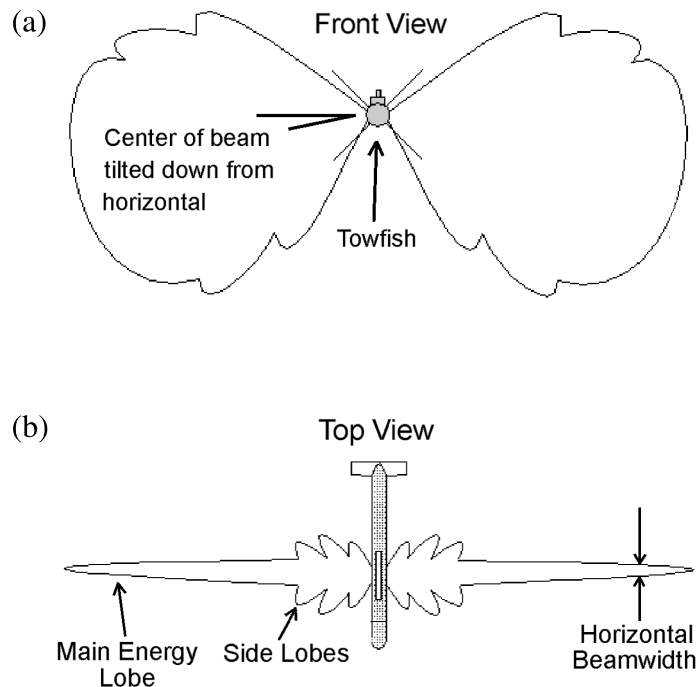


Figure 5.3 (a) Front view and (b) top view of sonar towfish with sonar beams. (*Courtesy of John Perry Fish*).



Figure 5.4 The *Empire Knight* imaged with sonar. (*Courtesy of Garry Kozak, L-3 Klein*)

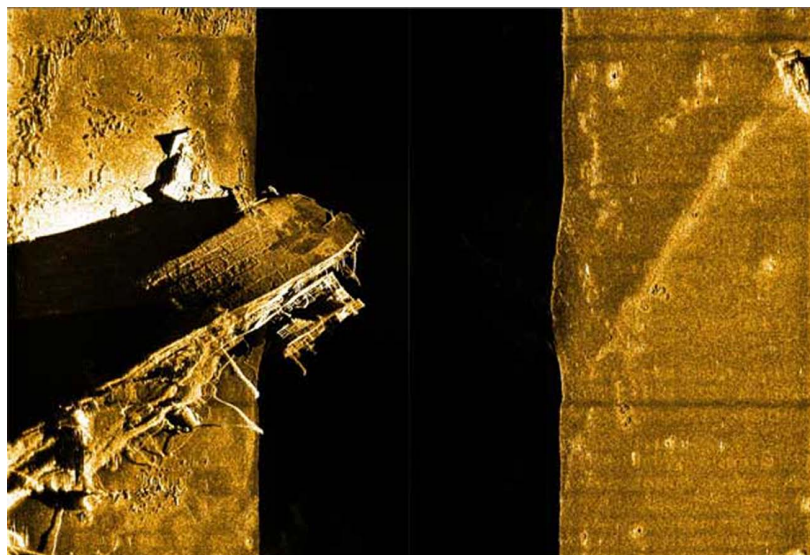


Figure 5.5 Another sonar image of the *Empire Knight*. (Courtesy of Garry Kozak, L-3 Klein)

Some high-resolution sonar images are particularly eerie, especially when the imaged objects are located on a bottom that is otherwise devoid of features. Figure 5.6(a) is a sonar image of the bottom of an inland lake that is 60 feet deep. The drowning victim can be seen lying on the bottom. The shape of the victim's body is clearly visible in Fig. 5.6(b). This sonar image was made with 455 kHz sound waves, corresponding to a wavelength in water of 3 mm.

Ultrasound Medical Imaging

The Japanese were the first to use acoustic imaging for medical applications. Their early work, which took place after World War II, started with simple ultrasonic devices that acted like depth finders, reading out a distance to an interface or boundary within tissue. The boundary might be something like the surface of a tumor, which is often denser than surrounding tissue and will reflect back an acoustic signal to a transducer. These devices were the precursors to modern ultrasound imaging systems that use intensive computer processing to produce startling imagery. Ultrasound imaging is very useful for examination of a fetus *in utero* (i.e., in the womb). One can non-invasively image the fetus through layers of the mother's tissue without potentially harmful radiation. The imaging system generates acoustic waves with wavelengths of a few millimeters or shorter, yielding very high-resolution imagery. The waves emerge from a transducer placed against the mother's abdomen and propagate inward, reflecting off of various boundaries, for example, the boundary between the amniotic fluid and the fetus' skin. Figure 5.7 shows a fetus *in utero* at eight months, imaged with sound waves with frequencies varying between 4 and 7 MHz.⁴ This frequency range corresponds

⁴1 MHz = 1 million cycles per second.

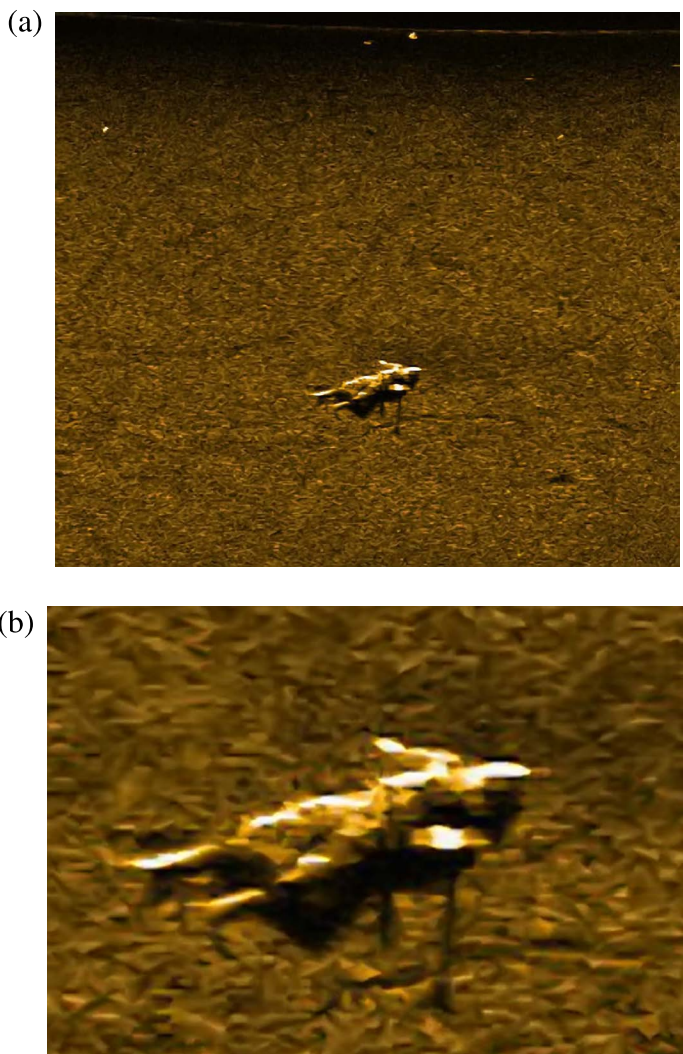


Figure 5.6 (a) Sonar scan of a lake with a drowning victim at the bottom; (b) detail of drowning victim. (*Courtesy of Gary Klein*).

to a wavelength range of about 200–400 μm in water. The ultrasound machine that made this image can produce a 3D view that can be rotated.

Figure 5.8 shows a side view of a fetus with the addition of pseudocolor to indicate the velocity of blood flow within the heart and main arteries. This view is one of a series of real-time images that are displayed as a movie, allowing medical workers to see the blood flow. The ultrasound machine has a mode in which it detects slight shifts in the frequency of the reflected sound waves from the moving blood. These Doppler shifts are similar to the shift in pitch of a train whistle that a stationary observer hears as the train goes by. The orange false color denotes blood flow away from the observer, and the blue denotes flow toward the observer.

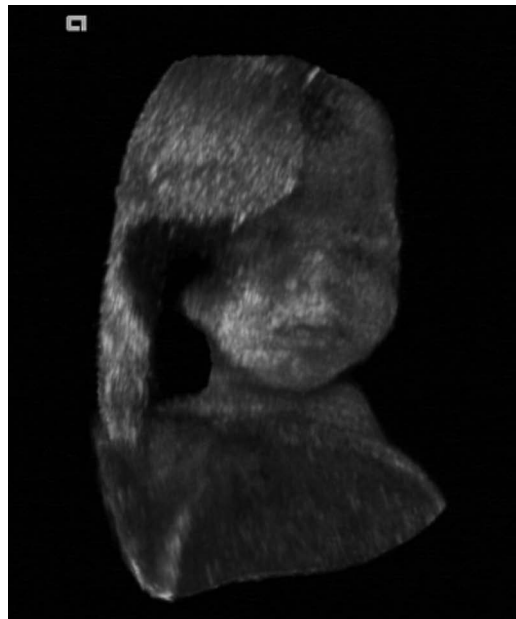


Figure 5.7 Fetal ultrasound image. (*Courtesy of Siemens Healthcare, Ultrasound*)

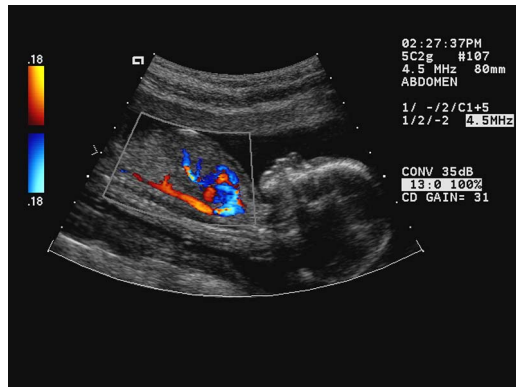


Figure 5.8 Ultrasound image of a fetus with Doppler false color. (*Courtesy of Siemens Healthcare, Ultrasound*)

This flow information helps early diagnosis of cardiac abnormalities. Motion of the heart muscle itself can be measured and viewed as a real-time movie. All these techniques can also be applied to people and animals.

Acoustic Daylight Imaging

The traditional approach to underwater acoustic imaging requires active “illumination” of the scene or object of interest. Sonar imaging begins with directed acoustic energy in the form of a staccato burst of pulses generated by the imaging system. This is the same approach we use for underwater optical imaging, where

we flood the scene with light and look at the reflected energy. A new approach to acoustic imaging is based on the existence of ambient sound in the underwater environment. This sound creates a “noise field” that is modified by the presence of objects in much the same way as scattered sunlight is reflected and absorbed by objects, making them visible to our eyes. The oceans are full of natural and artificial sources of noise, including sounds from breaking waves, fish, marine mammals, crustaceans, and motorboats, to name a few. Much of this noise is above our range of hearing, but electronic sensors can easily detect it.

In 1985, Michael Buckingham was working on sonar technology for the English Ministry of Defense when he realized that it might be possible to image objects underwater with the acoustic equivalent of daylight. Initial studies indicated that an acoustically reflective object placed at various distances in front of a single-element detector (a parabolic reflector with a single microphone at the focus) significantly increased the noise signal level measured by instruments connected to the detector. This experiment was the acoustic analogue of placing a white sheet of paper against a dark background in a person’s field of view. The Scripps group next designed and fabricated a larger acoustic “lens” with a cluster of 128 microphones located at the focus, like the compound eye of an insect. The signal from each microphone maps to a single “pixel” in the resulting acoustic image.

This group has finally built an instrument containing 900 sensors and extensive computing power in a flat geometry known as a phased array.⁵ The images it produces are nearly ten times higher in resolution than earlier images. This instrument, known as ROMANIS,⁶ was tested in the warm, shallow seas around Singapore, where millions of shrimp produce substantial levels of acoustic noise by the snapping of their claws—a behavior that is not well understood but serendipitously creates excellent conditions for acoustic noise imaging. The ROMANIS array is shown in Fig. 5.9.

Figure 5.10(a) shows a visible-light view of a test target imaged by ROMANIS. The 1-m square aluminum panels are covered with neoprene rubber, which acts as an effective reflector and diffuser of ambient noise. Figure 5.10(b) shows an acoustic image of the L-shaped pattern. The pseudocolor indicates the sound pressure level in decibels, as shown by the color bar to the right of the image. This image was made with sound in the 58–77-kHz frequency range, which corresponds to wavelengths in water between 1.9 and 2.5 cm.⁷

There are inherent limitations to the resolution of an ANI system, since the wavelength of the sound waves is a significant fraction of the size of the imaging system aperture. However, it offers an attractive alternative to sonar imaging, since

⁵The phased-array approach eliminates the need for a parabolic reflector and increases the field of view of the imaging system. The sensors in a phased array detect relative phase (timing) differences in incoming waves. This information is used to form an image without the need for a focusing lens. Phased arrays are also used in radar applications, like the passive millimeter-wave camera described in Chapter 3.

⁶ROMANIS stands for Remotely Operated Mobile Ambient Noise Imaging System.

⁷1 kHz = 1000 cycles per second.



Figure 5.9 ROMANIS acoustic imaging sensor. (*Courtesy of Mandar Chitre and Venugopalan Pallayil, Acoustic Research Lab, Tropical Marine Science Institute, National University of Singapore*)

it does not require that the target be illuminated with artificially produced sound waves, and it can produce images at much higher frame rates, making it capable of imaging moving objects.

Acoustic Imaging of Sound Sources

We have seen examples of active acoustic imaging (high resolution sonar), and acoustic imaging that is neither active nor passive (acoustic noise imaging). Now we will examine an example of passive acoustic imaging. Figure 5.11 is a series of acoustic “pictures” of a TGV (Train à Grande Vitesse, or high-speed train) trainset imaged with SYNTACAN, an acoustic microphone array that can produce visual images of moving objects that emit sound. The physical scale of the images is 6 m by 300 m, which is slightly larger than the trainset. The microphone array data build up a picture line by line, like an inkjet printer, using the motion of the object (in this case, the train) as the scanner. The TGV is especially loud because of its high speed, and these data help engineers to understand the various sources of noise in the TGV trains and to study methods of noise reduction. The sound waves that produced these images range in wavelength from 0.75 m for the top image to 10 m in the bottom. Note that the resolution of the image decreases as the wavelength increases. The pseudocolor indicates the sound intensity, where dark red indicates the highest intensity and blue the lowest. At the higher frequencies, we see the finest spatial resolution in the images. This is a recurring characteristic in imaging that is a manifestation of **diffraction**: for a fixed detector array geometry, the shorter the wavelength, the finer the angular resolution of the resulting images tends to be. Note that the most intense noise sources in the image are the power units at each end of the train. The pantographs (electrical wipers that engage the overhead power lines) at each end are sources of aerodynamically induced noise, and the “bogies” (wheelsets) with 17 m spacing are sources of high-pitched rolling wheel noise.

Figure 5.12 shows the SYNTACAN microphone array suspended from a manlifter. Instrumentation closer to the tracks measures the speed of the train so that the noise data from the microphones can be interpreted into an acoustic image.

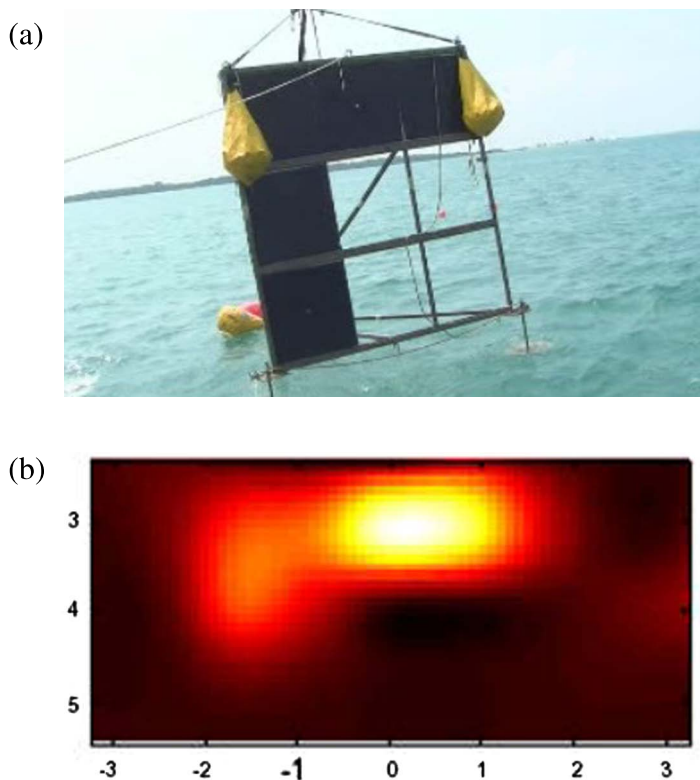


Figure 5.10 (a) ANI target and (b) an acoustic noise image of the target. (*Courtesy of Mandar Chitre and Venugopalan Pallayil, Acoustic Research Lab, Tropical Marine Science Institute, National University of Singapore*).

Acoustic imaging and light-wave imaging are complementary technologies. When one fails to work, the other often succeeds, since many materials that are opaque to light waves are transparent to sound waves, and vice-versa. Acoustic imaging can only work in situations where sound waves can travel from the target to the detector. It is thus not very useful in air, where sound is highly attenuated, and does not work at all through the vacuum of space, unlike light waves, which need no dense medium in which to propagate. Yet it allows us to see through materials opaque to light. We have seen images made through water and living tissue, for example, but acoustic imaging can see through denser materials like metal and rock. The Earth's internal structure has been mapped with seismic waves generated by earthquakes—an interesting example of acoustic noise imaging on a grand scale. Just as light-wave imaging allows us to look out into the universe, away from Earth, so acoustic imaging allows us to look inward: into our own bodies, into the depths of the ocean and the core of the planet.

The next chapter examines a single object imaged with light from a wide range of the electromagnetic spectrum. Each image shows a different aspect of the object, aspects that are not apparent with visible light alone.

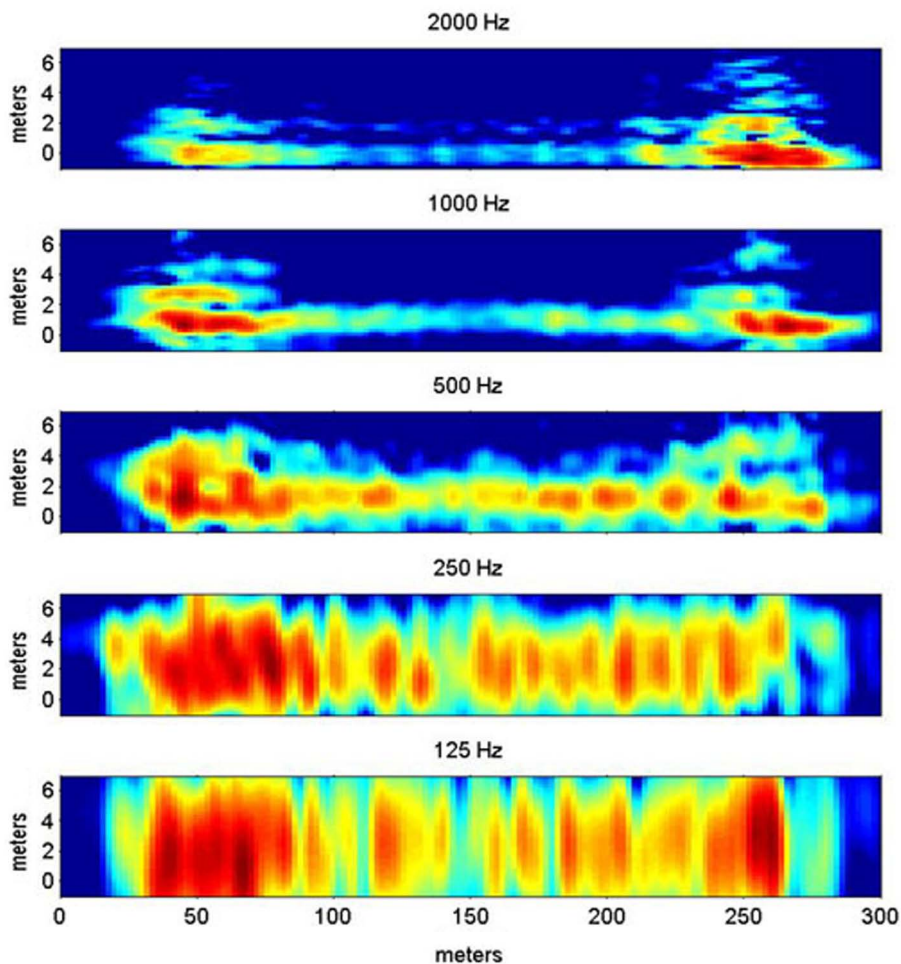


Figure 5.11 Acoustic image series of a TGV trainset. (*Courtesy of TNO-TPD, Delft, the Netherlands*)



Figure 5.12 TGV Thalys trainset and SYNTACAN acoustic imaging array. (*Courtesy of TNO-TPD, Delft, the Netherlands*).

Chapter 6

Sweeping through the Spectrum: Comparative Imagery

Having toured the known spectrum of light, from radio waves to gamma rays, one can appreciate the tiny slice of the spectrum that our unaided eyes can see is a fairly specialized band that permits vision in our water-drenched world. Yet the visible waveband provides an incomplete picture of the physical universe. Imaging technology permits us to transcend the limitations of our anatomy and see the universe with “alien vision.”

What would it be like if human eyes had an adjustable color response? Our eyes automatically adjust their focus and their sensitivity in response to varying object distance and light levels, yet their color response is fixed by their chemical structure. We can overcome this limitation with artificial eyes, each designed for a particular waveband of the electromagnetic spectrum. Consider a familiar object, a human face. The appearance of the face is highly dependent on wavelength—there are many “faces” to a face. I have been imaged in many wavelengths of light, from the millimeter-wave to the x-ray band. My familiar face, the one I see in the mirror, is only one of a larger set.

The millimeter-wave image seen in Fig. 6.1 was made with an imaging system that operates at a wavelength of 3.3 mm (3300 μm), corresponding to a **transmission window** in moist air. The image was taken outdoors under a clear sky. The cold sky reflects off my cheekbones, nose, ears, and forehead, giving the image a high degree of thermal contrast. This grayscale image is inverted so that black indicates hot and white indicates cold—it is easier to see the facial features this way. The image has a low resolution compared with some other imaging technologies, since the high-speed detector array has many fewer detector elements than an infrared or visible sensor, for example.

The infrared waveband contains a multitude of sub-bands, each with its own distinctive look. We see a different aspect of a human face in each sub-band – the LWIR and MWIR images convey the thermal emission of the skin with no external illumination required, while the near-IR band gives us insight into the reflectivity of the skin and eyes at wavelengths that are several times longer than visible light.

The LWIR face in Fig. 6.2 glows with its own light in the 8–9 micrometer waveband. A cooled infrared camera with a **QWIP FPA** captured this image, which is rendered in grayscale with white indicating hot and black indicating cold. The

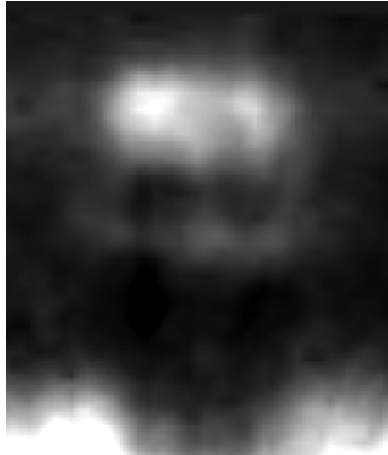


Figure 6.1 Millimeter-wave ($\lambda = 3300 \mu\text{m}$) photo. (Courtesy of Trex Enterprises)

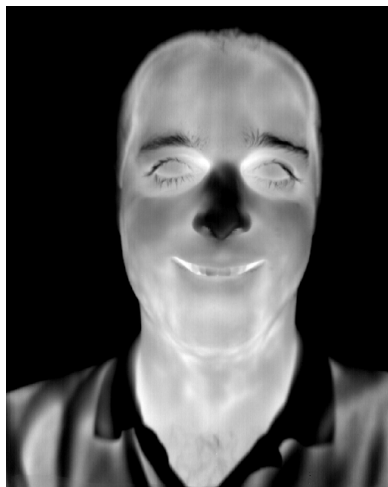


Figure 6.2 Longwave infrared ($\lambda = 8\text{--}9 \mu\text{m}$) photo. (Courtesy of FLIR)

eyes appear isothermal—there is little temperature variation over their surface, and no differentiation between the whites of the eyes and the iris. The nose and cheeks are noticeably cooler, the result of frostbite inflicted by severe weather during my time in Antarctica.

The MWIR face in Fig. 6.3 is very high in contrast, as captured by a cooled indium antimonide infrared camera. Small temperature changes on the surface translate into large intensity variations in the MWIR emission. This waveband conveys the maximum thermal contrast for objects that are close to room temperature, making it a powerful tool for diagnosis of thermal anomalies in both machines and living organisms.



Figure 6.3 Midwave infrared ($\lambda = 3\text{--}5 \mu\text{m}$) photo. (Courtesy of FLIR)

In the shortwave IR band, water absorbs very strongly. My water-filled skin looks completely black in Fig. 6.4, an image taken in the 2–2.5 micrometer band. The near-infrared band is too short in wavelength to convey any thermal information about a face—the skin is far too cold. Instead, we see reflected infrared light from hair and skin with no regard to visible color—light and dark skin appears equally reflective, and hair color disappears. The blue shirt looks white—near-IR light reflects off the cotton fibers without absorption by blue dye. The whites of the eyes are not nearly as “white” as they appear in visible light. The net result is a visible image gone wrong—I look like an old man with demon eyes! This image was taken indoors under tungsten lights with an indium gallium arsenide infrared camera.

Figure 6.5 is a near-infrared image taken with a silicon CCD camera that has a black glass infrared pass filter in front of the lens. The platform is a ten-year-old Nikon Coolpix camera with the internal blue glass **hot mirror** removed and replaced with a clear glass piece of the same size so that the camera becomes sensitive to both visible and infrared light.¹ I used a black glass filter in Fig. 6.6 that transmits light above 830 nm or 0.83 micrometers, making the image infrared only. The resulting image is pretty close to a monochrome visible-light image, with the exception that the blue shirt looks light grey.

The visible image in Fig. 6.7 returns to familiar territory, and the pigmentation in the hair and eyes asserts its effect on our perception of life-like color and contrast. The dye molecules in the shirt absorb the reds and greens in the room lights, letting only the blue component reflect back to the silicon CCD digital camera.

Sunblock absorbs heavily in the near-ultraviolet waveband. My face is coated with it in Fig. 6.8, all except for a few spots in the right ear and on the chest. This image was taken with a Wratten 18A filter over a standard 35-mm camera lens, with Kodak Tri-X black-and-white film, which has plenty of sensitivity in the 0.3–0.4 μm waveband. If you are wondering why my face looks different in some

¹The hot mirror is designed to block very near-infrared light from reaching the sensor. This is desirable in a color camera, where one wants the color response to closely match that of the human eye.



Figure 6.4 Shortwave infrared ($\lambda = 2\text{--}2.5 \mu\text{m}$) photo. (Courtesy of FLIR)



Figure 6.5 Near-infrared ($\lambda = 0.9\text{--}1.68 \mu\text{m}$) photo. (Courtesy of FLIR)



Figure 6.6 Very near-infrared ($\lambda = 0.83\text{--}1.1 \mu\text{m}$) photo.

images, that is purely a result of when the picture was taken during the last ten years!

Almost anything organic looks extremely dark in the shortwave UV band of the spectrum. The only surfaces that are reflective are the whites of my eyes and my



Figure 6.7 Visible ($\lambda = 0.4\text{--}0.7 \mu\text{m}$) photo.

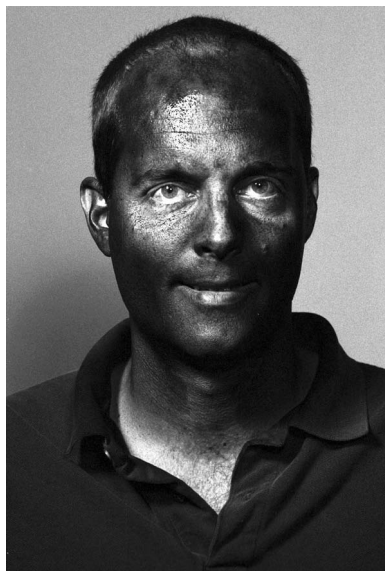


Figure 6.8 Near-ultraviolet ($\lambda = 0.35\text{--}0.38 \mu\text{m}$) photo. (Courtesy of Rand Molnar)

teeth in Fig. 6.9. This image was taken with a conventional film camera with a special fused silica and calcium fluoride lens that can transmit 254 nm radiation. The camera is equipped with a bandpass filter that transmits right around 254 nm but very little else. The light source is a xenon strobe without the usual UV blocking polymer coating on the strobe tube.

Hair and flesh disappear in the x-ray image in Fig. 6.10, except for a slight shadow of scalp, right on the vertex of the skull. The teeth and cheekbones interpose the highest density of matter between the x-ray source and film; consequently, they record as the darkest areas. The eye sockets act like windows into the skull, and therefore look lighter. For clarity, the values have been inverted from what they would be in a typical radiograph, making the regions of highest density black and lowest white. This image was actually taken in the 1920s, but



Figure 6.9 Shortwave ultraviolet ($\lambda = 0.254 \mu\text{m}$) photo. (Courtesy of Patrick Stanbro)



Figure 6.10 X ray ($\lambda \sim 2.5 \times 10^{-5} \text{ mm}$) of a human head. (Courtesy of LACMA).

the subject had a bone structure similar to mine, especially in the jaw area. The x-ray source was probably in the 100 keV range, and the image was captured onto fine-grained x-ray film.

Milky Way Images from Radio to Gamma Ray

Looking up at the night sky with our unaided eyes, we see light emitted by an amazing variety of objects. But we are only seeing one narrow view of the spectrum, and in many cases celestial objects emit light very differently in

other wavebands. Observing them at different wavelengths provides a much more complete picture of their structure. Because of this, observational astronomers have been a driving force in the development of multi-wavelength and invisible-light imaging. In some cases, visible-light astronomy (known as optical astronomy) is severely limited by the presence of light-obscuring matter between earth and a celestial object of interest. In other cases, there is not very much visible light emitted by the object of interest in the first place, yet the same object may be very bright in other wavebands. These revelations about the sky were made only in the latter part of the twentieth century, with the advent of invisible-light astronomical instruments. High-resolution radio telescopes permitted precise mapping of the radio sky, and orbiting telescopes made x-ray and gamma-ray astronomy possible, since the atmosphere absorbs the shortest wavelengths of light. As mentioned earlier, astronomers have now studied the heavens in twenty powers of ten in wavelength of the electromagnetic spectrum!

The Milky Way is a particularly rich area of study for multi-wavelength astronomy. It covers a full 360-degree field of view, and is quite wide in the narrow dimension as well. The Milky Way is a cross-sectional view of our galaxy taken from our vantage point about one third of the way from the center. Our galaxy is shaped like a disc with a bulge in the center; the bulge is a region with a high density of stars and other celestial objects. The comparative images shown in Fig. 6.11 are all registered the same way, with the galactic center corresponding to the center of the images. The radio images are all made with ground-based radio telescopes. The infrared images are made by satellite-based instruments, as are the x-ray and gamma-ray images. The optical image is a composite of long-exposure photographs made from ground level. Note that these images have quite different angular resolutions, owing to the vastly different imaging systems used to acquire them. As a result, some of the images show much less fine structure than the optical image, for example. Note the commonality of these images: the central area of the Milky Way is bright at all wavelengths.

Milky Way Image Descriptions

Scattering of electrons in interstellar plasma is the predominant mechanism that causes the diffuse glow visible in the 73-cm-wavelength microwave image. This waveband is called the radio continuum by astronomers. Plasma is gas that has electrons stripped off of it either by intense heating or by absorption of ultraviolet starlight. Strong radio emission by compact objects like Sagittarius A at the galactic center is associated with the interaction of electrons with strong magnetic fields. This image is courtesy of C.G. Haslam.

The second image is made with light with a 21-cm wavelength, which corresponds to an **emission line** found in atomic hydrogen. The presence of atomic hydrogen traces the warm interstellar medium, which consists of large clouds of gas and dust. This image is courtesy of W.B. Burton.

The third image at a 12-cm wavelength shows the radio continuum emission from hot, ionized gas, but at a higher spatial resolution than the 73-cm wavelength

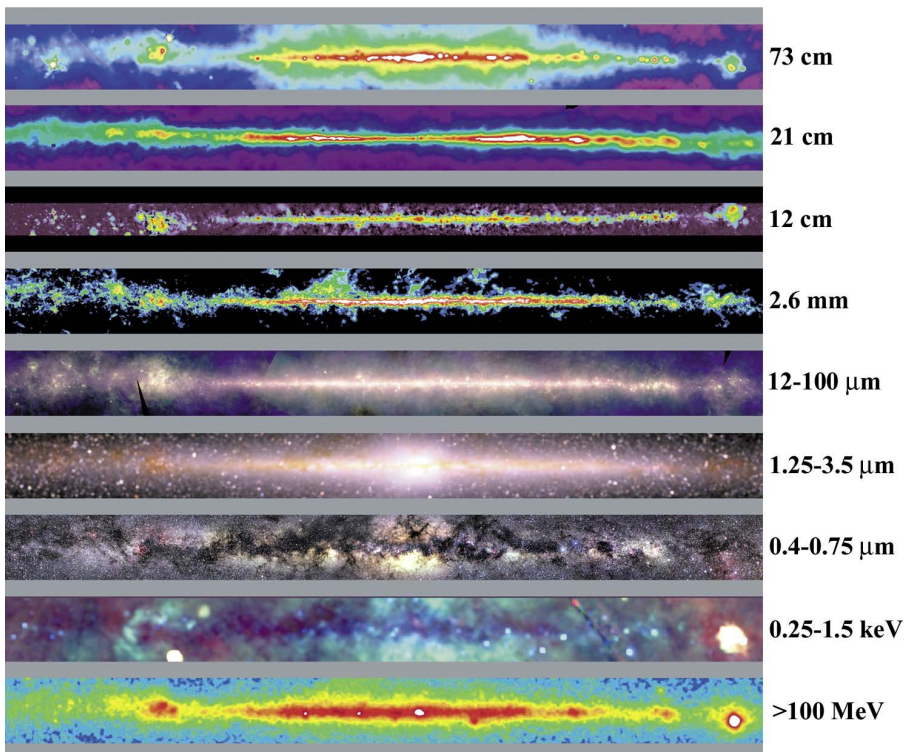


Figure 6.11 Multiwavelength Milky Way images

image. Finer details of the galactic center are visible because of this increased resolution. This image is courtesy of A.R. Duncan.

The fourth image shows emission from cold carbon monoxide. The wavelength of the emission is at a wavelength of 2.6 mm (the millimeter-wave band). Carbon monoxide is associated with molecular hydrogen that is difficult to observe directly. Molecular hydrogen is interesting to astronomers because large clouds of it are the precursors to star formation. This image is courtesy of T.M. Dame.

The fifth image shows emission at 12, 60, and 100 μm infrared wavelengths, which are indicated by blue, green, and red false color respectively. It is mostly thermal emission from interstellar dust warmed by the absorption of starlight. This image is courtesy of the Astrophysics Data Facility, NASA Goddard Space Flight Center.

The sixth image is also infrared, and shows mostly thermal emission from cool, low-mass stars throughout the galactic plane. The wavelengths indicated by blue, green, and red pseudocolor are 1.25, 2.2, and 3.5 μm respectively. The center bulge of the Milky Way is very clearly visible, since infrared light passes easily through the interstellar dust that blocks visible light. This image is courtesy of the Astrophysics Data Facility, NASA Goddard Space Flight Center.

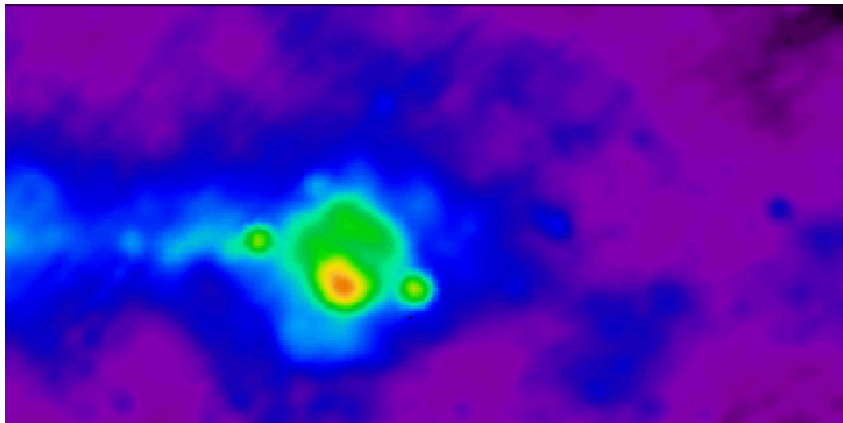
The seventh, an optical image with 0.4 to 0.75 μm waveband, shows the center of the Milky Way obscured by vast clouds of interstellar dust. This image is courtesy of S. Laustsen.

The eighth image, an x-ray image, shows that x-ray emissions from hot gas in shock waves make up the majority of the light seen. Shadows of cold gas clouds are evident in the central region. These gas clouds are strong absorbers of x-ray light, which scatters from the electrons within the atoms of the gases. The red, green, and blue false color denotes soft x rays in the 0.25, 0.75 and 1.5 keV wavebands, respectively. Several intense, compact sources are present, and are also visible in the gamma-ray image. Some of them are described below. This image is courtesy of the Astrophysics Data Facility, NASA Goddard Space Flight Center.

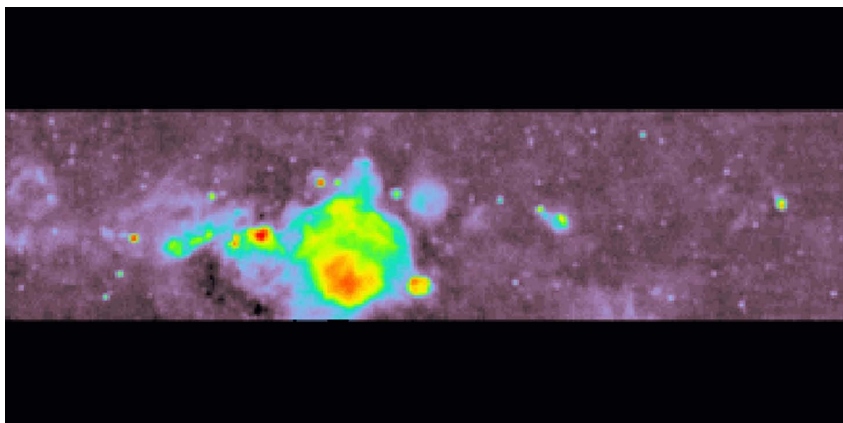
The last image shows gamma-ray light at the extreme end of the spectrum, with energies greater than 100 MeV. Most of this emission is caused by collisions between high-energy cosmic rays and atomic hydrogen nuclei in interstellar gas clouds. This image is courtesy of the Astrophysics Data Facility, NASA Goddard Space Flight Center.

One of the most striking features of this image set is the presence of a number of compact objects that are very bright at wavelengths other than the optical. Imaging technology revealed these new classes of celestial objects to astronomers only in the latter part of the twentieth century. Note the very bright object on the right side of the x-ray image, about one quarter of the total image width to the right of center. This is the Vela supernova remnant. This object was formed about 11,000 years ago when a star exploded, and a rapidly expanding shell of gas was blown off the star's surface. That shell is continually expanding in size, and as it expands into the interstellar medium, collisions between the two strips electrons off atoms. When the electrons recombine with the stripped atoms, they generate light at many wavelengths. The gas shell is especially bright in the soft x-ray band. Not all of the star's mass was blown into space. A significant portion of the core contracted to such an extent that atomic forces were overwhelmed, forming a rapidly rotating, extremely dense object known as a pulsar or neutron star. The Vela pulsar rotates 11 times per second, sweeping a powerful beam of radio waves (like the beam from a lighthouse) around in space. The Vela pulsar is thus clearly visible in both the 73-cm-wavelength and the 12-cm-wavelength images, and in the gamma-ray image as an intense, compact source. It is much less prominent in the optical image. Figure 6.12 shows five views of Vela in these five wavebands.

Two other pulsars are prominent on the far right side of the 73-cm microwave, x-ray and gamma-ray images. They are the Crab and Gemiga pulsars, both of which lie at the center of supernova remnants associated with the stars that formed them. On the left side of the center of the x-ray image, about the same distance to the left as Vela is to the right, is a very bright, compact object. This is Cygnus X-1, located in the constellation Cygnus and thought to be a black hole orbiting a companion



(a) Vela in microwave ($\lambda = 73$ cm).

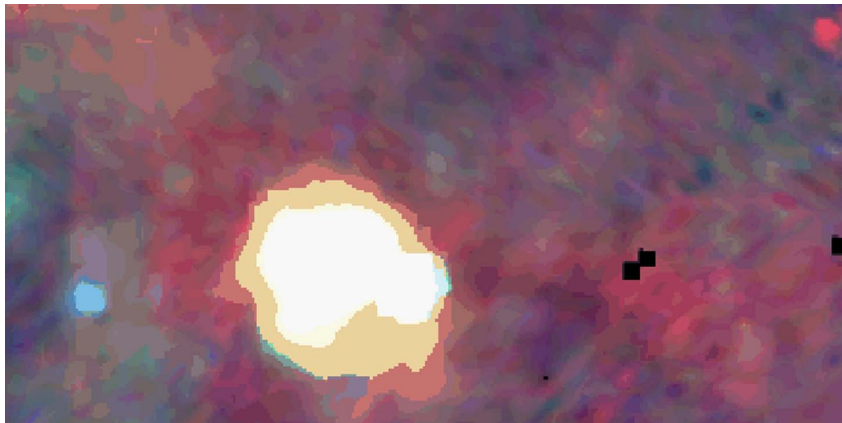
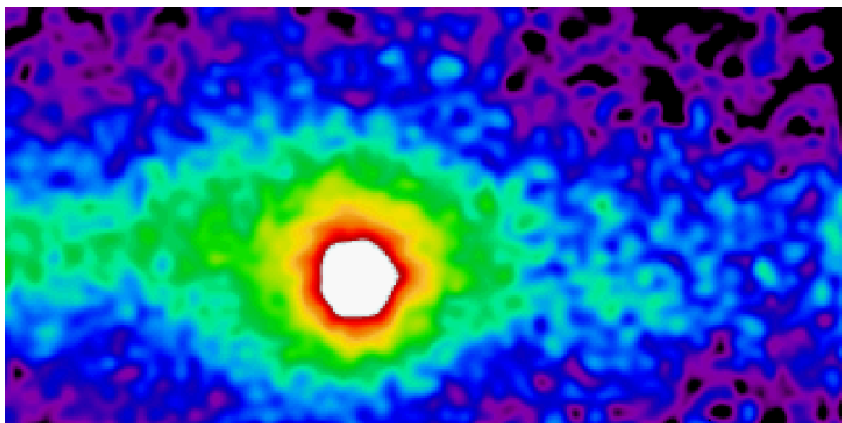


(b) Vela in microwave ($\lambda = 12$ cm).



(c) Vela in optical ($\lambda = 0.4\text{--}0.7$ mm).

Figure 6.12 Five images of Vela. (Courtesy of the Astrophysics Data Facility, NASA Goddard Space Flight Center).

(d) Vela in soft x ray ($E = 0.25\text{--}1.5 \text{ keV}$).(e) Vela in gamma ray ($E > 100 \text{ MeV}$).**Figure 6.12** (continued)

star. The intense gravitational field of the black hole (if that is what it really is) sucks gas from its companion, and as the gas falls into the hole, it heats up hot enough to emit soft x rays.

Epilogue

Invisible-light images and the imaging technology that makes them used to be obscure to the public, familiar only to scientists, engineers, and military specialists. That situation has changed in the last 20 years, as the technology has become more accessible to the general public and various devices have become declassified. What can we look forward to in the future? It is certain that many invisible-light imaging devices will become as common as camcorders, and that non-technical people will have opportunities to explore the electromagnetic spectrum on their own.

In the last ten years since the first edition of *Alien Vision* came out, there have been steady improvements in many areas of imaging technology, including reduced price and increased sensor resolution. The incredible growth of computer memory and storage have made it possible to create camera systems that can take images at extremely high frame rates and store all the raw digital image data for analysis.

The field of imaging technology is currently in a period of very rapid growth, with new applications and devices invented on a daily basis, and the imaging revolution shows no signs of slowing. Many wavebands are now accessible with commercial imaging devices that were unaffordable to all but the military a decade ago. Thermal imaging devices that used to cost US\$100,000 and weighed 100 pounds now cost under US\$2,000 and weigh a fraction of a pound, and the price, weight, and size continue to drop, while resolutions of sensors have improved dramatically. Ten years ago, the average thermal IR sensor was 320×256 pixels. Now 640×512 pixels is commonplace, and 1024×1024 and HD format sensors are also available commercially.

At some point in the next five years there will very likely be a huge proliferation in thermal imaging systems on automobiles, boats and other vehicles as the price drops to below US\$500. There are already handheld thermal viewers for sale to sportsmen for several thousand dollars. When they become several hundred dollars, a lot of people will get them for Christmas presents!

Many sensitive imaging devices operating in the near-IR band are now available for under US\$500, as restrictions on the availability of night-vision devices have eased. The end of the Cold War led to the availability of US\$100 Russian night-vision devices with near-IR sensitivity. Some consumer-grade camcorders have near-IR sensitivity and come with near-IR-only illuminators allowing video recording in total darkness. There are now some consumer digital cameras that have near-IR sensitivity, making digital near-IR photography an affordable option.

Ultraviolet cameras based on CCDs are made by a number of different CCD camera manufacturers. There are now commercially-available UV camera systems that see UV only, as well as special filters that enable UV-only imaging (effectively blocking visible and near-IR light that would contaminate the image). I am involved in a company that makes UV camera systems, and we are seeing many new applications for UV imaging, including paranormal investigation! Supposedly, ghosts and other paranormal “entities” emit UV light.

X-ray imaging is now used in many industrial applications that were impractical a few years ago. The technology of x-ray detection with electronic sensors has improved to the point where very low-intensity x-ray sources can be used to produce useful images without film, increasing safety and lowering cost. Gamma-ray imaging will probably always be very expensive and specialized, barring some breakthrough in gamma-ray source technology.

The increasing practicality of radar and sonar imaging is tied to the cost of computing power. As very high-speed computers became commodity items, the intensive data processing required for high-resolution sonar and synthetic-aperture radar became affordable to non-military users, and amazing systems for fish-finding and wreck imaging are on the commercial market. There are now prototype sonar systems that generate real-time, high-resolution imagery in a package that can be carried by a single diver, who sees a video image displayed on his or her diving mask. Commercial versions of these sonar systems will be invaluable for underwater tasks such as hull repair in zero-visibility water. In the not-too-distant future, we may see real-time imaging radar systems become standard equipment on aircraft, reducing the risk of controlled flight into terrain, which is the technical term for flying into the side of a mountain. Passive millimeter-wave imaging is almost a commercial reality, and could usher in a new era for airline transport, since aircraft equipped with mmW vision systems can safely land in low-visibility conditions that currently close airports. This technology is sorely needed, as the carrying capacity of airports in metropolitan areas has already been exceeded. Because of this, bad weather at one major U.S. airport causes a ripple effect, delaying hundreds of flights all over the country. The vision systems intended for flight control are more than just simple video display of an invisible-light imaging sensor; rather, several imaging devices working at various wavelengths can be incorporated into a single display using the technique of sensor fusion. The airline pilot sees a single video image that is a computer-enhanced composite of the video data from multiple sensors operating in various wavebands, including the visible. The pilot mostly sees a visible-light image in the display, but if he or she flies through a cloud, the displayed image could shift to the millimeter-wave video signal.

Astronomers continue to push the limits of invisible-light imaging on both ends of the electromagnetic spectrum and to fill in gaps in the spectrum where no one has yet observed the sky. Telescopes designed to detect gamma rays at extreme energies have recorded photons with energies in the 10^{21} -eV range. These photons have the same energy as a fast baseball! Continuing improvements in imaging technology are finding their way into nearly every band of the EM spectrum used in astronomy.

These efforts may lead to the discovery of new classes of celestial objects, as was the case with radio, x-ray, and gamma-ray astronomy.

This is a very exciting time for the field of imaging, and I hope that this book will stimulate the reader to explore imaging technology further and to invent new applications for imaging technology in other disciplines.

Glossary

Absorption band: A waveband of the electromagnetic spectrum where a material has a strong response, or resonance to light. This leads to the absorption of photons of light within that waveband by the material.

Aerothermal heating: The heating of an object, often a projectile by a rapid flow of gas, often at supersonic speeds.

Aitoff projection: A mapping of the entire sky onto an ellipse, just like Mercator's projection is a mapping of the earth's surface onto a flat piece of paper (a map). The Aitoff projection produces a great deal of distortion at the edges but is more accurate near the equator. Aitoff projections of the sky are in galactic coordinates, i.e., the center of our galaxy is mapped to the center of the ellipse, and the galactic plane (what we see as the Milky Way when we look at the sky) is mapped onto the "equator" of the projection.

Analog video: A video signal meant for a TV monitor. It is not as high fidelity as digital video, but it is easy to store in analog formats such as VHS tapes.

Antimatter: Matter made up of the antiparticles of normal matter. When antimatter and matter are combined, they annihilate each other, resulting in the production of gamma rays with energies equivalent to the mass of the annihilating particles.

Atomic number: The number of protons in the nucleus of an atom. The heavier the element, the higher the atomic number.

Backscatter x ray: An x-ray imaging technique that uses x rays scattered back in the direction of their source onto a detector. The backscatter signal is sensitive to the atomic number of atoms in the material being imaged, giving information about chemical composition as well as shape.

Back-thinned CCD: A charge-coupled device (CCD) sensor that is sensitive to UV light, since the silicon detector material is thin enough to detect UV light and convert it into electrical signals, rather than absorbing it.

Black hole: A celestial object resulting from the collapse of a star into a compact object that generates a gravitational field so intense that not even light can escape it. Many black hole candidates are thought to be associated with a companion star in a close orbit. The black hole absorbs matter from the companion star, and as the matter swirls into the hole, it heats up to temperatures as high as tens of millions

of degrees, generating a blast of x-ray light. See also *Black Holes and Warped Spacetime*, by W. Kaufmann.

Black light: An ultraviolet light source, usually of a gas-discharge type equipped with a filter that passes UV light only. The human eye perceives only a deep purple glow from the black light.

Closed-cycle cooler: A refrigerator used in some infrared cameras to cool the focal-plane array. These compact devices use an alternating expansion and contraction of helium gas that pumps heat out of the focal plane array to the outside air. Helium is used because it remains a gas even at extremely low temperatures.

Cobalt-60: Cobalt-60 is a radioactive isotope of cobalt that emits gamma rays through a radioactive decay process that converts the cobalt into nickel with the emission of a high-energy electron and a gamma ray. The 60 refers to the atomic mass—the number of protons and neutrons in the atom’s nucleus.

Coded-aperture mask: An array of tiny pinholes in a pattern known as a uniformly redundant array. The array produces a diffraction pattern on a detector that can be processed into an image. Coded-aperture masks were developed as imaging optics for very short wavelength light in the extreme ultraviolet, x-ray, and gamma-ray wavebands where traditional lens and mirror designs fail to operate.

Cooling curve: A cooling curve is a graph of temperature versus time for an object that has been heated up and then left to cool.

Cryostat: As used in this book, a device used to cool a focal plane array or other detector on a satellite or spacecraft that works on the principle of evaporation of hydrogen gas from ultracold hydrogen ice.

Depleted uranium: Depleted uranium is uranium with very little U-235 in it. U-235 is an unstable isotope of uranium that is used in some designs of fission weapons.

Diffraction: A wave phenomenon caused by interference between different portions of a wave. Diffraction causes spreading in beams of light, and is one of the reasons that dish antennas for radio astronomy have to be very large to achieve high pointing resolution. See *Optics*, by Hecht, for an excellent explanation of diffraction theory.

Diffraction pattern: A diffraction pattern from a slit is a series of light and dark lines produced on a detector by interference between tiny portions of the wave that

pass through the slit. A crystal can also produce an x-ray diffraction pattern due to the periodic arrangement of atoms in it.

Diffuse reflector: A surface that reflects incident light at random angles due to surface roughness.

Digital video: True digital video data is as faithful a reproduction as is possible of the original image stream. These data contain the digital intensity value for every pixel in a focal plane array.

Dish antenna: A radio antenna shaped in the form of a paraboloid with a detector element at the focus of the dish. Incoming parallel rays are focused onto the detector element.

Dispersion: This property of refracting materials is the dependence of the angle of refraction on the wavelength of a light wave.

Electromagnetic field: The electromagnetic field is an entity that interacts with matter via the exchange of photons with particles in the matter that have electrical charge. See *Optics*, by Hecht, for a more comprehensive explanation.

Electromagnetic spectrum: The known gamut of possible frequencies or wavelengths of light.

Electromagnetic wave: A wave composed of electric and magnetic fields that travels at the speed of light in empty space.

Emission line: An emission line is a waveband of light emitted by an atom or molecule that has been heated or otherwise excited.

Emissivity: The emissivity of a material is a measure of how much light it emits in a particular waveband relative to a perfect emitter (known as a blackbody) at the same temperature. Emissivity varies between 0 and 1, with shiny metallic objects tending to have low emissivities, and black objects (such as lumps of coal) having high emissivities.

Energy: The energy in a lightwave is transferred to matter in discrete bundles known as photons. The higher the frequency of a lightwave, the higher the energy of the associated photon.

Excitation mode: A frequency of vibration in an atom or molecule that leads to absorption and emission of light at that frequency. Objects such as organ pipes and

other musical instruments have acoustic excitation modes—these are the notes we hear.

Extreme light: a term coined to describe light with wavelengths that are either much shorter or much longer than the wavelengths of visible, infrared or ultraviolet light.

Extreme ultraviolet: Ultraviolet light in the 4-nm to 40-nm waveband. This light is highly absorbed by matter and is thus difficult or impossible to focus or reflect with conventional optical elements.

False color: Color added to images that do not contain color to indicate a property of the image. This is done to enhance slight changes in intensity within an image, to indicate regions at a particular intensity, and to indicate the intensity of invisible light which a priori has no color associated with it.

Focal plane array: A 2D array of detectors placed at the focal point of a lens, mirror, or other focusing optic. An image is focused onto the detectors, which then convert the light signal (or acoustic signal) into electrical signals that can be processed into images.

Frequency: The number of oscillations per unit time of a wave. The wavelength of light is related to the frequency via the expression: wavelength \times frequency = speed of light.

Gamma ray: Light with a wavelength shorter than 0.01 nm, or equivalently, light with photon energies higher than about 1 MeV. Gamma rays are typically generated by radioactive decay and have the ability to penetrate through materials such as thick steel, producing x-ray-like images of the interior.

Gamma-ray burster: Celestial objects of unknown origin that release powerful bursts of gamma rays in a random fashion. They are some of the most intensely studied gamma-ray sources in the sky.

Hard x ray: X-ray light with photon energies in the 100-keV range. Hard x rays are used for radiography, as the penetration of materials increases with energy.

Hot mirror: A near-infrared absorbing or reflecting optical element used in conjunction with silicon imaging sensors to prevent contamination of color images with near-IR light.

Imaging tube: A component used in sniperscopes and other imaging systems that converts invisible light signals from a scene or target into a visible image. A weak

light signal is imaged onto a light-sensitive surface that converts the light into electrons, which are then amplified and converted into a visible display.

Indium antimonide (InSb): A semiconductor detector material that is very sensitive to light in the 1–5 μm waveband. Indium antimonide must be cooled to temperatures around that of liquid nitrogen (-200°C) to work properly.

Indium gallium arsenide (InGaAs): A semiconductor detector material that is very sensitive to light in the 0.9–1.68 μm waveband. Indium gallium arsenide does not have to be cooled to operate properly, unlike indium antimonide, although it is usually temperature-stabilized at 10°C .

Infrared band: Light in the wavelength range between 0.75 μm and 100 μm .

Invisible light: Light that falls outside the waveband of visible light. Human beings require imaging technology to see invisible light.

Iridium-192: A radioactive isotope of the element iridium that emits gamma rays with an energy of 1.46 MeV.

Isotope: A chemical element with a different number of neutrons in the nucleus, which often makes the nucleus unstable and thus radioactive.

Light wave: An electromagnetic wave.

Logarithmic scale: A scale where successive divisions are powers of ten. Useful when displaying an enormous range of data, as it compresses the data down into a more intuitive form. A logarithmic scale of wavelength was used in Fig. 1 in the Introduction.

Longwave infrared (LWIR): Thermal infrared light in the 7–14 μm waveband, corresponding to the peak intensity of light emitted by mammals. LWIR light has the ability to penetrate through thick smoke and fog.

Medium light: Light falling in the middle of the known electromagnetic spectrum plotted with a logarithmic scale, particularly ultraviolet, visible, and infrared. Light in this center region of the spectrum interacts strongly with matter over very short

distance scales, since many atoms and molecules have strong absorption bands in the infrared and ultraviolet regions of the spectrum.

MeV: One million electron volts, equivalent to the kinetic energy of an electron at a potential of 1 million volts. Photons with MeV energies are in the gamma-ray waveband of the electromagnetic spectrum.

Micrometer (μm): A metric unit of distance equal to 1 millionth of a meter. A human hair is about 80 micrometers in diameter. The wavelength of visible light is about half a micrometer.

Microwave band: Light with a wavelength in the 1-cm to 1-m waveband. Microwaves can penetrate through many materials and can be used to detect objects at considerable distances through weather.

Midwave infrared waveband (MWIR): Light with a wavelength in the 3–5 μm range. Midwave infrared light is also known as thermal infrared light, since it is emitted by objects at terrestrial temperatures.

Milky Way: The disc-shaped galaxy we live in, and also the strip of white light made up of billions of stars in the night sky. We see the galaxy as a strip, since we are located within the plane of the disc.

Millimeter-wave (mmW) band: Light with a wavelength in the 1-mm to 1-cm range.

Molecular cloud: Very large clouds of cold gas molecules, typically molecular hydrogen and carbon monoxide. Hydrogen clouds can collapse from gravity and create star-forming regions.

Nanometer (nm): A metric unit of distance that equals 1 billionth of a meter. Visible light has wavelengths in the 400–750 nm range.

Near-infrared (near-IR) waveband: Light with a wavelength in the 0.75–1.1 μm range.

Near-ultraviolet (near-UV) waveband: Light with a wavelength in the 0.3–0.4 μm range.

Night glow: A naturally-occurring diffuse illumination that is caused by the excitation of gas in the upper atmosphere by radiation striking the Earth. Night

glow can be exploited for night vision through the use of a suitable imaging technology.

Nucleon: A proton or a neutron, the two particles found in the nucleus of atoms.

Photons: The smallest “particle” of light of a particular frequency. Light waves exchange energy with matter in discrete bundles known as photons.

Photoreceptors: Nerve cells in the eye that convert light into electrical signals that can be interpreted by the brain.

Planck’s constant: A fundamental constant that relates the energy of a photon to the frequency of its associated light wave.

Plutonium: An artificially generated radioactive element that is used in nuclear weapons as a source of neutrons.

Positron: The antimatter version of electrons. They have the same mass as an electron but have an opposite (positive) charge. They are emitted by some radioactive isotopes, and quickly annihilate with electrons, producing a pair of gamma rays with energies of 511 keV.

Pseudocolor: Color added to images that do not contain color to indicate a property of the image. This is done to enhance slight changes in intensity within an image, to indicate regions at a particular intensity, and to indicate the intensity of invisible light which a priori has no color associated with it.

Pulsar: A rapidly rotating core of a star that ended its life with a supernova explosion. Pulsars emit intense beams of light that sweep out a circle in space. See also *Black Holes and Warped Spacetime*, by W. Kaufmann.

Quantum theory: A theory that explains phenomena observed in the interaction of light waves with matter, whereby energy is transferred between lightwaves and matter in discrete bundles known as photons.

Quasar: Short for quasi-stellar radio source. Quasars are thought to be galaxies with powerful microwave sources located in the center. Quasars are among the brightest objects in the microwave sky. See also *Galaxies and Quasars*, by W. Kaufmann.

QWIP: An acronym for quantum well infrared photodetector, it is a detector material typically based on the semiconductor gallium arsenide.

Radar imaging: A technique of imaging invented during World War II that uses short pulses of microwave energy to measure the location of aircraft, ships, and

other objects in darkness and through all weather conditions. Radar can also be used to map surface features on Earth and other planets.

Radiance: A measure of the amount of light per unit area emitted by a target into a unit solid angle, often in units of watts per square centimeter per steradian for infrared measurements.

Radiography: A method of imaging the interior of object using highly penetrating x rays. X rays are directed through an object onto a sheet of special photographic film or an electronic detector, which records an x-ray “shadow” of the object that can show details of the interior that are not visible to the eye.

Radiometric measurement: Measurement of the in-band radiance or brightness of a target using a calibrated camera or other light detector.

Radiowave band: The region of the electromagnetic spectrum adjacent to the microwave band where light has a wavelength longer than a meter.

Refraction: The bending of waves caused by the change of the velocity of the wave. Refraction creates the illusion that a straight stick held partially in water appears bent. Refraction also is the reason why lenses focus light, since the lenses bend light rays into a common focal point.

Rhodopsin: A chemical found in the retina that changes in response to light, leading to the perception of light by the eye/brain/mind combination.

Sagittarius A: A compact radio source located at the center of the Milky Way galaxy. So-named because it is the brightest radio source in the constellation Sagittarius. Sagittarius A is believed to be a massive black hole that absorbs a huge quantity of gas and matter from stars in the dense galactic-core region.

Shortwave infrared (SWIR): Light in the 1.1–2.5 μm waveband.

Side lobe: The beam pattern from a dish or other directional antenna or sonar transponder consists of a main beam, where nearly all the energy is concentrated, and side lobes, which are less intense beams caused by diffraction.

Signature measurement: Measurement of the intensity and wavelength distribution of light emitted by a target using a calibrated light detector such as an infrared camera. Signature measurements may also include spatial and temporal structure measurements.

SIR-C/XSAR: SIR-C/XSAR stands for Spaceborne Imaging Radar–C/X-band Synthetic Aperture Radar. The orbital motion of the shuttle makes the radar system sweep out a path in space that synthesizes a large radar antenna, or aperture. SIR-C is the third imaging radar flown on the shuttle (the first two were A and B). The X band is a slice of the electromagnetic spectrum centered at a wavelength

of 3 centimeters. SIR-C/X-SAR actually operates in three different radar bands, the L-band (24 cm), C-band (6 cm) and X-band (3 cm).

Silicon-intensified target (SIT): A type of camera similar to the early vidicon sensors that is sensitive to ultraviolet light.

Sniperscope: An imaging device sensitive to light in the near-IR or other invisible waveband that is mounted on a rifle or other weapon and used for covert sniping under conditions that make visible riflescopes useless.

Solar loading: Heating of a surface due to impingement of sunlight, mostly in the near-infrared waveband. Solar loading can reduce contrast between targets and scenes.

Soft x ray: Low-energy x rays that are not as penetrating as hard x rays or gamma rays. Soft x-ray photons have energies that are typically 0.1–10 keV. Medical x rays are typically made with hard x rays.

Sonar imaging: Acoustic imaging method that can image underwater or through other liquid or solid material. Sound waves are generated, reflect off features of interest, and are detected by the transducer emitter.

Spectral signature: The characteristic brightness of light emission by a target as a function of wavelength. A solid rocket motor has a signature that is very distinctive from jet exhaust, for example.

Specular reflector: A surface, usually conductive but always optically smooth, where incident light is geometrically reflected at specific angles of reflection.

Speed of light: The speed of an electromagnetic wave in empty space is fixed at 300,000 km per second.

Sub-millimeter (sub-mmW) band: A region of the spectrum where light has wavelengths of a fraction of a millimeter. The infrared spectrum is considered to extend out to wavelengths of 100 mm, which is the lower limit of the sub-millimeter band. Light in this waveband has frequencies in the terahertz range—for this reason, these light waves are known as T-rays.

Supernova remnant: One possible ending for a star is a supernova event. The star exhausts its nuclear fuel, leading to the collapse of the star's core into a pulsar. The outer shell of the star blows off into space, forming an expanding shockwave that can interact with interstellar gas to emit x-ray light. The pulsar at the center of the supernova remnant emits radio waves and microwaves in a beam that revolves around like the light source in a lighthouse. Supernova remnants like the Crab, Geminga and Vela can appear bright in many invisible wavebands of light.

Swath: Synthetic aperture radar scans surfaces with a beam that lays down a track on the ground. The track is known as a swath, and is analogous to the track left in the wake of a mower. Many passes of a synthetic aperture radar system on a

satellite (for example) will cover an area—the image data can then be “stitched” together to create a complete (or nearly complete) radar map.

Synthetic aperture radar: A radar technique that synthesizes a large effective aperture or antenna size using the motion of a small radar dish or an array of small antennae spaced apart. This is a way to achieve high pointing resolution without having to build an enormous single antenna.

Thermal imaging: Imaging technology operating in the thermal infrared wavebands.

Thermal infrared: Light in the LWIR and MWIR wavebands, typically between 3–15 μm .

Thermal scarring: A persistent infrared feature in a scene caused by the heating or cooling of part of the scene, such as a shadow on a runway left by a departed aircraft. The heat source is often solar loading. The heat or lack of heat can persist for many minutes or even hours.

Thermography: The science of measuring temperatures using the emission of light from an object with known emissivity. Thermography is usually done in the MWIR and LWIR regions of the spectrum, although near-IR and visible light thermography are used in high-temperature applications such as measuring the temperature inside a blast furnace.

Tracers: Chemical compounds or molecules used in PET scans to introduce gamma-ray emitters into living tissue. Tracer molecules contain radioactive atoms in place of the conventional non-radioactive stable isotopes.

Transmission window: A waveband of light that freely penetrates through a medium, such as the atmosphere that is highly absorbent in adjacent wavebands. A good example is the transmission window in water in the visible waveband. Water is highly absorbent in both the near-UV and near-IR wavebands.

Trough and ridge: A type of geologic structure seen on the ocean floor and on the surface of the planet Venus. It is caused by the interaction of the large plates that make up the outer layers of both planets.

Ultraviolet: Light that has a wavelength in the range from 10–400 nm.

Visible light: Light that has a wavelength between 400 nm and 750 nm—the waveband that the unaided human eye sees. Astronomers call this the optical waveband.

Waveband: A range of wavelengths of light; for example, the infrared waveband is 750 nm to 100 μm .

Wavelength: The distance between successive crests of a wave.

X ray: Light in the wavelength range between 0.01–10 nm. X rays are often used to image through materials that are opaque to visible light.

Bibliography

I selected the following books and articles because they are introductory in nature or because they explain a particular subject described in this book that non-technical readers may have difficulty understanding.

General interest:

- H. Edgerton, *Stopping Time—The Photographs of Harold Edgerton*, Abrams, New York (1987).
- E. Hecht, *Optics*, Addison-Wesley, Reading, MA (1998).
- P. Kaiser and R. Boynton, *Human Color Vision*, OSA Press, Washington, D.C. (1996).
- W. Kaufmann, *Black Holes and Warped Spacetime*, W.H. Freeman, San Francisco, CA (1979).
- W. Kaufmann, *Galaxies and Quasars*, W.H. Freeman, San Francisco, CA (1979).
- W. Kaufmann, *Stars and Nebulas*, W.H. Freeman, San Francisco, CA (1978).
- P. P Morrison and the Office of Charles and Ray Eames, *The Powers of Ten*, Scientific American Library, New York, NY (1982).

Near-IR and near-UV imaging:

- L. Hayball, *Advanced Infrared Photography Handbook*, Amherst Media, Buffalo, NY (2001).
- J. Russ, *Forensic Uses of Digital Imaging*, CRC Press, Boca Raton, FL (2001).

Thermal imaging:

- G. Holst, *Common Sense Approach to Thermal Imaging*, SPIE Press, Bellingham, WA (2000).
- H. Kaplan, *Practical Applications of Infrared Thermal Sensing and Imaging Equipment, Third Ed.*, SPIE Press, Bellingham, WA (2007).
- J. Snell and D. Burleigh, Eds., *Thermal Sensing and Imaging 1980–1999*, Selected SPIE papers on CD-ROM, Volume 7, SPIE, Bellingham, WA (1999).

Millimeter-wave and microwave imaging:

- P. Bhartia and I. Bahl, *Millimeter Wave Engineering and Application*, John Wiley and Sons, Inc., New York, NY (1984).
- L. Klein, *Millimeter Wave and Infrared Multisensor Design and Signal Processing*, Artech House, Norwood, MA (1997).
- G. Stimson, *Introduction to Airborne Radar*, SciTech Publishing (1998).
- J. Toomay, *Radar Principles for the Non-Specialist*, SciTech Publishing (1999).
- F. Ulaby, R. Moore, and A. Fung, *Microwave Remote Sensing*, Addison-Wesley Publishing Co., Reading, MA (1981).

X-ray and gamma-ray imaging:

- R. Eisenberg, *Radiology: An Illustrated History*, Mosby-Year Book, St. Louis, MO (1991).
- B. Kevles, *Naked to the Bone: Medical Imaging in the 20th Century*, Perseus Press, Cambridge, MA (1998).
- L. Romans, *Introduction to Computed Tomography*, Lippincott, Williams & Wilkins, Philadelphia, PA (1995).
- W. Sweet and G. Brownell, “PET scanning,” *Nucleonics* **11**, 40–45 (1953).
- A. Wolbarst, *Looking Within: How X-Ray, CT, MRI, Ultrasound, and Other Medical Images Are Created, and How They Help Physicians Save Lives*, University of California Press, Berkeley, CA (1999).

Acoustic imaging:

- P. Callen, *Ultrasonography in Obstetrics and Gynecology*, W. B. Saunders Co., St. Louis, MO (2000).
- C. Mazel, *Side Scan Sonar Record Interpretation*, Peninsula Publications (1985).

Multiwavelength Astronomy:

- J. Bleeker and W. Larsen, *X-Ray and Gamma-Ray Astronomy*, Pergamon Press, New York, NY (1989).
- B. Burke, *An Introduction to Radio Astronomy*, Cambridge University Press, New York, NY (1997).
- K. Lang, *Sun, Earth and Sky*, Springer-Verlag, New York, NY (1995).
- S. Maran, *Astronomy for Dummies*, Hungry Minds, Inc., Indianapolis, IN (1999).
- C. Ronan, *Invisible Astronomy*, J.B. Lippincott Company, Philadelphia, PA (1972).

Index

A

absorption, 3, 12, 13, 31, 36, 41, 47, 64, 67, 72, 98, 102
atmospheric, 64
absorption bands, 36
acoustic beam pattern, 118
acoustic daylight imaging, 122
acoustic imaging, 116, 120, 124–126
acoustic microphone array, 124
acoustic noise imaging, 123–125
acoustic pictures, 115
acoustic waves, 115, 120
aerial photograph, 26
aerial reconnaissance, 10
aeronautical navigation, 71
Aitoff projection, 76, 77
alcohol, 3, 36
all-weather imaging, 72
analog video, 50
Angkor, Cambodia, 81
anode, 92
Antarctica, 82
antenna
 directional, 75
 dish, 68, 75
antimatter, 107, 109
aphakia, 5
Apis japonica, 62
archaeology, 80, 86
Arctic animals, 26
arteries
 heat signature of, 60
artificial vegetation, 10

astronomy, 41, 63

atomic number, 89, 102

B

back-thinned CCD, 6
ballpoint pen ink, 14
basal cells, 24, 27
bats, acoustic imaging in, 116
Becquerel, Henri, 107
biological systems, 62
black hole, 75, 135
black light, 24
black-and-white film, 129
black-and-white films, 6
Black-Eyed Susan flowers, 28
blue light, 5, 13, 43
brain, PET scan of, 111
bruises, 24
Buckingham, Michael, 123
buried objects, 80, 85
butterflies, 1, 29, 30

C

camera, 127–129, 131
cameras, xix, xxiii, 5, 6, 9, 32, 37, 38, 44, 48, 50, 51, 53, 73, 77
camouflage, 9–11, 20, 26, 27, 43
carcinoma, 96
CCD (charged-coupled device), 9, 14, 129
celestial objects, 74, 75, 132, 133, 135
charcoal, 16, 18
charged particles, 107
chemical elements, 102

chemical odor, 62
chlorophyll, 10
chromatic aberration, 5
circuit boards, 56
Cleopatra butterfly, 29
closed-cycle cooler, 49
cloth, 43
clutter, 80
cobalt-60, 90, 107
cocaine, detection of, 72
coded-aperture mask, 112
color, 1, 2, 9, 16, 19, 26–30, 32, 39
computer-aided tomography (CAT), 98
concealed weapons, detection of, 104
conductive materials, 87
contraband, 53, 71
coral reef, 29
Corona, 37
correcting fluid, 14
covert imaging, 71
cranial nerves, 60
craters, 64
criminologists, 17
Crouching Aphrodite, 108
cryogenic temperatures, 50
cryptic coloration, 26
crystals, scintillation, 109
Czerny, Marianus, 3

D

darkness, xx, 41, 42, 51, 57, 59
darkroom, 5
density, 43, 51, 64, 69, 87, 131, 133
depleted uranium, 112, 113
dermatology, 27
detectors
 antenna-type, 69
 gamma-ray, 109
diffraction, 68, 79
diffraction patterns, 89
digital video, 50
drug packets, detection of, 72

E

Earth, 80–82, 84, 90, 105, 113

Eastman Kodak, Inc., 10, 11
eclipse, 64
Effelsberg 100-meter telescope, 77
Eisner, Thomas, 29
electromagnetic energy, 71, 79
electromagnetic field, xxi
electromagnetic spectrum, xxi, xxiii, 115, 125
electromagnetic structure, 13
electromagnetic wave, xxi
electronic detectors, 48
electronic sensors, 6
electrons, 13, 22, 23, 30, 37, 67, 91–93, 107, 109, 133, 135
emission line, 133
emissivity, 72
Empire Knight, 118, 120
energy, xxi–xxiii
excitation modes, 13, 31
explosives, 53
extreme light, 67, 87
extreme ultraviolet, 89
eyes
 pupils, 9
 sclera, 32

F

false color, 10, 134, 135
fibers, forensic analysis of, 24
filters
 near-UV, 1
 passband, 64
 UV-transmitting, 29
fingerprint analysis, 23
flash photographs, 9
flavanols, 29
flowers, identification of, 29
fluorescence, 5, 24
fluorescent materials, 6
fluoroscope, 94, 96–99
focal plane array (FPA), 127
fog, 71, 72, 74
frequency, xxi, xxii, 1, 13, 56, 68, 69, 79

G

galaxy, 75, 77, 133
Galileo spacecraft, 84
gamma rays, 89–92, 107–109,
 111–113, 127
gamma-ray bursters, 105
gamma-ray imaging spectrometer
 (GRIS), 111, 112
gelatin photographic emulsions, 6
geology, 85
germanium, 48, 49

H

hair
 forensic analysis of, 24
 SWIR images of, 32
harp seals, 26
heat, 41, 43, 45, 46, 51, 53, 57, 59, 60,
 64, 82
hertz, 68
Hertz, Heinrich, 68
hidden compartments, 53
high-energy astronomy, 104
Hollow Man, 43
hornets, 62, 63
hot mirror, 129
hydrogen gas, 77
hydrophones, 116

I

imaging radar, 80, 83, 85
indium antimonide, 128
indium gallium arsenide, 14, 129
industrial radiography, 98
infrared film, 10
infrared imaging, 3, 13, 36
infrared light, 3, 5, 8, 9, 12, 18, 22,
 38, 39, 41–43, 48, 56, 59, 64
 longwave (LWIR), 38
 midwave (MWIR), 38
infrared photography, 10, 38
infrared telescopes, 63
insect pollination, 28
insect vision, 6
integrated circuits, 56

internal temperature, 62

interstellar dust, 77
interstellar medium, 133, 135
invisible light, xx, xxi
ionization, 93
ionizing radiation, 102

J

Jansky, Karl, 75
Jodrell Bank, 77

K

kilo-electron-Volts (keV), 91, 92, 106,
 109, 112, 113, 132, 135
Kodak Aero Infrared film, 10
Kodak Panchromatic Tri-X film, 6

L

Lake Ontario, 82
Lake Vostok, 82, 84
lakes, 82
landmines, 85, 86
lasers, 69
law enforcement, 9, 23, 51, 53
Lawrence Livermore National
 Laboratory, 111, 113, 114
lens
 antireflection coating on, 5
lesions, 28
light wave, xxi
lightning rod, 37
logarithmic scale, 67
longwave infrared (LWIR), 38, 41,
 44, 47, 48, 51–53, 63, 127

M

Maat Mons, 85
Magellan spacecraft, 84
Marin Headlands, 12
marine animals, 29
medium light, 67, 68
melanin, 27
metabolism, 109, 111
metal detectors, 85
methanol, 36, 37

- microwave, xxii, xxiii
microwave band, 68, 76, 79, 83, 85, 87
microwave energy, 68
microwaves, 67, 68, 76, 77, 79, 83, 85, 87
Midcourse Space Experiment (MSX) satellite, 64, 65
midwave infrared (MWIR), 38, 41–63, 127, 128
Milky Way, 77, 132–135
millimeter waves (mmW), 68, 71, 72, 74, 87
molecular clouds, 75, 77
molecular compounds, 36
molecules, 2, 10, 13, 22, 26, 30, 32, 41, 43, 48, 67, 72
moon, infrared imaging of, 64
moths, 29
mummy, noninvasive analysis of, 100
mutation, 89
- N**
nanometers, xxi
Natura (painting), 17, 19
near-infrared (near-IR), 1, 2, 5–11, 13, 14, 16–18, 20, 22, 30, 31, 34–36, 38–40
near-IR waveband, 2, 5
near-ultraviolet (near-UV), 1–6, 14, 15, 22–35, 38, 40
near-UV waveband, 1, 5, 29, 32
nectar guides, 28
Nelson machine, 95
night glow, 9
night vision, 7
nitrogen, 37
noise, 116, 123–125
noise field, 123
noncontact thermography, 56
noninvasive analysis, 27
nucleons, 91
- O**
oil paint, 19, 30
- ozone layer, 36
- P**
paintings, 17–19
pantographs, 124
Parkes 64-meter telescope, 77
parking lots, 12
passive radio imaging, 79
pencil, 16, 18, 19
perspiration, 62
phosphor, 92, 96
photocathode, 23
photodetectors, 69
photons, xxi, 1, 2, 22, 31, 89, 91, 97, 111
photoreceptors, 29, 30
Pieridae, 29
pigments, 18, 30, 32
pinhole camera, 6
pit vipers, 59
pixels, 43, 49, 60
Planck's constant, xxi
plankton, 30
plastic explosives, detection of, 72
plutonium, 112, 113
polar bear, 26
polyethylene, 47
poor visibility, 72
positron emission tomography (PET), 109
positrons, 109
Predator, 43
prism, xx
pseudocolor, 10, 41, 43, 53, 54, 60, 63, 64, 118, 121, 123, 124, 134
pulsars, 75, 76
pyramids, 43
- Q**
quantum theory, xxi
quantum well infrared photodetector (QWIP), 127
quasars, 75
- R**
radar, xxiii, 68, 72, 79–82, 84, 85, 87

- Radarsat*, 83
radiation, 53, 89, 107, 110
radio astronomy, 74
radio telescopes, 77, 79, 133
radio waves, xxiii, 127, 135
radioactive glucose, 110
radioactive isotopes, 90
radiography, 89
radiowave band, 68
rattlesnakes, 59
reflected ultraviolet light photography, 24
Ritter, Johann Wilhelm, 4
Roentgen, Wilhelm Konrad, 91, 92, 94, 107
ROMANIS, 123, 124
Rutherford, Ernest, 107
- S**
Sagittarius, 75, 77
Sagittarius A, 75, 77
Saint Elmo's Fire, 37
satellite imagery, 83
science fiction movies, 43
searchlights, 7
seismic data, 83
semen, forensic analysis of, 24
semiconductors, 49
shadowgram, 93, 98, 108
Shafter Airport, 74
shortwave infrared (SWIR), 1, 2, 12–15, 18–22, 26, 30–36, 39, 40
shrimp, 123
silicon, 5–7, 9, 14, 129
silicon detectors, 64
silicon dioxide, 48
silicon-intensified target (SIT), 6
SIR-C/X-SAR imaging system, 81
skin, 43, 45, 47, 56, 60, 62
ultraviolet damage to, 28
skin cancer, 28
smoke, 42, 51, 52, 56
sniperscope, 7, 8
soft x rays, 135, 137
- solar atmosphere, 106
solar flares, 105, 106
solar loading, 43, 53, 64
solid state device, 69
sonar, 116, 118, 121, 122
sonic energy, 117
sound waves, 115, 120, 121, 123–125
Spatial Infrared Imaging Telescope (SPIRIT), 64
speed of light, xxi
starlight, 9, 133, 134
stars, 74–77
stress injuries, 62
submarines, 116
Sun, x-ray image of, 105
sunblock, 33
sunspots, 106
supernova remnants, 76
surveillance, 9
swaths, 83
SWIR waveband, 2, 14, 36
- T**
T-ray imaging, 69
T-rays, 69, 70
terahertz, 69
thermal energy, 42, 60, 62
thermal equilibrium, 44
thermal imaging, 41–44, 48, 50, 51, 53, 54, 56, 62, 64
thermal imaging camera, 49, 51
thermal vision, 59
thermionic emission, 92
thermography, 53, 57
thermometer, 53
thunderstorm, 75
tracer, 109, 110
transformers, 54, 55
transmission window, 127
Tricho machine, 96
trigeminal nerve, 60
trough-and-ridge structure, 85
- U**
ulceration, 96

ultrasonic devices, 120
ultrasound imaging systems, 120
ultrasound medical imaging, 120
ultraviolet light, 5, 6, 22, 24, 27–29,
 35, 36
ultraviolet vision, 1, 29, 30
uncooled microbolometer camera, 63
underwater acoustic imaging, 122
uranyl potassium sulfate, 107
urban areas, 12
urine, forensic analysis of, 24

V

varnish, 17, 18, 30
vegetation, 10
veins, heat signature of, 60
Venus
 microwave imaging of, 84, 85
very long wave infrared (VLWIR), 41
visible light, xx–xxii, 3, 5, 7, 12, 13,
 18, 22–24, 26, 27, 29, 32, 34, 35,
 39, 127, 129, 133, 134

W

Wadi Kufra, 82

warm-blooded animals, 42
wavebands, xxii, xxiii, 1, 10, 13, 15,
 22, 26, 31, 32, 35, 39–43, 47, 48,
 64, 127–129, 133, 135
wavelengths, xxi–xxvii, 2, 5, 6, 9, 13,
 22, 31, 32, 36–41, 47, 48, 51, 56,
 64, 67–69, 71, 72, 74, 76, 77, 79,
 80, 83, 84, 87, 127, 129, 133–135
window glass, 47
wounds, detection of, 24

X

x rays, 22, 67, 68, 71, 89–92, 94, 96,
 98, 102, 105–107, 115
 hard, 106
 soft, 105, 106
x-ray telescopes, 105
xanthophyll, 10

Y

Yohkoh satellite, 106

Z

zero-visibility weather, 73

About the Author:

Austin Richards is a Senior Research Scientist at FLIR, a manufacturer of infrared imaging systems and digital imaging electronics based in Santa Barbara, CA. The author received his B.A. in physics from Amherst College in 1989 and his Ph.D. in astrophysics from UC Berkeley in 1995, and has held postdoctoral fellowships from Lawrence Berkeley National Laboratory and the University of Stockholm in Sweden, where he contributed to the AMANDA project, a kilometer-scale neutrino detector at the South Pole Station in Antarctica. He is currently an adjunct professor at the Brooks Institute of Photography in Santa Barbara, where he teaches digital imaging and digital infrared photography, and a partner in Oculus Photonics, a manufacturer of digital ultraviolet imaging systems.



(Image courtesy of FLIR)

This image of the author was taken with a large-format indium antimonide camera operating in the 3–5 μm waveband. Pseudocolor was added using Media Cybernetics Image Pro 4.1, and a median filter was applied using Photoshop to remove fixed-pattern noise.